

การแสดงออกและคุณลักษณะสองหน้าที่ของเอนไซม์ออโรทีดีน 5'-โมโนฟอสเฟต ดีคาร์บอกซิลเลส  
และออโรเทต ฟอสโฟไรโบซิลทรานสเฟอเรส ที่เชื่อมต่อกัน ในเชื้อพลาสมิเดียม ฟิลซิพาร์ม



นางสาวภัสราวดี เผ่าจินดา

จุฬาลงกรณ์มหาวิทยาลัย

CHULALONGKORN UNIVERSITY

บทคัดย่อและแฟ้มข้อมูลฉบับเต็มของวิทยานิพนธ์ตั้งแต่ปีการศึกษา 2554 ที่ให้บริการในคลังปัญญาจุฬาฯ (CUIR)  
เป็นแฟ้มข้อมูลของนิสิตเจ้าของวิทยานิพนธ์ ที่ส่งผ่านทางบัณฑิตวิทยาลัย

The abstract and full text of theses from the academic year 2011 in Chulalongkorn University Intellectual Repository (CUIR)  
are the thesis authors' files submitted through the University Graduate School.

วิทยานิพนธ์นี้เป็นส่วนหนึ่งของการศึกษาตามหลักสูตรปริญญาวิทยาศาสตรดุษฎีบัณฑิต

สาขาวิชาชีวเวชศาสตร์ (สหสาขาวิชา)

บัณฑิตวิทยาลัย จุฬาลงกรณ์มหาวิทยาลัย

ปีการศึกษา 2559

ลิขสิทธิ์ของจุฬาลงกรณ์มหาวิทยาลัย

Expression and bifunctional characterization of *Plasmodium falciparum* orotidine  
5'-monophosphate decarboxylase/ototate phosphoribosyltransferase fused enzyme

Miss Patsarawadee Paojinda



A Dissertation Submitted in Partial Fulfillment of the Requirements  
for the Degree of Doctor of Philosophy Program in Biomedical Sciences

(Interdisciplinary Program)

Graduate School

Chulalongkorn University

Academic Year 2016

Copyright of Chulalongkorn University

Thesis Title Expression and bifunctional characterization of  
*Plasmodium falciparum* orotidine 5'-  
monophosphate decarboxylase/orotate  
phosphoribosyltransferase fused enzyme

By Miss Patsarawadee Paojinda

Field of Study Biomedical Sciences

Thesis Advisor Professor Jerapan Krungkrai, Ph.D.

Thesis Co-Advisor Sudaratana Krungkrai, D.Eng.

---

Accepted by the Graduate School, Chulalongkorn University in Partial  
Fulfillment of the Requirements for the Doctoral Degree

..... Dean of the Graduate School  
(Associate Professor Sunait Chutintaranond, Ph.D.)

THESIS COMMITTEE

..... Chairman  
(Professor Apiwat Mutirangura, M.D., Ph.D.)

..... Thesis Advisor  
(Professor Jerapan Krungkrai, Ph.D.)

..... Thesis Co-Advisor  
(Sudaratana Krungkrai, D.Eng.)

..... Examiner  
(Professor Sittisak Honsawek, M.D., Ph.D.)

..... Examiner  
(Assistant Professor Nuchanat Wutipraditkul, Ph.D.)

..... External Examiner  
(Assistant Professor Sumet Wajanarogana, Ph.D.)

ภัสรารัตติ เฝ้าจินดา : การแสดงออกและคุณลักษณะสองหน้าที่ของเอนไซม์ออโรทีดีน 5'-โมโนฟอสเฟต ดีคาร์บอกซิลเลสและออโรเทต ฟอสฟอโรโบซิลทรานสเฟอเรส ที่เชื่อมต่อกันในเชื้อพลาสโมเดียม ฟัลซิพารัม (Expression and bifunctional characterization of *Plasmodium falciparum* orotidine 5'-monophosphate decarboxylase/orotate phosphoribosyltransferase fused enzyme) อ.ที่ปริกษาวิทยานิพนธ์หลัก: ศ. ดร. จิระพันธ์ กริ่งไกร, อ.ที่ปริกษาวิทยานิพนธ์ร่วม: ดร. สุदारัตน์ กริ่งไกร, 136 หน้า.

การเชื่อมต่อกันของเอนไซม์สองลำดับสุดท้ายในกระบวนการสังเคราะห์ไพริมิดีน ซึ่งมีลักษณะการเรียงแบบกลับกัน โดยเอนไซม์ออโรเทต ฟอสฟอโรโบซิลทรานสเฟอเรส อยู่ด้านหมู่คาร์บอกซิลิก และ เอนไซม์ออโรทีดีน 5'-โมโนฟอสเฟต ดีคาร์บอกซิลเลส อยู่ด้านหมู่อะมิโน (ออโรทีดีน 5'-โมโนฟอสเฟต ดีคาร์บอกซิลเลส-ออโรเทต ฟอสฟอโรโบซิลทรานสเฟอเรส) ที่พบในสิ่งมีชีวิตหลายชนิด การศึกษาครั้งนี้เราได้ทำการผลิตยีนที่เชื่อมต่อกัน แบบออโรทีดีน 5'-โมโนฟอสเฟต ดีคาร์บอกซิลเลส-ออโรเทต ฟอสฟอโรโบซิลทรานสเฟอเรสในเชื้อพลาสโมเดียม ฟัลซิพารัมและทำการแสดงออกของโปรตีนสองหน้าที่ในเชื้อเอสเซอริเซีย โคลิ หลังจากนั้นได้ทำให้เอนไซม์มีความบริสุทธิ์เกือบเป็นเนื้อเดียวกันโดยใช้แอฟฟินิตีโครมาโตกราฟี และแอนไอออนเอ็กซ์เชนจ์โครมาโตกราฟี โดยพบว่าเอนไซม์มีการทำงานในรูปของโมเลกุลคู่สองหน่วยพื้นฐานที่เหมือนกัน ถึงแม้ว่าการทำงานของเอนไซม์จะไม่เสถียรภาพแต่สามารถทำให้เก็บรักษาเอนไซม์ได้เป็นระยะเวลาที่นานขึ้นโดยการใส่สารตั้งต้นและผลิตภัณฑ์ของเอนไซม์ ในระหว่างขั้นตอนการทำให้บริสุทธิ์ นอกจากนี้เอนไซม์ยังแสดงออกถึงประสิทธิภาพการเร่งปฏิกิริยาของเอนไซม์ที่สมบูรณ์ ( $k_{cat}/K_m$ ) โดยการศึกษาครั้งนี้พบว่า มีผลต่อค่าจำนวนการกลับมาทำปฏิกิริยาซ้ำ ( $k_{cat}$ ) มากถึง 1,000 เท่า ในขณะที่ไม่ได้กระทบต่อค่าคงที่ของ Michaelis ( $K_m$ ) มากนักโดยอยู่ในระดับไมโครโมลาร์ เมื่อเปรียบเทียบกับเอนไซม์ในรูปแบบการทำงานเดี่ยว และแบบจับกันเป็นคอมเพล็กซ์ที่ตีพิมพ์เผยแพร่มาก่อนนี้ การเชื่อมต่อกันของทั้งสองเอนไซม์อยู่บนโปรตีนเดียวกันเป็นการสร้าง "ซูเปอร์เอนไซม์" ที่มีประสิทธิภาพในการเร่งปฏิกิริยาที่สมบูรณ์ และความยืดหยุ่นของเอนไซม์ แสดงถึงความสัมพันธ์ในการวิวัฒนาการระดับโมเลกุลของปฏิกิริยาเอนไซม์ และการทำงานของเมแทบอลิซึม

สาขาวิชา ชีวเวชศาสตร์

ปีการศึกษา 2559

ลายมือชื่อนิสิต .....

ลายมือชื่อ อ.ที่ปริกษาหลัก .....

ลายมือชื่อ อ.ที่ปริกษาร่วม .....

# # 5587829220 : MAJOR BIOMEDICAL SCIENCES

KEYWORDS: MALARIA / PLASMODIUM FALCIPARUM / PYRIMIDINE DE NOVO BIOSYNTHESIS / OROTATE PHOSPHORIBOSYLTRANSFERASE / OROTIDINE 5'-MONOPHOSPHATE DECARBOXYLASE / FUSED BIFUNCTIONAL ENZYME / CATALYTIC EFFICIENCY

PATSARAWADEE PAOJINDA: Expression and bifunctional characterization of *Plasmodium falciparum* orotidine 5'-monophosphate decarboxylase/orotate phosphoribosyltransferase fused enzyme. ADVISOR: PROF. JERAPAN KRUNGKRAI, Ph.D., CO-ADVISOR: SUDARATANA KRUNGKRAI, D.Eng., 136 pp.

Fusion of the last two enzymes in the pyrimidine biosynthetic pathway in the inversed order by having a COOH-terminal orotate phosphoribosyltransferase (OPRT) and an NH<sub>2</sub>-terminal orotidine 5'-monophosphate decarboxylase (OMPDC), as OMPDC-OPRT, are described in some organisms. Here, we produced gene fusions of *Plasmodium falciparum* OMPDC-OPRT, and expressed as the bifunctional enzyme in *Escherichia coli*. The enzyme was purified to near homogeneity using affinity and anion-exchange chromatography, exhibited enzymatic activities and functioned as a dimer. The enzymatic activities, although unstable, were stabilized by its substrate and product during purification and long-term storage. Furthermore, the enzyme expressed a perfect catalytic efficiency ( $k_{cat}/K_m$ ). The turnover number ( $k_{cat}$ ) was selectively enhanced up to three orders of magnitude, while the Michaelis constant ( $K_m$ ) was not much affected and remained at low  $\mu$ M levels, when compared to the enzymes in the monofunctional and in the complex forms, as published earlier. The fusion of the two enzymes, creating a “super-enzyme” with perfect catalytic power and more flexibility, reflects cryptic relationship of enzymatic reactivities and metabolic functions on molecular evolution.

Field of Study: Biomedical Sciences

Academic Year: 2016

Student's Signature .....

Advisor's Signature .....

Co-Advisor's Signature .....

## ACKNOWLEDGEMENTS

First, I would like to express my sincere thanks to my thesis advisor, Professor Dr. Jerapan Krungkrai for his invaluable help and constant encouragement throughout the course of this research. I am most grateful for his teaching and advice, not only the research methodologies but also many other methodologies in life. I would not have achieved this far and this thesis would not have been completed without all the support that I have always received from him.

Next, I am grateful to Dr. Sudaratana Krungkrai and Dr. Waranya Imprasittichai for kindly helps and precious comments and suggestions in laboratory techniques and all their helpfuls. I would like to thank Professor Dr. Toshihiro Horii and Associate Professor Dr. Nirianne Marie Q. Palacpac of Osaka University, Japan, for their kindness and suggestions in this study.

I would like to express the deepest appreciation to my committee chair Professor Dr. Apiwat Mutirangura. And I would like to thank my committee members, Professor Dr. Sittisak Honsawek, Assistant Professor Dr. Nuchanat Wutipraditkul, and Assistant Professor Dr. Sumet Wajanarogana for valuable suggestions and criticisms.

My acknowledgements are extended to all staffs in Department of Biochemistry, Faculty of Medicine, Chulalongkorn university for their helpfuls and supports during my study.

This work was supported by the 90th Anniversary of Chulalongkorn University, Rachadapisek Sompote Fund.

Finally, I most gratefully acknowledge my parents and my friends for all their supports throughout the period of this study.

## CONTENTS

	Page
THAI ABSTRACT .....	iv
ENGLISH ABSTRACT .....	v
ACKNOWLEDGEMENTS .....	vi
CONTENTS .....	vii
LIST OF TABLES .....	xi
LIST OF FIGURES .....	xii
LIST OF ABBREVIATIONS .....	xv
CHAPTER I INTRODUCTION .....	1
1.1. Background and Rationale .....	1
1.2. Research questions.....	5
1.3. Hypothesis.....	6
1.4. Objectives.....	6
1.5. Conceptual framework .....	7
1.6. Key words.....	8
1.7. Expected Benefits .....	8
CHAPTER II LITERATURE REVIEWS.....	9
2.1. Background of malaria infection .....	9
2.2. Life cycle of malaria.....	11
2.3. Genomic of malaria parasite.....	14
2.4. Pyrimidine biosynthesis .....	17
2.4.1. Synthesis of pyrimidine nucleotides by <i>de novo</i> pathway.....	17
2.4.2. Synthesis of pyrimidine nucleotide by salvage pathway.....	20

	Page
2.5. Pyrimidine biosynthesis in <i>Plasmodium</i> parasite .....	20
2.6. Orotidine 5'-monophosphate decarboxylase and orotate phosphoribosyltransferase .....	23
2.6.1. Orotidine 5'-monophosphate decarboxylase .....	23
2.6.2. Orotate phosphoribosyltransferase .....	26
2.7. Evolution of orotidine 5'-monophosphate decarboxylase and orotate phosphoribosyltransferase .....	31
2.8. Organization of aspartate transcarbamoylase (ATC) and dihydroorotase (DHO) in eubacterial <i>Aquifex aeolicus</i> .....	39
2.9. Other bifunctional enzymes in the malaria parasite .....	40
2.10. Evolutional origin of protein-protein co-localization .....	42
CHAPTER III MATERIALS AND METHODS .....	43
3.1. Materials .....	43
3.2. Equipments .....	44
3.3. Reagents .....	46
3.3.1. General reagents.....	46
3.3.2. Reagent kits.....	49
3.4. Methods.....	49
3.4.1. Cloning and construction of recombinant fused bifunctional <i>PfOMPDC-PfOPRT</i> gene .....	49
3.4.2. Preparation of competent <i>E. coli</i> .....	52
3.4.3. Expression and purification of recombinant fused bifunctional <i>PfOMPDC-OPRT</i> enzyme .....	52



	Page
3.4.4. Confirmation of recombinant fused <i>PfOMPDC</i> - <i>OPRT</i> enzyme by Western blotting .....	54
3.4.5. Determination of molecular mass of recombinant fused <i>PfOMPDC</i> - <i>OPRT</i> enzyme .....	55
3.4.6. Enzymatic assays and kinetic studies .....	55
3.4.7. Enzymatic stability test .....	58
3.4.8. Bioinformatics and proteomics .....	58
3.4.9. Agarose gel electrophoresis and density analysis of DNA bands .....	59
3.4.10. SDS-Polyacrylamide gel electrophoresis (SDS-PAGE) and density analysis of protein bands .....	59
3.4.11. Protein assay .....	60
3.4.12. Statistical analysis .....	60
CHAPTER IV RESULTS .....	61
4.1. Preparation of fused bifunctional <i>PfOMPDC-PfOPRT</i> gene and recombinant enzyme .....	61
4.1.1. Construction of recombinant plasmid containing fused bifunctional <i>PfOMPDC-PfOPRT</i> gene and confirmation of the fused gene by restriction map .....	61
4.1.2. Expression and purification of fused bifunctional <i>PfOMPDC-PfOPRT</i> enzyme .....	63
4.1.3. Confirmation of fused bifunctional <i>PfOMPDC-PfOPRT</i> enzyme by Western blot analysis .....	67
4.2. Physical property of fused bifunctional <i>PfOMPDC-PfOPRT</i> enzyme .....	69
4.2.1. Determination of molecular mass of native bifunctional enzyme .....	69
4.2.2. Stabilization of recombinant bifunctional enzyme .....	71

	Page
4.3. Kinetic property of fused bifunctional <i>Pf</i> OMPDC- <i>Pf</i> OPRT enzyme .....	79
4.3.1. Kinetic constants of fused bifunctional <i>Pf</i> OMPDC- <i>Pf</i> OPRT enzyme ....	79
4.4. Bioinformatics and proteomics of fused bifunctional <i>Pf</i> OMPDC- <i>Pf</i> OPRT enzyme .....	84
4.4.1. Multiple sequence alignments of all bifunctional OMPDC-OPRT enzymes .....	84
4.4.2. Proteomic analysis of bifunctional <i>Pf</i> OMPDC- <i>Pf</i> OPRT enzyme .....	87
4.4.3. Homology models of the bifunctional <i>Pf</i> OMPDC- <i>Pf</i> OPRT enzyme .....	89
CHAPTER V DISCUSSION AND CONCLUSION.....	95
REFERENCES .....	121
APPENDIX .....	131
Nucleotide sequence <i>P. falciparum</i> OMPDC-OPRT gene .....	132
Map of pTrcHis A vector .....	134
The Best Presentations .....	135
VITA.....	136

## LIST OF TABLES

	Page
Table 1 Purification of bifunctional <i>Pf</i> OMPDC- <i>Pf</i> OPRT enzyme. ....	66
Table 2 Purification of bifunctional <i>Pf</i> OMPDC- <i>Pf</i> OPRT enzyme in the presence of stabilizers. ....	75
Table 3 Kinetic constants of <i>Pf</i> OPRT and <i>Pf</i> OMPDC components in the bifunctional enzyme. ....	83
Table 4 LC-MS/MS data analysis of the bifunctional <i>Pf</i> OMPDC- <i>Pf</i> OPRT enzyme. ....	88
Table 5 Comparison of kinetic constants of <i>P. falciparum</i> OPRT and OMPDC domains in bifunctional, enzyme complex and monofunctional enzymes. ....	102
Table 6 Comparison of kinetic constants of OPRT and OMPDC domains in bifunctional <i>P. falciparum</i> ( <i>Pf</i> ) OMPDC-OPRT and <i>L. donovani</i> ( <i>Ld</i> ) UMPS enzyme. ....	104
Table 7 Comparison of kinetic constants of OPRT and OMPDC domains in bifunctional <i>P. falciparum</i> OMPDC-OPRT and human UMPS enzyme. ....	106
Table 8 Comparison of kinetic constants of OPRT and OMPDC in <i>P. falciparum</i> and human monofunctional enzymes. ....	107

## LIST OF FIGURES

	Page
Figure 1 Proposed model for multienzyme (OPRT) <sub>2</sub> (OMPDC) <sub>2</sub> complex formation of <i>P. falciparum</i> OPRT and OMPDC.....	4
Figure 2 The world map showing the area of malaria infection. ....	10
Figure 3 Life cycle of human malaria. ....	12
Figure 4 Pyrimidine <i>de novo</i> pathway in human. ....	19
Figure 5 <i>De novo</i> pyrimidine biosynthesis of malaria parasites. ....	22
Figure 6 Multiple sequence alignment of OMPDCs. ....	25
Figure 7 3D structure of dimeric <i>P. falciparum</i> OMPDC.....	26
Figure 8 Multiple sequence alignment of OPRTs. ....	29
Figure 9 3D structure of dimeric <i>P. falciparum</i> OPRT. ....	30
Figure 10 Evolution of <i>OPRT</i> and <i>OMPDC</i> genes. ....	33
Figure 11 Evolution of <i>OMPDC-OPRT</i> gene and its organization. ....	35
Figure 12 Cloning of recombinant plasmid containing designed <i>PfOMPDC-PfOPRT</i> fused gene.....	51
Figure 13 Agarose gel electrophoresis analysis of <i>PfOMPDC-PfOPRT</i> -pTrcHisA plasmid. ....	62
Figure 14 Ni-NTA affinity and HiTrapQ anion-exchange chromatographic profiles of the fused bifunctional <i>PfOMPDC-PfOPRT</i> enzyme. ....	64
Figure 15 SDS-PAGE analysis on a 10% polyacrylamide gel of the bifunctional <i>PfOMPDC-PfOPRT</i> enzyme.....	67
Figure 16 SDS-PAGE and Western blot analysis of the purified bifunctional <i>PfOMPDC-PfOPRT</i> enzyme.....	68

Figure 17	Superose 12 gel-filtration FPLC of the purified bifunctional <i>PfOMPDC-PfOPRT</i> enzyme.....	70
Figure 18	SDS-PAGE analysis on a 10% polyacrylamide gel of the purified bifunctional enzyme after subjecting onto a Superose 12 gel-filtration FPLC column. ....	71
Figure 19	Ni-NTA affinity and HiTrapQ anion-exchange chromatographic profiles of the bifunctional <i>PfOMPDC-PfOPRT</i> enzyme with stabilizers.....	73
Figure 20	Stabilization of the bifunctional enzyme by stabilizers, PRPP and UMP. ....	77
Figure 21	SDS-PAGE analysis of the purified bifunctional enzyme <i>PfOMPDC-PfOPRT</i> during storage in the absence of stabilizers.....	78
Figure 22	Michaelis-Menten and Lineweaver-Burk plots of the forward reaction of <i>PfOPRT</i> component in the bifunctional <i>PfOMPDC-PfOPRT</i> enzyme.	80
Figure 23	Michaelis-Menten and Lineweaver-Burk plots of the forward reaction of <i>PfOPRT</i> component in the bifunctional <i>PfOMPDC-PfOPRT</i> enzyme.	81
Figure 24	Michaelis-Menten and Lineweaver-Burk plots of the reaction of <i>PfOMPDC</i> component in <i>PfOMPDC-PfOPRT</i> bifunctional enzyme. ....	82
Figure 25	Multiple sequence alignments of all known bifunctional OMPDC-OPRT enzymes. ....	87
Figure 26	Proposed homology model of the bifunctional <i>PfOMPDC-PfOPRT</i> enzyme in monomeric form. ....	90
Figure 27	Crystal structure of the <i>L. donovani</i> UMPS ( <i>LdUMPS</i> ) enzyme in monomeric form.....	91
Figure 28	Proposed homology model of the bifunctional <i>PfOMPDC-PfOPRT</i> enzyme in dimeric form.....	93
Figure 29	Homology model of the <i>LdUMPS</i> enzyme in dimeric form.....	94

Figure 30	The sequential steps for monomer and dimer formation of the bifunctional <i>Pf</i> OPRT- <i>Pf</i> OMPDC enzyme.....	111
Figure 31	Rosetta Stone hypothesis of evolution for protein-protein interactions in colocalization and allostery by mutations.....	113
Figure 32	Evolution of protein-protein interactions of the fused bifunctional <i>Pf</i> OMPDC- <i>Pf</i> OPRT enzyme.....	114
Figure 33	Comparative structural models of <i>P. falciparum</i> OMPDC-OPRT, <i>L. donovani</i> and human UMPS.....	116



## LIST OF ABBREVIATIONS

3D	=	three dimensional structures
μg	=	microgram
μl	=	microliter
μM	=	micromolar
μmol	=	micromole
A	=	absorbance
aa	=	amino acids residue
Arg	=	arginine
APS	=	ammonium persulfate
ATC	=	aspartate transcarbamoylase
ATP	=	adenosine triphosphate
Asp	=	aspartate
Bis	=	N,N-Methylene-bis-acrylamide
BSA	=	bovine serum albumin
bp	=	base pair
°C	=	degree Celsius
CAD	=	carbamoylphosphate synthetase- aspartate transcarbamoylase-dihydroorotase trifunctional enzyme

CaCl <sub>2</sub>	=	calcium chloride
CO <sub>2</sub>	=	carbon dioxide
COOH-terminal	=	carboxyl-terminal
CPS II	=	carbamoylphosphate synthetase II
CDP	=	cytidine diphosphate
CTP	=	cytidine triphosphate
CTPS	=	cytidine triphosphate synthase
Da	=	Dalton
DHFR-TS	=	dihydrofolate reductase-thymidylate synthase
DHO	=	dihydroorotase
DHOD	=	dihydroorotate dehydrogenase
DNA	=	deoxyribonucleic acid
dCDP	=	deoxycytidine diphosphate
dCTP	=	deoxycytidine triphosphate
dTDP	=	deoxythymidine diphosphate
dTMP	=	deoxythymidine monophosphate
dTTP	=	deoxythymidine triphosphate
dUDP	=	deoxyuridine diphosphate
dUMP	=	deoxyuridine monophosphate
DTT	=	dithiothreitol
EC	=	enzyme commission



<i>E. coli</i>	=	<i>Escherichia coli</i>
EDTA	=	ethylene diamine tetraacetic acid
e.g.	=	for example
<i>et.al.</i>	=	et alia (and other)
etc.	=	et cetera
EtBr	=	ethidium bromide
FPLC	=	fast protein liquid chromatography
Gln	=	glutamine
G6PD-6PGL	=	glucose 6-phosphate dehydrogenase-6-phosphogluconolactonase
h	=	hour
HCl	=	hydrochloric acid
$\text{HCO}_3^-$	=	bicarbonate ion
<i>Hs</i>	=	Human, <i>Homo sapiens</i>
i.e.	=	id est (that is)
IPTG	=	isopropyl $\beta$ -D-1-thiogalactopyranoside
$k_{\text{cat}}$	=	turnover number
$k_{\text{cat}}/K_m$	=	catalytic efficiency
$K_m$	=	Michaelis constant
kb	=	kilo base pair
kDa	=	kilodalton

LB media	=	Luria-Bertani media
LC-MS/MS	=	liquid chromatography-mass spectrometry/ mass spectrometry
LCR	=	low complexity region
<i>Ld</i>	=	<i>Leishmania donovani</i>
LGT	=	lateral gene transfer
Lys	=	lysine
M	=	molar
mA	=	milliamps
mg	=	milligram
Mg <sup>2+</sup>	=	magnesium ion
MgCl <sub>2</sub>	=	magnesium chloride
min	=	minute
ml	=	millilitre
mM	=	millimolar
mm	=	millimeter
NaCl	=	sodium chloride
ng	=	nanogram
NH <sub>2</sub> -terminal	=	amino-terminal
nM	=	nanomolar
nm	=	nanometer

Ni-NTA	=	nickel-nitrilotriacetate
nmol	=	nanomole
OA	=	orotic acid
OD	=	optical density
OMP	=	orotidine 5'-monophosphate
OMPDC	=	orotidine 5'-monophosphate decarboxylase
OPRT	=	orotate phosphoribosyltransferase
ORF	=	open reading frame
PBS	=	phosphate-buffered saline
PCR	=	polymerase chain reaction
PDB ID	=	protein data bank identification
<i>Pf</i>	=	<i>Plasmodium falciparum</i>
<i>Pfu</i> DNA polymerase	=	<i>Pyrococcus furiosus</i> deoxyribonucleic acid polymerase
pH	=	potential of hydrogen ion
Phe	=	phenylalanine
PP <sub>i</sub>	=	pyrophosphate
PRPP	=	5'-phosphoribosyl-1-pyrophosphate
RNA	=	ribonucleic acid
rpm	=	round per minute
R <sup>2</sup>	=	regression coefficient

[S]	=	concentration of substrate
SDS-PAGE	=	sodium dodecyl sulfate polyacrylamide gel electrophoresis
<i>Sc</i>	=	<i>Saccharomyces cerevisiae</i>
sec	=	second
<i>sp./ spp.</i>	=	species
TAE	=	tris-acetate- ethylene diamine tetraacetic acid
TEMED	=	N,N,N',N'-tetramethylethane-1,2-diamine
TLCK	=	N-[(3S)-7-Amino-1-chloro-2-oxoheptan-3-yl]-4-methylbenzenesulfonamide hydrochloride
Thr	=	threonine
UMP	=	uridine 5'-monophosphate
UMPS	=	uridine monophosphate synthase
UDP	=	uridine diphosphate
UTP	=	uridine 5'-triphosphate
UV	=	ultraviolet
v	=	volt
$V_0$	=	void volume
$V$	=	initial velocity
$V_{\max}$	=	maximum velocity
$V_t$	=	total eluting volume

v/v = volume per volume

w/v = weight per volume



## CHAPTER I

### INTRODUCTION

#### 1.1. Background and Rationale

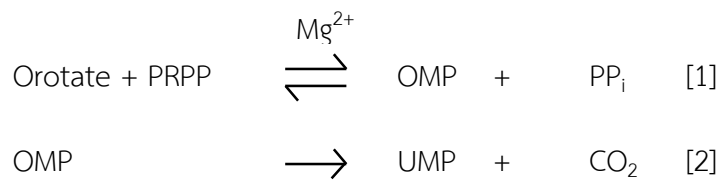
Malaria is a mosquito-borne infectious disease of humans in tropical and subtropical zones. Four kinds of malaria parasites infect humans: *Plasmodium falciparum*, *P. vivax*, *P. ovale*, and *P. malariae*. In addition, *P. knowlesi*, a type of malaria that naturally infects macaques in southeast asia, also infects humans, causing malaria that is transmitted from animal to human (1, 2). Of these, *P. falciparum* is the most dangerous, with the highest rate of complications and mortality. The disease control efforts are threatened by resistance of the parasite to current therapies (3) and lack of a highly effective vaccine (4). Malaria remains a major and growing threat to the public health of population living in the endemic areas (5). In humans, infections are approximately 515 million cases a year and 1.5-2.7 million deaths each year (6), *P. falciparum* is responsible for over hundreds of million clinical cases. It is the greatest toll on human health, primarily in children of age less the five years old. People who got malaria is very sick with high fevers, shaking chills, and flu-like illness (7, 8).

Malaria is caused by *Plasmodium spp.* that commonly transmitted a certain type of female *Anopheles* mosquito which feeds on human. Most infections can be

effectively treat with existing drugs, although resistance is a serious problem. Nevertheless, their continued use poses considerable risk to widespread of drug-resistant parasites. Therefore, antimalarial agent will be developed for new drug target (2).

The malaria parasite depends on *de novo* synthesis (from small metabolites) of pyrimidine nucleotides, the important target for new antimalarial drug development (9), whereas the mammalian host cells obtain the pyrimidine nucleotides from both *de novo* and salvage pathways (from preformed pyrimidine bases and nucleosides) (10, 11). This has spawned a great deal of interest. For instance, inhibition of the *de novo* pyrimidine synthesis by specific enzyme inhibitors, thus lead to identify new potential antimalarials and to develop thereafter a novel chemotherapy for malaria (12, 13).

Six enzymatic reactions are involved in the *de novo* pathway. The enzymes catalyze the sequential conversions of the following precursors ( $\text{HCO}_3^-$ , ATP, glutamine (Gln), aspartate (Asp), and 5-phosphoribosyl-1-pyrophosphate (PRPP)), to form uridine 5'-monophosphate (UMP). In the final two reactions: [1] orotidine 5'-monophosphate (OMP) synthesis requires the addition of ribose 5-phosphate moiety from PRPP to orotate by orotate phosphoribosyltransferase (EC 2.4.2.10, OPRT), requiring  $\text{Mg}^{2+}$  as cofactor, and [2] OMP is subsequently decarboxylated to yield UMP by orotidine 5'-monophosphate decarboxylase (EC 4.1.1.23, OMPDC) respectively:



For most prokaryotes and yeast (14, 15), the OPRT and OMPDC enzymes are encoded by two separate genes, while in majority of multicellular eukaryotes including human, the genes for both enzymes are fused into a single gene and expressed as a bifunctional form, generating bifunctional UMP synthase (UMPS) which bears an NH<sub>2</sub>-terminal OPRT covalently linked to a COOH-terminal OMPDC or OPRT-OMPDC fused enzyme (10, 11, 16, 17).

Until recently, fusions of OPRT and OMPDC in the inversed order, where the OMPDC is at the N-terminus and OPRT is at the C-terminus (OMPDC-OPRT), have been described in some single-cell eukaryotic organisms, i. e. , kinetoplastids (*Leishmania donovani*, *Trypanosoma cruzi*), diatoms (*Thalassiosira pseudonana*), and in subset of cyanobacteria (e.g., *Noctoc punctiforme*, *Oscillatoria sp.*) (18-20). These gene fusion events appear to have occurred independently, nevertheless, near the base of kinetoplastid and apicomplexan protozoan lineages (18, 19, 21, 22).

In *P. falciparum*, the *OPRT* and *OMPDC* genes are located on two separate chromosomes (23), at chromosome 5, *OPRT* gene encoding a protein with 281 amino acids (32 ± 3 kDa) and at chromosome 10, *OMPDC* gene encoding a protein with 323 amino acids (38 ± 3 kDa) (24-26). The native and recombinant forms of the monofunctional *PfOPRT* and *PfOMPDC* have been carried out in our laboratory during



the past 10 years. In *in vivo* and *in vitro* studies, both enzymes form a heterotetrameric multienzyme complex ( $140 \pm 8$  kDa) bearing two molecules of each *Pf*OPRT (~67 kDa) and *Pf*OMPDC (~76 kDa) with the efficient functional kinetic advantages (26) (Figure 1).

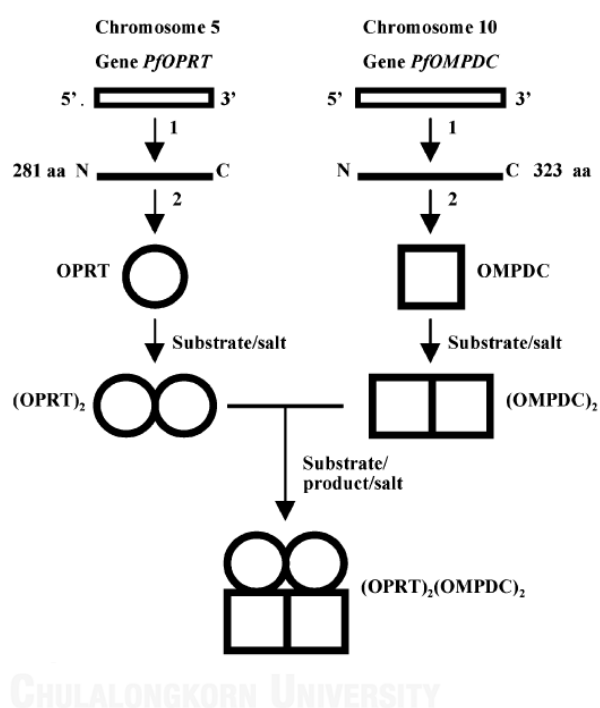


Figure 1 Proposed model for multienzyme (OPRT)<sub>2</sub>(OMPDC)<sub>2</sub> complex formation of *P. falciparum* OPRT and OMPDC.

The genes encoding OPRT and OMPDC are distinctive. When the recombinant proteins are produced separately, the individual monofunctional enzymes form homodimers. Both enzymes are functioned with optimal kinetic constants (e.g.,  $K_m$ ,  $k_{cat}$  and  $K_m/k_{cat}$  values) in a tightly associated heterotetrameric form (26).

Using molecular biological and biochemical approaches, it is therefore plausible to construct a plasmid containing fused genes of *PfOPRT* and *PfOMPDC* in the inversed order (e.g., *PfOMPDC-PfOPRT*, or *PfUMPS*), as found in many bacteria and eukaryotes, and then express and purify the bifunctional *PfUMPS* in the heterologous system of *Escherichia coli* (*E. coli*). The kinetic parameters (e.g.,  $V_{max}$ ,  $K_m$ ) and catalytic efficiency (e.g.,  $k_{cat}/K_m$ ) of the recombinant *PfUMPS* will be then determined, comparing to those of the monofunctional and multienzyme complex forms which had been previously reported (26-28). This study will elucidate evolution of the last two enzymes (monofunctional → multienzyme complex → fused bifunctional protein) in the *de novo* pyrimidine pathway of the malaria parasite.

## 1.2. Research questions

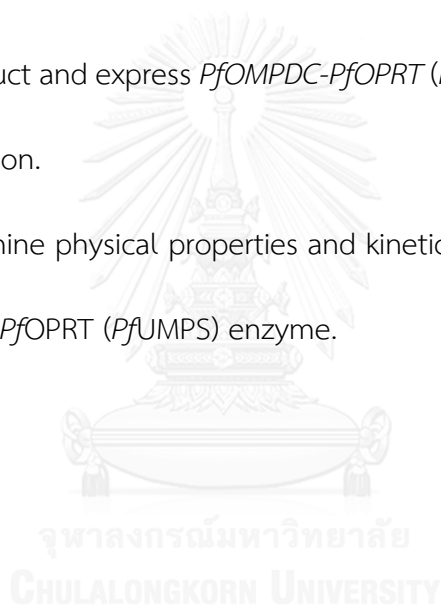
- 1) Does the fused *PfOMPDC-PfOPRT* (*PfUMPS*) gene functionally express in *E. coli*?
- 2) Does the fused bifunctional *PfOMPDC-PfOPRT* (*PfUMPS*) enzyme exhibit the highest catalytic efficiency ( $k_{cat}/K_m$ )?

### 1.3. Hypothesis

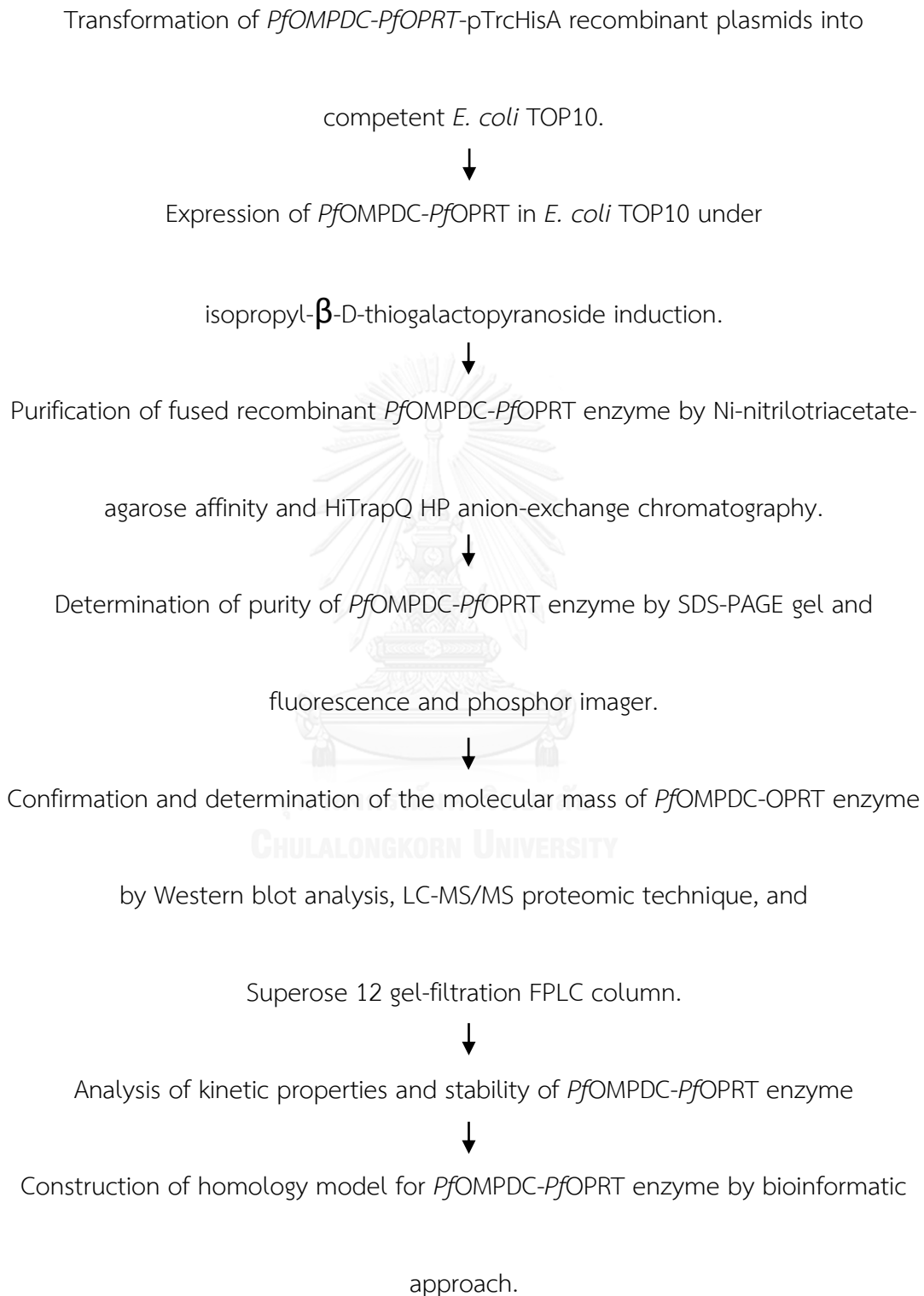
The fused bifunctional *PfOMPDC-PfOPRT* (*PfUMPS*) enzyme might have greater catalytic efficiency than the multienzyme complex and the monofunctional enzymes.

### 1.4. Objectives

- 1) To construct and express *PfOMPDC-PfOPRT* (*PfUMPS*) gene in an inversed linked fusion.
- 2) To determine physical properties and kinetic parameters of bifunctional *PfOMPDC-PfOPRT* (*PfUMPS*) enzyme.



## 1.5. Conceptual framework



**1.6. Key words:** Malaria; *Plasmodium falciparum*; Pyrimidine *de novo* biosynthesis; Orotate phosphoribosyltransferase; Orotidine 5'- monophosphate decarboxylase; Fused bifunctional enzyme; Catalytic efficiency

### 1.7. Expected Benefits

- 1) Understanding the basic knowledge of the physical and kinetic properties of fused bifunctional *PfOMPDC-PfOPRT* synthetic enzyme, especially its high catalytic efficiency to a perfect enzyme (29, 30).
- 2) Elucidating the enzyme evolution, especially *PfOPRT* and *PfOMPDC* of the *de novo* pyrimidine pathway in *P. falciparum*, this will accelerate the development of more potential antimalarial drugs (29, 30).

## CHAPTER II

### LITERATURE REVIEWS

#### 2.1. Background of malaria infection

Malaria is one of the world's major public health problems. The majority of malarial related mortality occurs in children below the age of five years, mostly in sub-Saharan region of Africa, due to their lack of naturally acquired malarial immunity (31, 32). The human malaria is caused by five species of *Plasmodium* such as *P. falciparum* (60-75%), *P. vivax* (25-40%), *P. ovale*, *P. malariae* and *P. knowlesi*, and mainly caused by either *P. falciparum* or *P. vivax*, and most malaria-associated deaths are due to *P. falciparum*. Of the two most common species of human malaria, *P. falciparum* is the most pathogenic, with approximately 1% of human infections giving rise to severe disease. The severe disease encompasses a range of presentation including severe anemia, cerebral malaria, hypoglycemia and a systemic syndrome analogous to toxic shock (33, 34). The transmission area of malaria infection are tropical and sub-tropical zones in the world (e.g., Africa, South America and Asia) (Figure 2) (35).

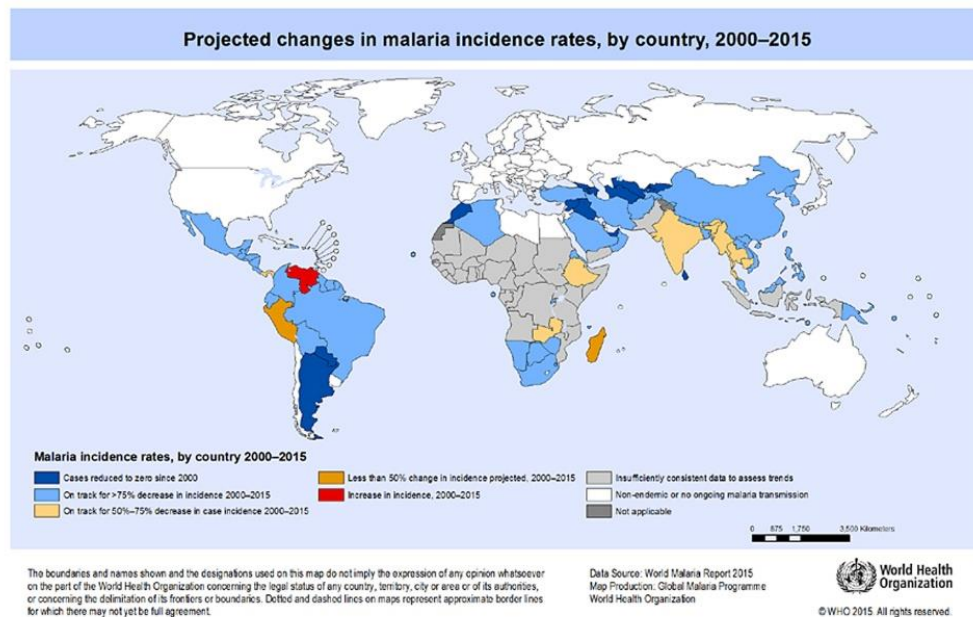
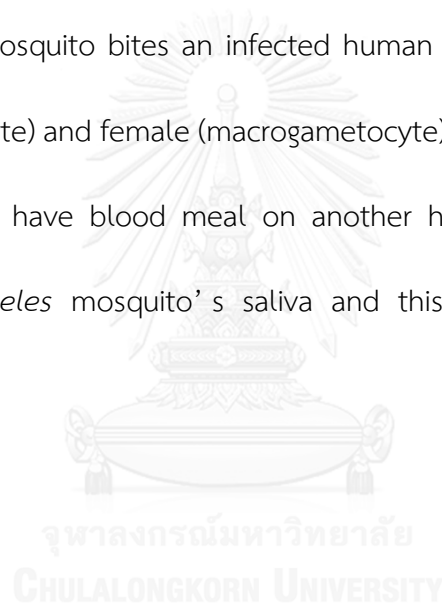


**Figure 2** The world map showing the area of malaria infection.

The transmission of malaria exists in five WHO regions. There were around 3.2 billion people in 95 countries at risk of malaria infection and developing disease (see details in map), and on high risk around 1.2 billion (more than 1 in 1,000 for feasibility of getting malaria per year). Regarding to the report of world malaria in 2015, 214 million cases of malaria were reported (range 149-303 millions) and deaths of malaria were 438,000 (range 236,000-635,000), indicating a decline of malaria cases and deaths of 37% and 60% since 2000, respectively. In African region, there were 90% of all malaria deaths existed which in children whose age under 5 years, who accounted for more than two thirds of all deaths (35).

## 2.2. Life cycle of malaria

The life cycle of *Plasmodium* has sexual and asexual phases in two hosts (Figure 3). The first asexual phase, termed schizogony, occurs in human where the parasites grown and multiplied in liver cell and then in the red blood cells. The sexual phase or gamegony occurs in female *Anopheles* mosquito, as does the second asexual phase, termed sporogony. The sexual stage develops when the female *Anopheles* mosquito bites an infected human and takes blood contained male (microgametocyte) and female (macrogametocyte) gametocyte. Of course, the *Anopheles* mosquito have blood meal on another human, the sporozoites are injected with *Anopheles* mosquito's saliva and this to begin another human infection.







In the mosquito's saliva gland, if it has sporozoites during feeding, it secretes sporozoites into blood circulation of human, around 24 to 48 h later in the liver, sporozoites infect liver cells and mature into schizonts, where the exo-erythrocytic schizogonic phase starts. The schizonts rupture and release merozoites out of liver cells. After the initial replication in the liver, the parasites undergo asexual multiplication in the erythrocytes. Then the merozoites enter to blood circulation and infect red blood cell, the merozoites grown to the trophozoites, the trophozoites mature into schizonts, beginning the erythrocytic schizogonic phase, which rupture releasing merozoites. In case, immature trophozoites differentiate into sexual erythrocytic phase (gametocyte), male (microgametocyte) and female (macrogametocyte).

The sexual phase gametocytes are ingested by the female *Anopheles* mosquito during a blood meal containing microgametocyte and macrogametocyte. The parasite multiplication in the mosquito is known as the sporogonic cycle. In the mosquito's stomach, lysis of the infected red blood cell releases the microgametes penetrate the macrogametes generating zygotes. The zygotes in turn become motile and elongated (ookinetes), invade the midgut wall of the mosquito where develop into new stage, oocysts. The oocysts grow, rupture, and release sporozoites, make their way to the mosquito's salivary glands. Inoculation of the sporozoites into a next human host perpetuates the malaria life cycle (32, 36).

### 2.3. Genomic of malaria parasite

In 1996, the malaria genome project was initiated to determine the nucleotide sequence of *P. falciparum* genome by the Institute for Genomic Research, the Wellcome Trust Sanger Institute and Stanford Genome Technology Center. The complete genome sequence of *P. falciparum* was established in 2002 (37). In 2005, the genome sequence of other rodent malaria parasite (*P. yoelii*) was published (38), and the genome sequence of *P. vivax* and *P. knowlesi* were completed in 2008 (39, 40).

The *Plasmodium* genomes were estimated to include 23-27 million bases, they are rich in low complexity region (LCR) since nucleic acid level correlates with LCR at protein level for function (41). The characterized LCR was either single amino acid or group of amino acids repeat, and nearly 50% of *Plasmodium* protein were longer than their yeast homologues, contain the insert segments, these inserts correspond to LCR (42). The genome of *P. falciparum* has 14 chromosomes and the genes encoding proteins are approximately 5,500 genes, in which 51% of these have only one intron (3). The nuclear genome of *P. falciparum* 3D7 strain was composed of 22.8 million bases, distributed among 14 chromosomes ranging in size from approximately 0.6 to 3.3 million bases (37). Of course, about 5,268 protein-encoding genes were predicted. The *P. falciparum* genomes have high AT content (AT-rich) with approximately 82% (43, 44). However, the *P. vivax* genome showed lower level

of AT-rich with approximately 67.7%. The previous understanding indicated that the extreme AT content in itself have probably not too much to do with disease severity (45). The 54% of *P. falciparum* genes had introns, similar to that found in *Schizosaccharomyces pombe* and *Dictyostelium discoideum*, however, much higher than *Saccharomyces cerevisiae* where only 5% of genes had introns. Abstracting introns, the *P. falciparum* genes was about 2.3 kb in length, substantially larger than in other organisms which had the genes length, ranging 1.3-1.6 kb. A greater proportion of genes (15.5%) which longer than 4 kb was shown in the *P. falciparum* genes, when compared to *S. pombe* and *S. cerevisiae* containing 3.0% and 3.6%, respectively. A lot of the large genes encode many unknown proteins, which may be localized in cytosol by having no signal peptides. In addition, there were no transposable elements and retrotransposons. As detected by high-resolution liquid chromatography and tandem mass spectrometry (LC-MS/MS), 52% of the predicted gene products (2,731 proteins) were associated in cell lysates taken from many development stages of the parasite, which many identified proteins had no similarity to proteins in other organisms (37).

In addition, 5,268 predicted proteins, about 60% were not sufficiently similar to proteins detected in other organisms to provide reasons for determining the function. Nearly two-thirds of the proteins seem to be unique to *P. falciparum*, a proportion higher than identified in other eukaryotic organisms, reflecting an

increased evolutionary distance between *Plasmodium* and other eukaryotes by notably reducing similarity of the sequence due to the AT-richness of the parasite genome. The other 257 proteins (5% of total protein) had significant similarity to the functional proteins in other organisms, so far examined. There were 31% proteins showing one or more transmembrane domains. The putative signal peptide containing proteins were 17.3% (37).

The evolution of malaria genome are compared to the genome analysis of other eukaryotes for which the complete genomes are available. It is demonstrated that *P. falciparum* is similar to plant *Arabidopsis thaliana* than to other taxa, in terms of genomic content. Nevertheless, this is consistent with phylogenetic analysis. *P. falciparum* nuclear genome has genes derived from plastids or from the nuclear genome of the secondary endosymbiont. Therefore, the closed relations of *Plasmodium* and *Arabidopsis* do not reflect the true phylogenetic history of the *P. falciparum* evolutionary lineage. As comparative genomic analysis in gene duplication, there were 237 proteins in *P. falciparum* expressing strong matches to proteins in all completed eukaryotic genomes, but having no matches to proteins at low stringency, in all complete prokaryotic proteome. These proteins are used to determine the definitively differences between eukaryotes and prokaryotes. The proteins include those play functional roles in cytoskeleton formation and

maintenance, packaging of chromosome and modification, cell cycle regulation, intracellular signalling, transcription, translation, replication (37).

## 2.4. Pyrimidine biosynthesis

Human and malaria parasites have a different mode of pyrimidine synthesis, the human obtains pyrimidines from 2 routes: salvage of the preexisting compounds and *de novo* synthesis, but the parasites have only *de novo* synthetic pathway.

### 2.4.1. Synthesis of pyrimidine nucleotides by *de novo* pathway

The *de novo* pyrimidine synthesis requires Asp, Gln and  $\text{HCO}_3^-$  as precursors. Pyrimidines are assembling the single pyrimidine ring before starting attached to PRPP. First step in *de novo* pyrimidine biosynthesis is the formation of carbamoyl phosphate by carbamoylphosphate synthetase II (CPS II). Carbamoylphosphate is condensed with Asp in a reaction catalyzed by the aspartate carbamoyl transferase (ATC), then cyclized to dihydroorotate by dihydroorotase (DHO). The activities of CPS II, ATC and DHO found on a trifunctional protein in one gene (CAD). Dihydroorotate diffuses into the mitochondria, and then converts into orotate by dihydroorotate dehydrogenase (DHOD). The DHOD is located on outer surface of inner mitochondrial membrane. This is the only mitochondrial step in the nucleotide

ring biosynthesis. Orotate is converted to OMP by OPRT. And then OMP is decarboxylated to UMP by OMPDC. In the pathway of final two steps, OPRT and OMPDC found on a bifunctional protein in one gene is called UMPS. Five of six reactions appear in the cytosol of the cell, whereas the DHOD reaction operates in mitochondria.

The UMP conversion to uridine diphosphate (UDP) and uridine triphosphate (UTP) were catalyzed by nucleotide kinases (46, 47). The ribonucleotide reductase converts CDP to deoxyribonucleotide derivative. The precursor for synthesis of thymidine nucleotide is UDP. UDP is also converted to dUDP by ribonucleotide reductase. Dephosphorylation of dUDP to dUMP was then achieved. The thymidylate synthase converts dUMP to deoxythymidine monophosphate (dTMP), requiring transfer of a single carbon from 5, 10-methylenetetrahydrofolate (48) (Figure 4).

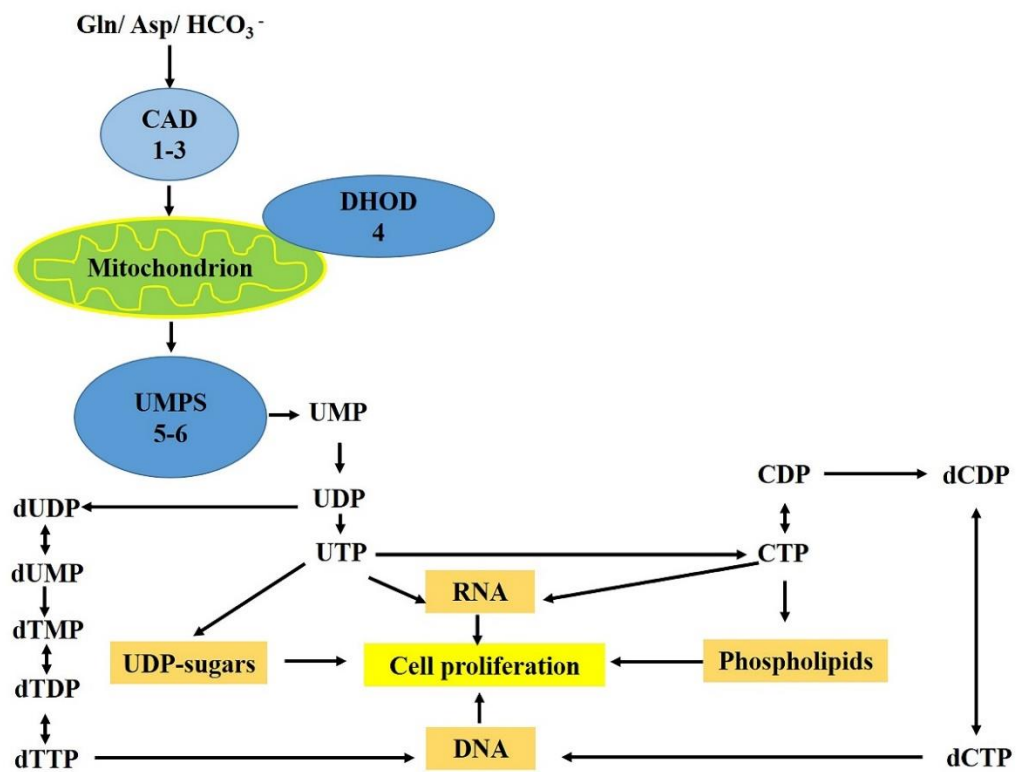


Figure 4 Pyrimidine *de novo* pathway in human.

The *de novo* pyrimidine biosynthetic pathway requires six enzymes. The first three enzymes are catalyzed on trifunctional protein, a cytosolic enzyme known as CAD. The fourth enzyme is DHOD, a mitochondrial enzyme. The fifth and sixth enzymes are catalyzed on a bifunctional protein UMPS, a cytosolic enzyme (48).



#### 2.4.2. Synthesis of pyrimidine nucleotide by salvage pathway

The salvage pathway is a process in which pyrimidine nucleotides, synthesized from intermediates in the degradative pathway for nucleotides. Salvage pathways are used to recover bases and nucleosides that are formed during degradation of RNA and DNA. This is important in some organs because some tissues cannot undergo *de novo* synthesis. The salvaged bases and nucleosides can then be converted back into nucleotides. The pathway beginning with deoxycytidine, deoxyuridine, or deoxythymidine nucleosides, in the first step, appropriate kinases converted to nucleoside monophosphates. Uridine phosphorylase has an activity to inter convert uracil, uridine and deoxyuridine. In contrast uridine kinase phosphorylates the nucleoside into UMP. Then, dTMP generate from deoxythymidine phosphorylase adds to deoxyribose-1-phosphate, and thymidine kinase phosphorylates this nucleoside into dTDP and dTTP.

#### 2.5. Pyrimidine biosynthesis in *Plasmodium* parasite

The *de novo* pathway has the six sequential enzymes, CPS II, ATC, DHO, DHOD, OPRT and OMPDC, using  $\text{HCO}_3^-$ , ATP, Gln, Asp and PRPP as precursors. The *P. falciparum* enzymes in the *de novo* pathway were encoded from their separated genes.

Figure 5 shows that the final two steps of UMP synthesis in *de novo* pathway require the addition of ribose 5-phosphate from PRPP to orotate by OPRT to form OMP and the subsequent decarboxylation of OMP to produce UMP by OMPDC. These enzymes are encoded by two separate genes in most prokaryotes, whereas their genes in most multicellular organisms are joined into a single gene, resulting in the bifunctional UMPS (18, 22, 49).





## 2.6. Orotidine 5'- monophosphate decarboxylase and orotate phosphoribosyltransferase

### 2.6.1. Orotidine 5'-monophosphate decarboxylase

The sixth enzyme in the *de novo* pyrimidine biosynthetic pathway is OMPDC, decarboxylation of OMP to form UMP, where the reaction is  $\text{OMP} \rightarrow \text{UMP} + \text{CO}_2$ . The monofunctional protein of *P. falciparum* OMPDC is a novel form. The single open reading frame of *PfOMPDC* genes contains 969 bp, one exon and encode a protein with 323 amino acid residues having a molecular mass of about 38 kDa, located on chromosome 10 locus PF10\_0225. Dimeric enzyme is an active form and with molecular mass about 76 kDa (26). Furthermore, it demonstrates that malaria parasite enzyme has also an extension of 32 amino acids at the N-terminus (Figure 6).

The alignment of *PfOMPDC* with those of the seven amino acid sequences known (Figure 6) indicate a large insertion at the N-terminal region in all *Plasmodium*. It has been proposed that these domains used to bind between *PfOPRT* and *PfOMPDC* for tetrameric formation (24-26, 50). The 3D structure of *PfOMPDC* has eight  $\beta$ -strands and 13  $\alpha$ -helices (Figure 7). The dimeric interface consists a network of 10 hydrogen bonds. The active site is located at the open end of the  $(\alpha/\beta)_8$  barrel (50).

```

E.coli -----MTLTASSSSRAVTVVPPVWLDYHNR-----D----- 28
B.subtilis -----MKNMLPIIPLDFASA-----E----- 17
H.sapiens KEAPKELSGARAELPRIHPVASKLLRLMQKKEINLCLADVSLA-----R----- 47
S.cerevisiae ---MSKATYKERAAT-HPSPVAAKLFNIMHEKQINLCAALDVRTT-----K----- 43
L.donovani -----MSFFDLLNER--AKRLLLCVLDLPRAKTAAAAVE----- 33
T.cruzi -----MPMAFFDMLNER--AKSLLLCIQLDPRAKTAAEAAB----- 35
P.falciparum -----MGFKVKLEKRRNAINLCLCIQLDPEKDIENFMKLEKENNYN 42

E.coli -----ALAVVDKIDPRDCRLK----- 44
B.subtilis -----TLAQLLAPFQQEPLFVK----- 33
H.sapiens -----LLQADALGPSICMLK----- 63
S.cerevisiae -----LLELVEALGPKICLLK----- 59
L.donovani -----CKRLIEQTHEYAAAYK----- 49
T.cruzi -----CMRLIDATAEYAAAYK----- 51
P.falciparum NIKKNLKEKYINNVS IKKDILKAPDNI IREKSEEFFYFFNHFCFYINETNKYALTFK 102

E.coli VGKEFTLFGPQ-----VRELQQRGFDIQLDLKFHDIPNTLAHAVAA---AADLGVW 94
B.subtilis VGMEFYQEGPS-----TVKQLKERNCELQLDLKLDHDIPTTANKAMKR---LASLQVD 83
H.sapiens THVDLNDFTLD---VMKEIITLAKCHEFLIQLEDRKFADIGNTYKQYEGGIFKIASWAD 120
S.cerevisiae THVDLTDFSMEG---TVKPLKALS AKYNFLLEDRKFADIGNTYKQYSAGVYRIAEWAD 117
L.donovani PNAAFBFFFGAEGWAALSEVIRAVPAG-IPVQLDAKRGDIADTADAYATS--AFKHLNAH 106
T.cruzi PNAAFBFFFGAEGWKALQQVI AHVPAN-IPVQLDAKRGDIADTAEAYAKS--AFEHLKAH 108
P.falciparum MNFAFYIPYGSVGDVVLKNVFDYLYELNIPTQLDMKINDIGNTYKNYRKF--IFEYLKSD 160

E.coli MVNTHASGGARMTAAREAL---VFFGKDAPLLIAVTVLTSMEASDLVD-LGMTLSPAAY 150
B.subtilis LVNTHAAGGKKMQAALEGLEEGTPAGKKRPSLIAVTVLTSSEQIMKDELLIEKSLIIT 143
H.sapiens LVNTHVVPGSGVWVKGLEQEVG---LPLH---RGCLLIAEMSSTGS-----LATGAY 164
S.cerevisiae ITNTHGVVGPVIGSGLKQAA---EEVTKEPRGLLMLAELSCKGS-----LATGAY 164
L.donovani AITTHSPYMGSDSLQPFMRYPDK---AVFVLCKTSNKGSNLDLQC-LRVGDRYLYEAVAR 161
T.cruzi AITTHSPYMGSDSLSPFLQYASK---GVFVLCKTSNKGSNIEIQC-LRVNGRHLYESVAH 163
P.falciparum SCTTHNIYMGTNMLKDI CYDEEKNKYSAFVLVKTTPNPSAIFQKNLSLDNKQAYVIMAE 220

E.coli PERLAALTQKCGLDGVCSAQEAVRFKQVFGQEFKLVIPGIRPQGSEAGDQRRIMPEQA 210
B.subtilis VVHYSKQABESGLDGVVCSVHEAKAIYQAVSPSFLTVIPGIRMSEDAANDQVRVAPATA 203
H.sapiens IRAAVRMAEE-HSEFVYGFISGSRVSMKP---EFLHLIPGQLEAGGDNLGQQYNPQEV 220
S.cerevisiae VKGTVDIAKS-DKDFVYGFIAQRDMGGRDEGYDWLIMIPGIRGLDDKGDALGQQYRIVDDV 223
L.donovani VEGPWNVN-----GNVGLVVGATDPVALARVRARAPLWPLVPGIGAQQGSLKALDAG 215
T.cruzi VETVWNYN-----KNVGLVVGATDPIALSRRVVRAPLWPLVPGIGAQQGDLKALNAG 217
P.falciparum VLNMSYYLNLEQNNEFGFVVGANSYDEMNYIRTYFPVICYLSPGIGAQNGLHKLTLTNG 280

E.coli LS-AGVDYVY-IGRPVYVQ--SVDPAQTLKAINASLQRSA----- 245
B.subtilis RE-KGSSAIV-VGRSIVTK--AEDPVKAYKAVRLEWEGIKS----- 239
H.sapiens IGRGSDIIT-VGRGIVIS--AADRLEAAEMYRKAWEAYLSRLGV-- 262
S.cerevisiae VS-TGSDIIT-VGRGLFAKGRDAKVEGERYRKAGWEAYLRRCGQQN 267
L.donovani LRADGSGMLINVSRG----- 231
T.cruzi LRADGSGMLINVSRG----- 233
P.falciparum YHKSYEKILINIGRAITK--NFYPQKAAQMYVDQINAILKQNMES- 323

```

### Figure 6 Multiple sequence alignment of OMPDCs.

A sequence alignment of seven different OMPDCs was performed using Clustal Omega. Species name and accession number are as follows: *E.coli* (*Escherichia coli*) (P08244.1), *B. subtilis* (*Bacillus subtilis*) (P25971.1), *H. sapiens* (*Homo sapiens*) (NP\_000364), *S. Cerevisiae* (*Saccharomyces cerevisiae*) (AAB64498.1), *L. donovani* (*Leishmania donovani*) (XP\_003859743), *T. cruzi* (*Trypanosoma cruzi*) (EKG07751.1), and *P. falciparum* (*Plasmodium falciparum*) (BAB92089.1). The yellow and pink highlighted boxes indicate identical and similar amino acids, respectively.

Additionally, percent identity of the sequence of *Pf*OMPDC comparing among *E. coli*, *B. subtilis*, *H. sapiens*, *S. cerevisiae*, *L. donovani* and *T. cruzi* are 13%, 17%, 15%, 14%, 33% and 37%, respectively, according to Clustal Omega calculation (Figure 6). From the percent identity determination, it is suggested that *Pf*OMPDC sequence is the most similar to that of *T. cruzi*.



**Figure 7** 3D structure of dimeric *P. falciparum* OMPDC.

Homodimeric *Pf*OMPDC contains subunit A (red) and subunit B (blue), PDB ID: 2ZA2 (50).

### 2.6.2. Orotate phosphoribosyltransferase

The fifth enzyme in the *de novo* pyrimidine biosynthesis pathway is OPRT, UMP synthesis requires the addition of ribose 5-phosphate moiety from PRPP to orotate by OPRT to produce OMP and pyrophosphate (PP<sub>i</sub>). The reaction is orotate + PRPP → OMP + PP<sub>i</sub>. The amino acid residues of Lys89, Phe97, Phe98, Thr212 and Arg241 are located at the active site of *Pf*OPRT enzyme, and interacting by extended hydrogen bonds among orotate, PRPP, environment amino acid residues and water molecules (51). The single open reading frame of *Pf*OPRT gene

contains 843 bp, one exon and encodes a protein with 281 amino acid residues with a molecular mass of about 33 kDa, located on chromosome 5 locus PFE0630C. Dimeric enzyme is an active form having molecular mass of about 66 kDa (24, 25). The extension of malaria parasite enzyme was found with 66 amino acids at N-terminus and also the unique insertion of 19 amino acids at 178-196, with high hydrophobic index of +1.0 - +3.0 (24, 25).

The alignment of *PfOPRT* with those of the nine sequences known (Figure 8) indicate a large insertion at the N-terminal region in all *Plasmodium*. It has been proposed that these regions used to bind between *PfOPRT* and *PfOMPDC* for tetrameric formation (24-26, 50).

The 3D structure of *PfOPRT* (Figure 9) has ten  $\beta$ -strands and seven  $\alpha$ -helices, in addition to one *cis*-peptide. The *PfOPRT* is the most closely related to that from *S. cerevisiae* (*ScOPRT*) in amino acid sequence as well as in structure (52). The catalytic dimer in *PfOPRT* structure was bound together exclusively by hydrogen bonds. In especially,  $\alpha 4$  and the loop residues drag into it make dominant interactions that bind the catalytic homodimer together. Nearly all of the surface residues of  $\alpha 4$ , which is comprised of the residues 136-KGIPMVSLTSHFLFE-150, are buried at this dimeric interface (52).



```

T.cruzi          -----ARAKDPRAAAKKLSEIDNL 19
L.donovani      -----
H.sapiens       -----
E.coli          -----
S.cerevisiae    -----M 1
B.subtilis      -----
M.thermautotrop -----
D.melanogaster  -----
P.falciparum    MTTIKENEFLCDEEYKSFVHLKDKICEERKKKELVNNNIDNVFNDDDDNNYDDGNSY 60

T.cruzi          VRFGKACSTDLAAALVASRCVRFNGFTLKS GKNSP--IYDLRRLVTHPS-ILRVVAREY 76
L.donovani      -----IMRLVAREY 9
H.sapiens       MAVARAALGPLVTGLYDVQAFKFGDFVLKSGLSPP--IYDLRGIVSRPR-LLSQVADIL 57
E.coli          ---MKPYQRQFIEFALSKQVLKFGFETLKSGRKSP--YFFNAG-LFNTGR-DLALLGRFY 53
S.cerevisiae    PIMLEDYQKNFLELAI ECQALRFGSFKLKSGRESP--YFFNLG-LFNTGK-LLSNLATAY 57
B.subtilis      ---MKQIIAKHLLDIQAVFLRPNPFTWASGILSP--IYCDNRLTSLFPE-VRNDVASGI 54
M.thermautotrop GFTTGEIADELNVSKDTARWLTQTTSVSRKEAPVDFAINWESLGGSSS-RMRVVSAAAM 74
D.melanogaster  --MILDENNLIKEFKEAEAILHGHFVLSGLHSD--TYIQCAKIFENPSRAMKVCALLA 56
P.falciparum    SSIKEMKLLKVVLLKYKALKFGEFILKSKRKS--YFFSSG-VLNNIV-SSNICFLL 116

T.cruzi          ANVLR--TLQFRIVMLLYAALPIATAISLEM-----NPLVYPRREAKSYGTKAA 125
L.donovani      AKVLR--HYKFRVLAALYAAPIASAINSEM-----NPLIYPRREAKIYGTCAA 58
H.sapiens       FQTAQNAGISFIVTVCVYTAIPLATVICSTN-----QPMILIRRKETKDYGTKRL 108
E.coli          AEALVDSGIEFLLFPPYKGGPIATTTAVALAEHHD---LDIYCFNRKKAADHGEGBN 110
S.cerevisiae    AIAIIQSDLKFIVTFPPYKGGPLAAIVCVKLAIEIGGSKFQNYQYAFNRKKAADHGEGBN 117
B.subtilis      SKLVKEHFPEAFMIACTTAGI PHAALAADHL-----NPMCYVRSRKPKAHKGKNQ 105
M.thermautotrop ADMALK-YGVAIVLIIISVPPFATLMADVGAETG-LETSIAVFPVKHRKDEGAEGA 132
D.melanogaster  DKIKKELNSSIHLIPLPIIGGIVGYEIGRQLG-----KTMFCERVN---GKFEL 104
P.falciparum    SELILKNKLSFYLLAAYKGGPMVSLTSHFLFESKK--YSNIFLYDRKEKKEYGDKNV 174

T.cruzi          IEG-----DYKKGDRVWVDDVVTGGKLEAIEKLA--AGLEIV 164
L.donovani      IEG-----EYKKGDRVVIIDDVSTGEMKVEAIEKLR--AGLEV 97
H.sapiens       VEG-----TINPGETCLIEDVVTSGSVLETVEVLQK--EGLKVT 147
E.coli          LVG-----SALQG-RVVLVDDVITAGTIAIRESMEIQA--NGATLA 148
S.cerevisiae    IVG-----SALENKRILIIDVMTAGTINEAFEIISN--AKGQVV 156
B.subtilis      IEG-----AVQEGQKTVIDLDTGGVLEACAALQA--AGCEVL 144
M.thermautotrop ISGN-----FAKVKGRVWVDDVITSGRTIAEVVEVLKN--QGAKPI 173
D.melanogaster  RRG-----FKIKKGEKILLIEDVITTKKSLAEVCAEGEGEGKVV 146
P.falciparum    IVGNLDDDDKDIILNLKKTKNQDEBEKNI IIDDVFTCGTLETELLAKLKT-Y-EHLKVV 233

T.cruzi          SIVVLDREM-----GAKQLLGS LGYELEAVVTLSPPLPWRQAGAITQQQMKD 213
L.donovani      SIVVLD RDM-----GAKAFNLKLG YDFEAVVGLHQPLPWRKSNAITSQQEAD 146
H.sapiens       DAIVLDREQ-----GGKDKLQAHGIRLHSVCTLSKLEILEQQKVKDAETVGR 196
E.coli          GVLISLDRQERGRGE---ISAIQEVERDYNCKVISIITLKDIAYLEEKPEMAEHLAA 203
S.cerevisiae    GSIIADRQEVVSTDDKEGLSATQTVSKKYGIPVLSIVSLIHITYLEGR--ITABEKS 214
B.subtilis      GVVSITTYGLP-----KAEBFAKAE LPPYSLTDYDTTEVALENGNIHSDDLKK 194
M.thermautotrop AVTVLIDKKG-----ISEVDGVEVESLIRVSRIG----- 202
D.melanogaster  AEASLTKRNS-----ETKLPPFVISLIELN--KNYSEEBLPSLKLQPLI 189
P.falciparum    AFIVLNRNE-----YEINENNQKIYKIDIFEKRVGIPLYSILS 272

T.cruzi          VQSFMLEAS-SKL----- 225
L.donovani      VRAF LGQWKQSKL----- 159
H.sapiens       VKRFIQENVFVAANHNGSPLSI 218
E.coli          VKAYREEFGV----- 213
S.cerevisiae    IEQYLQTYGASA----- 226
B.subtilis      LQTWKRNPESKDFKK----- 210
M.thermautotrop -----
D.melanogaster  TKPGSREYLT----- 200
P.falciparum    YKDDIQSMI----- 281

```

### Figure 8 Multiple sequence alignment of OPRTs.

A sequence alignment of nine different OPRTs was performed using Clustal Omega. Species name and accession number are as follows: *T. Cruzi* (*Trypanosoma cruzi*) (EKG07751.1), *L. donovani* (*Leishmania donovani*) (XP\_003859743), *H. sapiens* (*Homo sapiens*) (NP\_000364), *E. coli* (*Escherichia coli*) (X00781), *S. cerevisiae* (*Saccharomyces cerevisiae*) (NP\_013601), *P. falciparum* (*Plasmodium falciparum*) (BAB92089.1), *B. Subtilis* (*Bacillus subtilis*) (AIY97169.1), *M. thermautotrop* (*Methanothermobacter thermautotrophicus*) (AAB85374.1) and *D. melanogaster* (*Drosophila melanogaster*) (NP\_966038.1). The yellow and pink highlighted boxes indicate identical and similar amino acids, respectively.

It is noted that percent identity of the sequence of PfOPRT comparing among *T. cruzi*, *L. donovani*, *H. sapiens*, *E. coli*, *S. cerevisiae*, *B. Subtilis*, *M. thermautotrophicus* and *D. melanogaster* are 22%, 23%, 26%, 27%, 32%, 16%, 17% and 20%, respectively, according to Clustal Omega calculation (Figure 8). From the percent identity result, it is suggested that PfOPRT sequence is the most similar to that of *S. cerevisiae*.

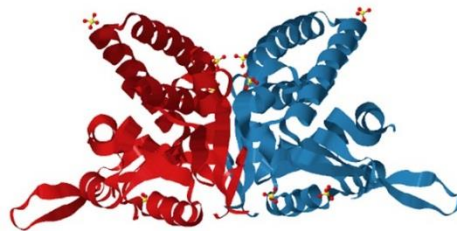


**Figure 9** 3D structure of dimeric *P. falciparum* OPRT.

Homodimeric *Pf*OPRT contains subunit A (red) and subunit B (blue), PDB ID: 4FYM (52).

The alignment of *Pf*OPRT sequence with those of other organisms show large insertion present at the N-terminal and internal regions (Figure 8). The alignment of *Pf*OMPDC sequence with those of the ten known crystal structures (Figure 6) indicate a large insertion at the N-terminal region in all *Plasmodium* species. It has been proposed that these regions are responsible for binding between *Pf*OPRT and *Pf*OMPDC for tetrameric formation (26, 50).

## 2.7. Evolution of orotidine 5'-monophosphate decarboxylase and orotate phosphoribosyltransferase

The single open reading frame of *PfOPRT* and *PfOMPDC* genes encode the proteins with 281 and 323 amino acid residues, respectively (26). Both enzymes from *P. falciparum* have been purified and found to be multienzyme complex with a molecular mass of 140 kDa, containing two subunit of each *PfOPRT* and *PfOMPDC* are 33 kDa and 38 kDa, respectively (24, 25). The multienzyme complex forms  $\alpha_2\beta_2$  conformation, representing the  $(PfOPRT)_2(PfOMPDC)_2$  as a heterotetrameric form (24-26).

The *PfOPRT* and *PfOMPDC* contribute their functions in a multienzyme complex, which are indicated by the chromatographic experiments of *PfOPRT* and *PfOMPDC* on the Superose 12 gel filtration FPLC column, demonstrating a single peak with molecular mass of 140 kDa, and also by the SDS-PAGE, showing the result of a monomeric form of both *PfOPRT* and *PfOMPDC* with molecular masses of 33 and 38 kDa, respectively (24, 25). The dimeric forms of *PfOPRT* and *PfOMPDC* are 67 and 76 kDa, respectively, as determined on the Superose 12 gel filtration FPLC column (26).

Taken together, the multiple sequence alignments indicate that the *OPRT* gene of the fused *OMPDC-OPRT* is originated from the eukaryotic ancestor (e.g., fungi, yeast (*S. cerevisiae*)). In case of the cyanobacteria, it was demonstrated

that the fused *OMPDC-OPRT* gene occurs via lateral gene transfer (LGT) (18, 53).

The possible evolutionary scenario of *OPRT* and *OMPDC* genes in eukaryotes is shown in Figure 10. Many of the eukaryotic groups (e.g., Metazoa, Amoebozoa, Plantae, Heterolobosea, and euglenoids), share *OPRT-OMPDC* gene and form monophyletic clusters, the most likely description is that the *OPRT-OMPDC* gene fusion was established once in the common ancestor of eukaryotes. Nonetheless, there is a possibility that the *OPRT-OMPDC* gene fusion occurred independently or was subsequently transferred via LGT among distantly related eukaryotic groups. The *OPRT-OMPDC* gene is defined in eukaryotic groups: fungi and alveolata are stand-alone genes, kinetoplastids and stramenopiles are inversely *OMPDC-OPRT* fusion. The previous information indicated that the *OPRT* genes in fungi, alveolata, and stramenopiles and the *OMPDC* genes in alveolata, kinetoplastids, and stramenopiles are acquired from bacterial origin via LGT. The *OPRT-OMPDC* gene in fungi is split and acquired the replaced *OPRT* gene from bacterial origin as the split gene. The alveolata and stramenopiles thoroughly have loss the original *OPRT-OMPDC* gene fusion and acquired the *OPRT* and *OMPDC* genes by LGT. In kinetoplastids, the *OMPDC-OPRT* gene is taken through LGT, acquiring the of *OMPDC* gene, splitting the original *OPRT-OMPDC* gene, and re-fusion between the acquired *OMPDC* gene and the *OPRT* genes in the inversed order. However, the evolutionary history for the origin of the transferred genes in both *OPRT* and *OMPDC* gene, it is still unclear, whether its common ancestor is originated (18, 53).

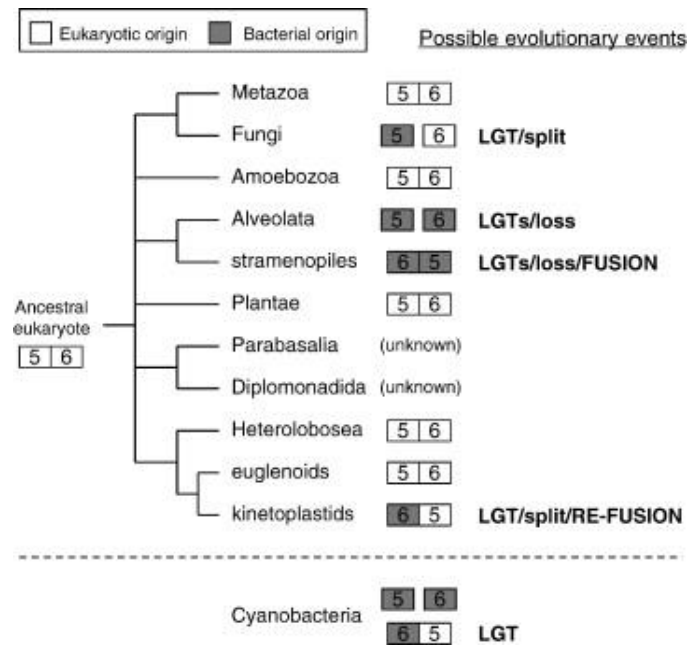
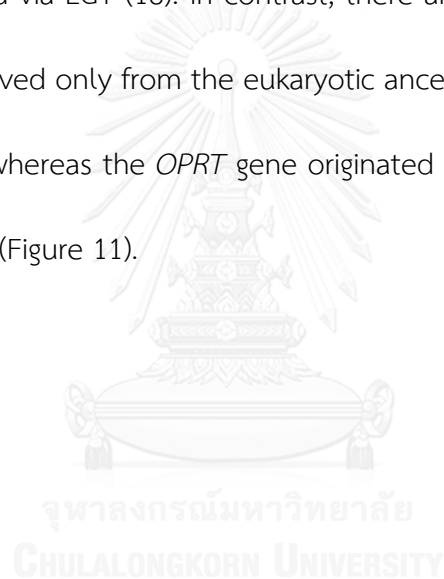


Figure 10 Evolution of *OPRT* and *OMPDC* genes.

*OPRT* and *OMPDC* are the last two enzymes in *de novo* pathway encoding by genes 5 and 6, respectively. The eukaryotic origin and bacterial origin are represented by open and gray boxes, respectively. It is unknown for the presence and organization of *OPRT* and *OMPDC* genes in parabasalia and diplomonadida. The possibility of evolutionary events, LGT, for example in the corresponding groups, secondary gene splitting and subsequent gene fusion are shown. In the evolutionary scenario, the cyanobacterial *OMPDC-OPRT* gene fusion is acquired subsequently via LGT, as shown below the dashed line (18).

As for the literature reviewed for the *OMPDC-OPRT* gene fusion, there are lines of existing evidence for the *OMPDC* gene originating from prokaryotic ancestor (e.g., cyanobacteria), and for the *OPRT* gene descending from eukaryotic origin of unicellular eukaryotic organisms, such as kinetoplastids and apicomplexans. Nevertheless, the cyanobacterial *OMPDC-OPRT* has a monophyletic origin and that this fused gene is not derived from their fusion of the cyanobacterial stand-alone genes, but is acquired via LGT (18). In contrast, there are no lines of evidence for the *OMPDC* gene derived only from the eukaryotic ancestor in the inversely linked *OMPDC-OPRT* gene, whereas the *OPRT* gene originated from both prokaryotic and eukaryotic organisms (Figure 11).



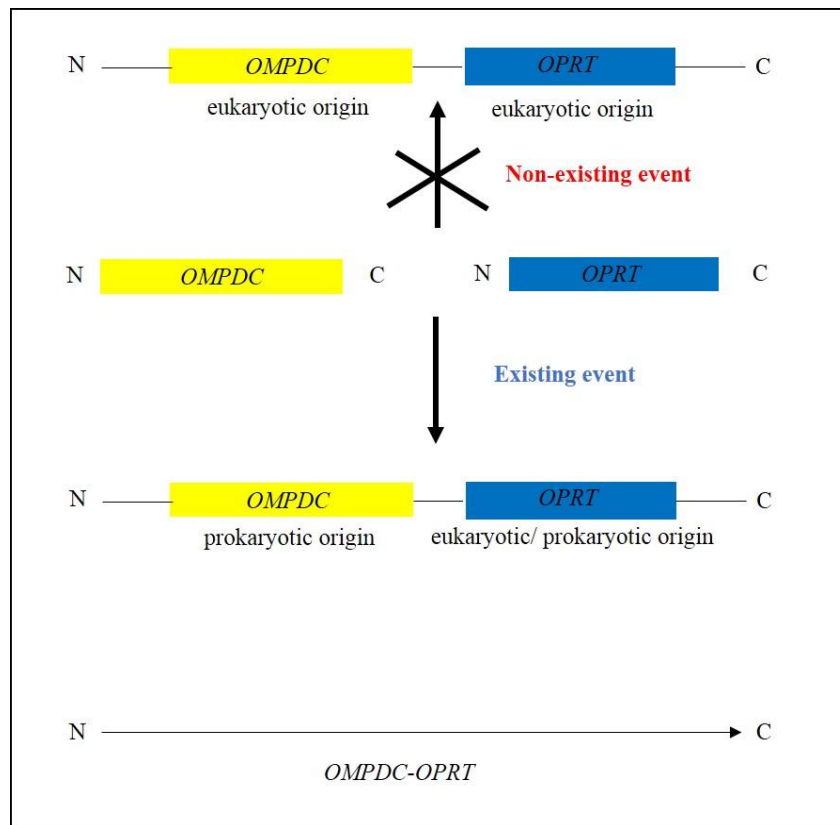


Figure 11 Evolution of *OMPDC-OPRT* gene and its organization.

The *OMPDC-OPRT* gene organization in kinetoplastids (e.g., *Trypanosoma cruzi* and *Leishmania donovani*), diatom (e.g., *Stramenopiles*), and cyanobacteria (e.g., *Nostoc punctiforme*) (18, 19, 53).



The OPRT and OMPDC enzymes are encoded by two separate genes in most prokaryotes, on the contrary these nucleotides sequences in most eukaryotic organisms are joined into a single gene, know as the bifunctional UMPS (16, 54), However, in the eukaryotes, the organization of *OPRT* and *OMPDC* genes are polytypic, and is therefore suitable for investigation of whether multiple gene fusion/fission events have occurred in this set of genes (18).

So far as literature concerned, there are three types of *OPRT* and *OMPDC* gene organization. The order linked *OPRT-OMPDC* gene fusion is present in the majority of eukaryotic groups, i.e., multicellular organisms, plants and mammals, including humans. On the other hand, they exist as separate genes (stand-alone) in yeast, fungi, apicomplexans (e.g., *Toxoplasma*, *Plasmodium*), and in most prokaryotes (18, 20). Interestingly, the inversely linked *OMPDC-OPRT* gene fusion is present in the parasitic kinetoplastids (e.g., *Trypanosoma cruzi*, *Leishmania donovani*), and diatom (*Stramenopiles*), which are single-cell eukaryotes, representing an independent fusion event of both genes (18). The inversed fusion genes are also found in some prokaryotes, e.g., cyanobacteria (e.g., *Gloeobacter violaceus*, *Anabaena sp.* and *Nostoc punctiforme*).

Evolutionary, the stand-alone *OMPDC* presence in diplomonids, which appears to have the same origin as euglenoid, may provide important insights into the evolutionary process of rearrangement of gene fusion. Our previous analyses suggested that the kinetoplastid *OMPDC-OPRT* appear through three events as follows:

(1) Splitting of the original *OMPDC-OPRT* gene

(2) LGT-based acquisition of the *OMPDC* gene

(3) Re-fusion between the acquired *OMPDC* and the resident *OPRT* genes in the reverse order, although the temporal order of gene splitting and LGT is not conclusively.

Significantly, diplomonids are found at an intermediate branch between euglenoids and kinetoplastids in euglenozoa. Wherefore, it is likely that the splitting of *OPRT-OMPDC* occurred first, in a common ancestor of diplomonids and kinetoplastids, and that, after separation of the diplomonid lineage, a common ancestor of kinetoplastids acquired *OMPDC* gene via LGT, and then re-fusion to *OMPDC-OPRT* gene. However, the possibility rearrangement of *OPRT-OMPDC* gene appears to be independently in the diplomonid and kinetoplastid lineages (21, 53).

Based on the current knowledge, the rationality of originated fused gene can be used as a phylogenetic marker. The contention of reasons are that it is difficult to exclude possibility of LGT. There is ample evidence of eukaryote-to-eukaryote

LGT events and LGT between faraway related groups is an important evolutionary mechanism in eukaryotes and prokaryotes. Another reason of fused gene was the possibility of independent fused gene in different groups, readjustment of gene fusion including secondary splitting of fused genes and subsequent re-fusion, as found in green algae (e.g., *Mougeotia scalaris*). So the *OPRT* genes in fungi, alveolate (e.g., malaria parasite), and diatoms (e.g., *Stramenopiles*) and the *OMPDC* genes in alveolata, kinetoplastids, and diatoms are acquired from bacterial LGT (18). The feasible evolution scenario in these groups is as follows: in fungi, *OPRT-OMPDC* is split and the bacterial type *OPRT* gene is acquired instead of the split gene (55). Alveolata and diatoms have lost their original *OPRT-OMPDC* fused genes, and acquired *OPRT* and *OMPDC* genes separately by LGT, whereas the diatoms have then developed as *OMPDC-OPRT* gene fusion.

In 2011, French JB *et. al.*, provided an evidence showing the organization of the genes encoding the enzymes for last two steps of the pyrimidine biosynthetic pathway of *L. donovani*. The *OPRT* and *OMPDC* encoding regions are fused, leading to the bifunctional inversely linked *OMPDC-OPRT* gene. They also elucidated the three-dimensional structure of this protein by X-ray crystallography. The structure of *L. donovani* UMPS (*LdUMPS*) was determined by molecular replacement using *LdOMPDC* and *Corynebacterium diphtheriae* *OPRT* (PDB code 2P1Z) as a template. The dimeric form of *LdUMPS* with molecular mass of 90 kDa is demonstrated. The

$k_{cat}/K_m$  catalytic value of *LdOMPDC* in *LdUMPS* is consistent with the highly efficient nature of this decarboxylase activity, whereas the catalytic efficiency of *LdOPRT* component is an order of magnitude slower than that of the *LdOMPDC* component (20).

## 2.8. Organization of aspartate transcarbamoylase (ATC) and dihydroorotase (DHO) in eubacterial *Aquifex aeolicus*

In eukaryotes, there are two types of gene and enzyme organization for *CPS II*, *ATC*, and *DHO* encoding the first three enzymes in this pathway, *CPS II*, *ATC*, and *DHO*, respectively. The first type is the fusion of these enzymes of *CPS II-DHO-ATC* (*CAD*), which is found in animals, amoebozoans, and also in the red alga *Cyanidioschyzon merolae*. The second type is the stand-alone enzyme, which is common among the remaining eukaryotic groups.

Additionally, many enzymes are found to be active in the multienzyme complex including the pyrimidine enzymes. In an eubacterial *Aquifex aeolicus*, *ATC* and *DHO*, the second and the third enzymes of the pathway are encoded by separate genes and form the enzyme complex after their expression. Both *ATC* and *DHO* are catalytically active in trimeric forms and associate into a hexamer of  $(ATC)_3(DHO)_3$  (56, 57). The multifunctional enzyme complex shows also that catalytic efficiency ( $k_{cat}/K_m$ ) is higher than that of the separate enzyme, however,

the lower  $K_m$  values for multifunctional complex is noted. In contrast, the first three enzymes of the pyrimidine pathway in human and other animals exist as a trifunctional CAD protein, in which the responding genes are fused (57). In most plants and prokaryotes (e.g., *E. coli*), their genes are stand-alone organization and expressed as monofunctional enzymes.

## 2.9. Other bifunctional enzymes in the malaria parasite

There are also lines of evidence demonstrating few the bifunctional enzymes existing in the malaria parasite. The previous study of the bifunctional enzyme dihydrofolate reductase-thymidylate synthase (DHFR-TS), proved that DHFR is a key enzyme in folate metabolism, linked to the production of thymidylate by TS. In several protozoa, the catalytic activities of both DHFR and TS active sites are carried on a single polypeptide chain of the enzyme, constituting a bifunctional DHFR-TS enzyme with high catalytic efficiency (58-61). Nearly all known TS enzymes exist as a dimeric, including bifunctional DHFR-TS in the protozoan parasites. The crystal structures of *L. casei* TS, and *P. falciparum* DHFR-TS, reveal that the TS domains are hold together, and form active sites near the dimeric interface. Each TS active site is composed of residues from both monomers (62). Additionally, there are independent inversely fusions of glucose-6-phosphate dehydrogenase (G6PD) and 6-phosphogluconolactonase (6PGL) in the pentose phosphate pathway existing

in malaria parasite (63). The evolutionary scenario of these fused genes in phylogenetic tree explain three phenomena as follows: the first type, since the apicomplexan fusion genes branch with a non-fused gene from dinoflagellates, the closest relatives of apicomplexans, assume the fused between *G6PD* and *6PGL* genes occurred after divergence of apicomplexans and dinoflagellates. Secondly, the *G6PD-6PGL* fused gene was clearly an ancestral feature common to *Trichomonas* and *Giardia*, and expected to find this gene in any species that diverged recently from either lineage. And thirdly, the *G6PD* gene part of the fused gene in *Trichomonas* and *Giardia* come from horizontal gene transferred from a bacteria ancestor. In *Giardia* genome, the gene may have been transferred with a *6PGL* gene, commonly found in the same operon in most bacteria, or they may have been fused prior to the horizontal transfer. The origin of inversely fusion *6PGL-G6PD* gene was identified in all *Plasmodium spp.*, and the fusion must have occurred in an ancestor of the *Plasmodium spp.*. So, no data of genomic available for many of the species has been analyzed, and it is not possible to determine how long ago the fusion occurred. Interestingly, the insertion sequence, unique character present in only *Plasmodium spp.* is functionally important for enzymatic activity (63). This unique property is similar to the well characterized OPRT and OMPDC in *P. falciparum* (24-26).

## 2.10. Evolutional origin of protein-protein co-localization

The structural complex of the malarial parasite enzyme, as described in section 2.6, thus, represents an efficient functional kinetic benefit, which is in line with co-localization principles for evolutionary origin, that increases random mutation in the proteins, possibly decreasing the free energy enough to create a tightly binding dimer resulted in increasing their concentrations, which can amplify the effect of protein function, i.e., increased catalytic efficiency of the corresponding enzymes. And also with allosteric property in the protein-protein interaction, in which the complex system is regulated by allosteric control (64, 65). This advanced understanding would help for new antimalarial drugs designed by targeting the protein-protein fusion of *PfOMPDC* and *PfOPRT* in the bifunctional form (66, 67).

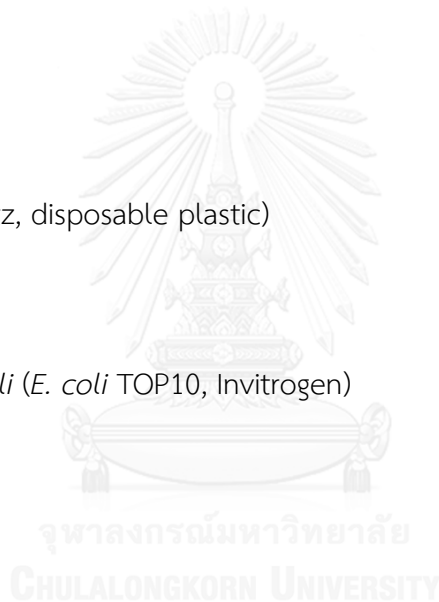
As far as the literature concerned, the bifunctional enzymes might have the highest performance in terms of catalytic efficiency, which is the best advantage of the functioning enzyme, i.e., *LdOMPDC-OPRT* (20), *PfDHFR-TS* (62, 68).

## CHAPTER III

### MATERIALS AND METHODS

#### 3.1. Materials

- 1) Alcohol lamp
- 2) Autopipet (Gilson pipetman model P2, P10, P20, P100 and P1000)
- 3) Autopipet tips
- 4) Beaker
- 5) Cuvette (quartz, disposable plastic)
- 6) Cylinder
- 7) *Escherichia coli* (*E. coli* TOP10, Invitrogen)
- 8) Flask
- 9) Magnetic bar
- 10) Microcentrifuge tube (Eppendorf)
- 11) Microcentrifuge tube rack
- 12) Parafilm
- 13) Petridish (90 x 15 mm)
- 14) *Pfu* DNA polymerase (Promega)
- 15) Pipet rack
- 16) Plastic wrap





- 17) Platinum loop
- 18) Polaroid film
- 19) Polypropylene conical centrifuge tube
- 20) Screw cap tube
- 21) Spreader (glass)
- 22) Test tube
- 23) Thermometer

### 3.2. Equipments

- 1) Applied Biosystems model 377 sequencer
- 2) Balance (Shimadzu)
- 3) Deep freezer -20 °C, -80 °C (Sharp, Revco)
- 4) DNA Thermal cycler (Thermo Hybaid)
- 5) Electrophoresis apparatus for agarose gel (Bio-Rad)
- 6) Fast Protein Liquid Chromatography (FPLC) system, equipped with a Superose 12 HR 10/30 column (1.5 x 30 cm) and a sample loop of 0.5 ml (Pharmacia).
- 7) Fluorescence and phosphor imager (Storm model 865)
- 8) Gel-document (Bio-Rad)
- 9) High speed centrifuge (Sorvall)

- 10) High Performance Liquid Chromatography Quadrupole-Time of Flight model SYNAPT™ High-Definition Mass Spectrometry (HPLC Q-TOF model SYNAPT™ HDMS) equipped with a symmetry C<sub>18</sub> 5 μm, 180-μm x 20-mm trap column and a BEH130 C<sub>18</sub> 1.7 μm, 100-μm x 100-mm analytical reversed-phase column (Waters corporation)
- 11) Incubator (Mettler, 37 °C)
- 12) Magnetic stirrer
- 13) Microcentrifuge (Heraeus)
- 14) pH meter (WPA)
- 15) Polaroid camera (Polaroid)
- 16) Power supply (Bio-Rad)
- 17) Refrigerator (Sanyo)
- 18) Shaking incubator (Kuhner, 18 °C and 37 °C)
- 19) Thermostat shaking water bath (GFL, 37 °C)
- 20) Ultrasonic homogenizer (Bandelin Sonoplus)
- 21) UV transilluminator (Spectroline)
- 22) UV-visible spectrophotometer model UV 1601 equipped with a temperature-controller (Shimadzu)
- 23) Vertical electrophoresis apparatus for polyacrylamide gel (mini-gel) (Bio-Rad)
- 24) Vortex (Scientific industry)

### 3.3. Reagents

#### 3.3.1. General reagents

- 1) 5- Phospho- D- ribose- 1- diphosphate sodium salt ( 5- phosphoribosyl- 1- pyrophosphate, PRPP) (Sigma)
- 2) Acetic acid, glacial (Merck)
- 3) Acrylamide (Sigma)
- 4) Agar (Becton, Dickinson and company)
- 5) Agarose (SeaKem)
- 6) Ammonium persulfate (APS) (Sigma)
- 7) Ampicillin sodium salt (Sigma)
- 8) Bromophenol blue (Fluka)
- 9) Bovine serum albumin (BSA) (Sigma)
- 10) Butanol (Merck)
- 11) Calcium chloride (Merck)
- 12) Comassie brilliant blue R250 (Sigma)
- 13) Disodium hydrogen phosphate (Merck)
- 14) Dithiothreitol (DTT) (Sigma)
- 15) DNA size marker (1 kb DNA ladder) (Vivantis)
- 16) Endonuclease: *Bam*HI, *Pst*I and *Xho*I (New England Bio Labs)
- 17) Ethanol, absolute (Merck)

- 18) Ethidium bromide (Sigma)
- 19) Ethylene diamine tetraacetic acid (disodium salt) (EDTA) (Fluka)
- 20) Formic acid (Fluka)
- 21) Glucose (Fluka)
- 22) Glycerol (Sigma)
- 23) Glycine (Vivantis)
- 24) Hydrochloric acid (Merck)
- 25) Imidazol (Sigma)
- 26) Iodoacetamide (Sigma)
- 27) Isopropanol (Merck)
- 28) Isopropyl  $\beta$ -D-thiogalactopyranoside (IPTG) (Sigma)
- 29) Lysozyme (Sigma)
- 30) Magnesium chloride (Merck)
- 31) Magnesium sulfate (Merck)
- 32) Methanol, absolute (Merck)
- 33) Mercaptoethanol (Sigma)
- 34) N,N-Methylene-bis-acrylamide (BIS) (Sigma)
- 35) N,N,N',N'-Tetramethylethylenediamine (TEMED) (Sigma)
- 36) Orotic acid monosodium (OA) (Sigma)
- 37) Orotidine 5'-monophosphate trisodium salt (OMP) (Sigma)
- 38) Phenol-chloroform (1:1, v/v) (Pierce)

- 39) Potassium chloride (Merck)
- 40) Potassium hydrogen phosphate (Merck)
- 41) Protease inhibitor cocktail (phosphoramidon (6  $\mu\text{g/ml}$ ), leupeptin (1  $\mu\text{g/ml}$ ), antipain (2  $\mu\text{g/ml}$ ), bestatin (1  $\mu\text{g/ml}$ ), pepstatin (1  $\mu\text{g/ml}$ ), E-64 (6  $\mu\text{g/ml}$ ), aprotinin (1  $\mu\text{g/ml}$ ), chymostatin (1  $\mu\text{g/ml}$ ) and *N*-*p*-tosyl-L-lysine chloromethyl ketone (TLCK, 20  $\mu\text{g/ml}$ )) (Roche)
- 42) Protein molecular mass marker for SDS-PAGE (low range) (Bio-Rad)
- 43) RNase (Sigma)
- 44) Sodium acetate (Merck)
- 45) Sodium dodecyl sulfate (SDS) (Sigma)
- 46) Sodium hydroxide (Merck)
- 47) Triton-X-100 (Sigma)
- 48) Trizma base (Sigma)
- 49) Trypsin (Promega)
- 50) Tryptone (Becton, Dickinson and company)
- 51) Uracil (Sigma)
- 52) Uridine (Sigma)
- 53) Uridine 5'-monophosphate (UMP) (Sigma)
- 54) Yeast extract (Becton, Dickinson and company)

### 3.3.2. Reagent kits

- 1) HiTrapQ HP anion-exchange column (Pharmacia BioSciences)
- 2) Protein assay dry reagent concentrate (Bio-Rad)
- 3) QIAexpress™ kit (Qiagen), containing monoclonal antibody directed against His<sub>6</sub>-tag with horseradish peroxidase conjugates
- 4) Qiagen nickel-nitrilotriacetic acid (Ni-NTA) agarose affinity resin
- 5) Qiagen plasmid midi kit
- 6) pTrcHisA expression vector (Invitrogen)
- 7) Zero Blunt TOPO cloning vector (Invitrogen)

### 3.4. Methods

#### 3.4.1. Cloning and construction of recombinant fused bifunctional *PfOMPDC-PfOPRT* gene

*P. falciparum* *OMPDC* (969 bp) and *OPRT* (846 bp) genes were separately cloned by using PCR with designed primers as follows:

for *OMPDC* gene,

forward primer 5'**CGGGATCC**GCCATGGGTTTTAAGGTAAAATTAG3' 33 mers

reverse primer 5'**GCCTCGAGC**GATTCCATATTTTGCTTTAAG3' 30 mers

which introduced *Bam*HI and *Xho*I restriction sites, respectively (shown in bold)

for *OPRT* gene,

forward primer 5'GC**CTCGAG**ATGACGACGATAAAAAGAGAATG3' 30 mers

reverse primer 5'GC**CTGCAG**CGCTCATATCATCGACTGTATATCGTC3' 30 mers

which introduced *XhoI* and *PstI* restriction sites, respectively (shown in bold).

High fidelity *Pfu* DNA polymerase was used for the PCR reaction. The PCR cycling parameters include denaturation at 95 °C (1 min), annealing at 55 °C (1 min) and extension at 68 °C (3 min) for 40 cycles. The PCR reaction (50 µl total volume) was prepared as shown previously (24). After 40 cycles, a single band of the predicted size was visualized on an 0.8% agarose gel, after electrophoresis.

The PCR cycling parameters and the PCR products processing and ligating into a Zero Blunt TOPO cloning vector, were essentially described (24, 26). The cloned *OMPDC* and *OPRT* were sequenced by the dideoxy chain termination method using an automated Applied Biosystems model 377 sequencer. The cloned *OMPDC* gene was firstly subcloned into a pTrcHisA expression vector, using *BamHI* and *XhoI* restriction sites. The *OPRT* gene was secondly subcloned into the pTrcHisA containing the *OMPDC*, using *XhoI* and *PstI* restriction sites. Finally, the pTrcHisA containing the inversed order fusion as *OMPDC-OPRT*, were constructed and expressed as fused bifunctional NH<sub>2</sub>-OMPDC-OPRT-COOH enzyme. The freshly prepared competent *E. coli* TOP10 cells were transformed with the construct

plasmid (Figure 12) and propagated in the Luria-Bertani (LB) medium containing ampicillin (100 µg/ml).

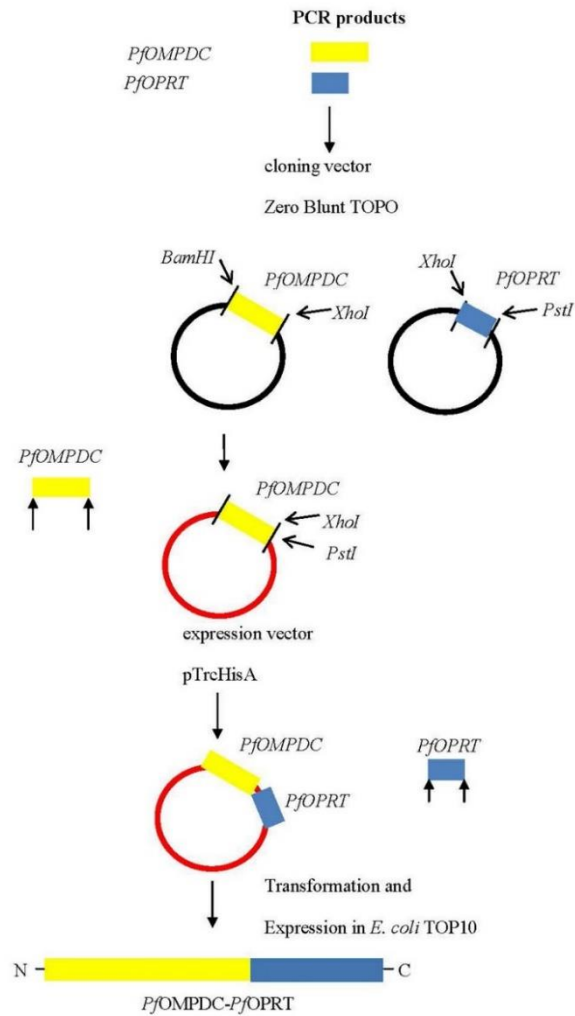


Figure 12 Cloning of recombinant plasmid containing designed *PfOMPDC-PfOPRT* fused gene.



### 3.4.2. Preparation of competent *E. coli*

An *E. coli* Top10 colony from a LB plate was inoculated in LB broth at 37 °C for overnight and transferred into 50 ml LB broth and incubated at 37 °C until absorbance (A) 600 nm of the culture was about 0.4-0.6. The culture was centrifuged at 6,000 rpm for 10 min at 4 °C. The supernatant was discarded. The cell pellet was then suspended in 10 ml of iced-cold 50 mM CaCl<sub>2</sub> and left on ice for 40 min. The treated cell was centrifuged at 6,000 rpm for 10 min at 4 °C. The cell pellet was resuspended in 5 ml of cold 50 mM CaCl<sub>2</sub> and cooled on ice for another 15 min. The cell was then centrifuged at 6,000 rpm for 10 min at 4 °C. The cell pellet was resuspended in 500 µl of cold 50 mM CaCl<sub>2</sub> and 30-50% glycerol by gentle vortexing. The competent cells were freshly prepared for each transformation.

### 3.4.3. Expression and purification of recombinant fused bifunctional

#### *PfOMPDC-OPRT* enzyme

The competent *E. coli* TOP10 cells were transformed with the construct plasmid, cultivated in LB medium at 37 °C until the cell density of 0.4-0.6 at A 600 nm, then induced with 1 mM IPTG at 18 °C for 18 h, harvested at 8,000 rpm for 10 min, washed at least two times with 5 mM phosphate buffered saline (PBS), and finally stored as cell paste at -80 °C until use.

Frozen cell paste was resuspended in a lysis buffer (50 mM TrisHCl pH 8.0, 300 mM NaCl, 10 mM imidazole, glycerol, 10 mg/ml lysozyme, 10 mg/ml RNase, Triton X-100 and one tablet of protease inhibitor cocktail) (24). Lysozyme and Triton X-100 were added to final concentrations of 0.1%. The mixture was sonicated by an ultrasonic Sonoplus homogenizer. The *E. coli* lysate was centrifuged at 10,000 rpm at 4 °C for 30 min.

The obtained supernatant fluid was loaded onto a Ni-NTA agarose affinity column (0.5 ml bed volume) which had been equilibrated with a buffer A containing 50 mM TrisHCl pH 8.0, 150 mM NaCl and 10 mM imidazole. The column was washed twice with 5 ml of a buffer B containing 50 mM TrisHCl pH 8.0, 150 mM NaCl and 20 mM imidazole, and then eluted with 3 ml of a buffer C containing 50 mM TrisHCl pH 8.0, 150 mM NaCl and 250 mM imidazole. The eluting fractions of 0.5 ml were collected and assayed for enzymatic activities of OPRT and OMPDC. The eluent containing the enzymatic activities from Ni-NTA agarose affinity column was pooled and added onto a HiTrapQ anion-exchange chromatography column which had been equilibrated with 50 mM TrisHCl pH 8.0, and then eluted with 50 mM TrisHCl containing 500 mM NaCl. The 0.5-ml fractions were collected and assayed for enzymatic activities of OPRT and OMPDC (24).

#### 3.4.4. Confirmation of recombinant fused *Pf*OMPDC-OPRT enzyme by Western blotting

The Western blot analysis was performed to confirm the authenticity of the His<sub>6</sub>-tagged recombinant protein according to the manufacture's instruction. The detection system was QIAexpress™ kit, containing monoclonal antibody directed against His<sub>6</sub>-tag with horseradish peroxidase conjugates. The recombinant protein was then analyzed. Firstly, a SDS-PAGE gel was washed with water several times, and then with blotting buffer (25 mM TrisHCl, 150 mM glycine and 10% methanol). The filter papers were also soaked with the blotting buffer. The nitrocellulose membrane was flashed with methanol and then soaked in blotting buffer. Secondly, the SDS-PAGE gel to be blotted was put onto the nitrocellulose membrane, and care was taken to remove all air bubbles. Thirdly, the assembly was put into an electrophoretic chamber of mini-gel apparatus with the nitrocellulose membrane facing the cathode. A voltage gradient of 12 V or 80 mA was applied for 1 h (69). Finally, the blotted nitrocellulose membrane was then processed for the QIAexpress™ detection system as described before.

### 3.4.5. Determination of molecular mass of recombinant fused *Pf*OMPDC-OPRT enzyme

The Superose 12 HR gel-filtration FPLC system was performed to determine molecular mass in a native form of recombinant fused *Pf*OMPDC-*Pf*OPRT enzyme. The eluent containing both OPRT and OMPDC activities from the HiTrapQ anion-exchange chromatography column, as described previously (section 3.4.3) were pooled and then loaded onto the Superose 12 gel-filtration FPLC column which had been equilibrated with 50 mM TrisHCl pH 8.0 containing 250 mM NaCl. The fused *Pf*OMPDC-OPRT enzyme was then eluted with this buffer at flow rate of 0.5 ml/min for 45 min, the 0.5-ml fractions were collected and assayed for both enzymatic activities. The FPLC column was calibrated with molecular mass markers: blue dextran (2,000 kDa), thyroglobulin (670 kDa), immunoglobulin (158 kDa), bovine serum albumin (66 kDa), ovalbumin (44 kDa), myoglobin (17 kDa) and vitamin B12 (1.35 kDa).

### 3.4.6. Enzymatic assays and kinetic studies

The OPRT and OMPDC activities of the fused bifunctional enzyme were measured according to previously described, using spectrophotometric methods by monitoring decrease of absorbance for orotate and OMP, respectively (24-26). Each enzymatic assay was performed in a quartz cuvette with a UV-visible Shimadzu

spectrophotometer model UV1601 equipped with a temperature controlled cuvette holder at 37 °C. For all kinetic analyses, the purified enzyme (> 90% purity) was used at concentrations of 5-10 μM in 1.0 ml reaction assays, and their kinetics were measured in three to five different preparations. The  $K_m$  and  $V_{max}$  values were calculated by measurement of initial velocities ( $V$ ) in triplicate with at least five substrate concentrations ( $[S]$ ). The turnover number ( $k_{cat}$ ) and catalytic efficiency ( $k_{cat}/K_m$ ) values were then calculated as described (70, 71).

In this study, two kinetic equations were used as follows:

Michaelis-Menten equation [3]:

$$V = \frac{V_{max} \cdot [S]}{K_m + [S]} \quad [3]$$

Lineweaver-Burk equation [4]:

$$\frac{1}{V} = \frac{K_m}{V_{max}} \cdot \frac{1}{[S]} + \frac{1}{V_{max}} \quad [4]$$

Since the enzymatic reaction of OPRT has two substrates, orotate and PRPP. For orotate substrate, the reaction mixture (1 ml) contained 50 mM TrisHCl pH 8.0, 5 mM MgCl<sub>2</sub>, 250 μM DTT, and concentrations of orotate were varied from 6.25 to 250 μM, at fixed saturating concentration of PRPP (250 μM). The *Pf*OMPDC-*Pf*OPRT enzyme (100 μl) was incubated for 1 min at 37 °C with all components except PRPP.

The reaction was started by adding 250  $\mu\text{M}$  PRPP and followed a linear graph of absorbance change at 295 nm for 3 min (24, 25). For PRPP substrate, the reaction mixture (1 ml) contained 50 mM TrisHCl pH 8.0, 5 mM  $\text{MgCl}_2$ , 250  $\mu\text{M}$  DTT, and concentrations of PRPP were varied from 6.25 to 250  $\mu\text{M}$ , at fixed saturating concentration of orotate (250  $\mu\text{M}$ ). The *Pf*OMPDC-*Pf*OPRT enzyme was incubated for 1 min at 37 °C with all components except PRPP. The reaction was started by adding PRPP and followed a linear graph of absorbance change at 295 nm for 3 min (24, 25).

The reaction of OMPDC activity assay (1 ml) contained 50 mM TrisHCl pH 8.0, 250  $\mu\text{M}$  DTT. The concentrations of OMP were varied from 6.25 to 125  $\mu\text{M}$ . The *Pf*OMPDC-*Pf*OPRT enzyme (100  $\mu\text{l}$ ) was incubated for 1 min at 37 °C with all components except OMP. The reaction was started by adding OMP and followed a linear graph of absorbance change at 285 nm for 3 min (24, 25).

The absorbance changes of both enzymes were then calculated for enzymatic activities, as  $\mu\text{mol}/\text{min}$ , using their extinction coefficients values of the conversion were  $3.67 \times 10^3 \text{ M}^{-1} \text{ cm}^{-1}$  for OPRT, and  $1.65 \times 10^3 \text{ M}^{-1} \text{ cm}^{-1}$  for OMPDC, respectively (24, 25).

### 3.4.7. Enzymatic stability test

To stabilize the recombinant OMPDC-OPRT enzyme upon purification and storage, the substrate PRPP for OPRT and the product UMP for OMPDC were included during two purification steps and storage at a final concentration of 0.5 mM in all buffers used. The purified enzyme (~60  $\mu$ M) was stored at 4 °C in a buffer with 10% glycerol and 2.5 mM DTT with/without PRPP and UMP, and tested for enzymatic activities of both OPRT and OMPDC at time intervals of ~2-3 days up to 45 days.

### 3.4.8. Bioinformatics and proteomics

Multiple alignments of amino acid sequences of OMPDC-OPRT enzymes were performed using the Clustal Omega program (72). Homology models of the three-dimensional (3D) structures were generated by the Phyre2 program (73). An 3D structure of the bifunctional *Pf*OMPDC-*Pf*OPRT (residues 1-323 and 324-604, respectively) was constructed by using the crystal structure of *L. donovani* UMPS (PDB code 3QW4) as template, having OMPDC (residues 1-323) and OPRT (residues 387-604), in which residues 324-386 of OPRT component were not present in the homology model.

The amino acid sequences of the bifunctional enzyme were determined using a liquid chromatography-mass spectrometry/mass spectrometry (LC-MS/MS) as essentially described previously (74, 75). The protein score in the result taken from

an MS/MS search is derived from an ion score. The ion score is the MS/MS match on the data based, with significance threshold at  $p < 0.05$ , representing the total numbers of protein/peptide molecular mass matches for each query.

#### **3.4.9. Agarose gel electrophoresis and density analysis of DNA bands**

Agarose gel electrophoresis was performed with 0.8% agarose gel in 1x Tris-acetate-EDTA (TAE) at a voltage of 100 V for 30 min. Ethidium bromide (EtBr) stained DNA bands were photographed using a *Polaroid camera*. Using VC 1 kb and 100 bp DNA ladder for the agarose gel electrophoresis, comparing to the bands density of DNA ladder of 2500 bp, 1000 bp and 500 bp (76).

#### **3.4.10. SDS-Polyacrylamide gel electrophoresis (SDS-PAGE) and density analysis of protein bands**

SDS-PAGE was performed on a Bio-Rad mini-gel apparatus with 10% polyacrylamide gel in the Laemmli buffer system (77), using Bio-Rad molecular mass markers for the SDS-PAGE. The gels were stained with Coomassie brilliant blue R, visualized by Gel document (Bio-Rad), and then analyzed density of protein bands by a Storm fluorescence and phosphor imager (model 865).



### 3.4.11. Protein assay

Protein concentrations were determined by the Bradford method (78) using bovine serum albumin as standard.

### 3.4.12. Statistical analysis

For statistical analysis, data are means  $\pm$  SD of at least three independent experiments unless otherwise specified.



## CHAPTER IV

### RESULTS

#### 4.1. Preparation of fused bifunctional *PfOMPDC-PfOPRT* gene and recombinant enzyme

##### 4.1.1. Construction of recombinant plasmid containing fused bifunctional *PfOMPDC-PfOPRT* gene and confirmation of the fused gene by restriction map

The *PfOMPDC* (ORF, 969 bp) and *PfOPRT* (ORF, 843 bp) of PCR products were separately ligated into a cloning vector, Zero Blunt TOPO plasmid, and then inserted into an expression vector, pTrcHisA plasmid (4.4 kb). The selected clone containing *PfOMPDC-PfOPRT*-pTrcHisA plasmid was checked by plasmid extraction and digestion at restriction sites with corresponding endonuclease enzymes. Firstly, the size of *PfOMPDC-PfOPRT*-pTrcHisA plasmid was 6.212 kb, confirmed by single cut with *Bam*HI digestion of *PfOMPDC-PfOPRT*-pTrcHisA plasmid to linear-like DNA with a size of 6.212 kb. Secondly, the plasmid was double cut with *Bam*HI and *Pst*I digestions to generate inserting genes (1.813 kb) and the pTrcHisA plasmid (4.4 kb). Thirdly, The plasmid was triple cut with *Bam*HI, *Pst*I and *Xho*I digestions to give three DNA fragments, pTrcHisA plasmid (4.4 kb), *PfOMPDC* (969 bp), and *PfOPRT* (846 bp). The restriction maps were analyzed on an agarose gel electrophoresis (Figure 13).

These results suggest the constructed pTrcHisA plasmid have *PfOMPDC* and *PfOPRT* inserting genes, corresponding to the design inserts with restriction sites for the cloning of fused bifunctional *PfOMPDC-PfOPRT* gene for heterologous expression in *E. coli*.

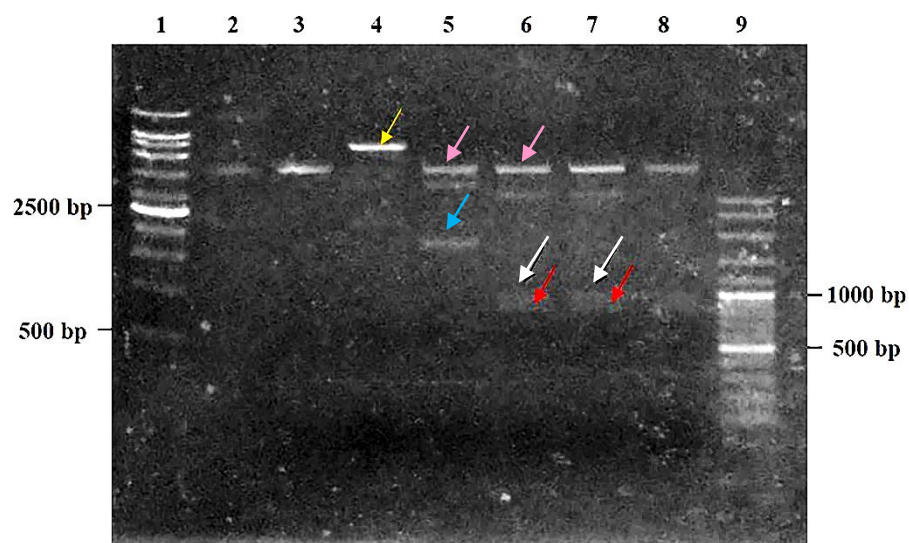


Figure 13 Agarose gel electrophoresis analysis of *PfOMPDC-PfOPRT-pTrcHisA* plasmid.

Agarose gel was used at 1%. Lane 1: 1 kb DNA ladder marker, Lane 2: pTrcHisA plasmid, Lane 3: Negative control, Lane 4: *PfOMPDC-PfOPRT-pTrcHisA* plasmid digested with *Bam*HI, Lane 5: *PfOMPDC-PfOPRT-pTrcHisA* plasmid digested with *Bam*HI and *Pst*I, Lane 6: *PfOMPDC-PfOPRT-pTrcHisA* plasmid digested with *Bam*HI, *Pst*I and *Xho*I, Lane 7: Positive control, digested with *Bam*HI, *Pst*I and *Xho*I, Lane 8: Negative control, digested with *Bam*HI, *Pst*I and *Xho*I and Lane 9: 100 bp DNA ladder

marker. The white arrow indicates band of *PfOMPDC* gene (upper band), the red arrow indicates band of *PfOPRT* gene (lower band), the yellow arrow indicates band of uncut fused bifunctional *PfOMPDC-PfOPRT* gene, the pink arrows indicates band of pTrcHisA plasmid and the blue arrow indicates band of *PfOMPDC-PfOPRT* gene. The negative control is pTrcHisA plasmid only, and positive control is a *PfOMPDC-PfOPRT*-pTrcHisA plasmid as control of the fused bifunctional gene in our laboratory.

#### 4.1.2. Expression and purification of fused bifunctional *PfOMPDC-PfOPRT* enzyme

The *PfOMPDC-PfOPRT* fused gene was expressed in *E. coli* TOP10, under 1mM IPTG induction at 18 °C for 18 h, as soluble form. The enzyme was purified by two sequential steps of Ni-NTA affinity and HiTrapQ anion-exchange chromatographic techniques. The fused *PfOMPDC-PfOPRT* enzyme were eluted with 50 mM TrisHCl, pH 8.0, 300 mM NaCl and 250 mM imidazole on the Ni-NTA affinity column and subsequently eluted with 50 mM TrisHCl, pH 8.0, 500 mM NaCl on the HiTrapQ anion-exchange column, respectively (Figure 14). The enzymatic activities of *PfOMPDC* and *PfOPRT* were co-eluted in both columns, as overlapping peaks.

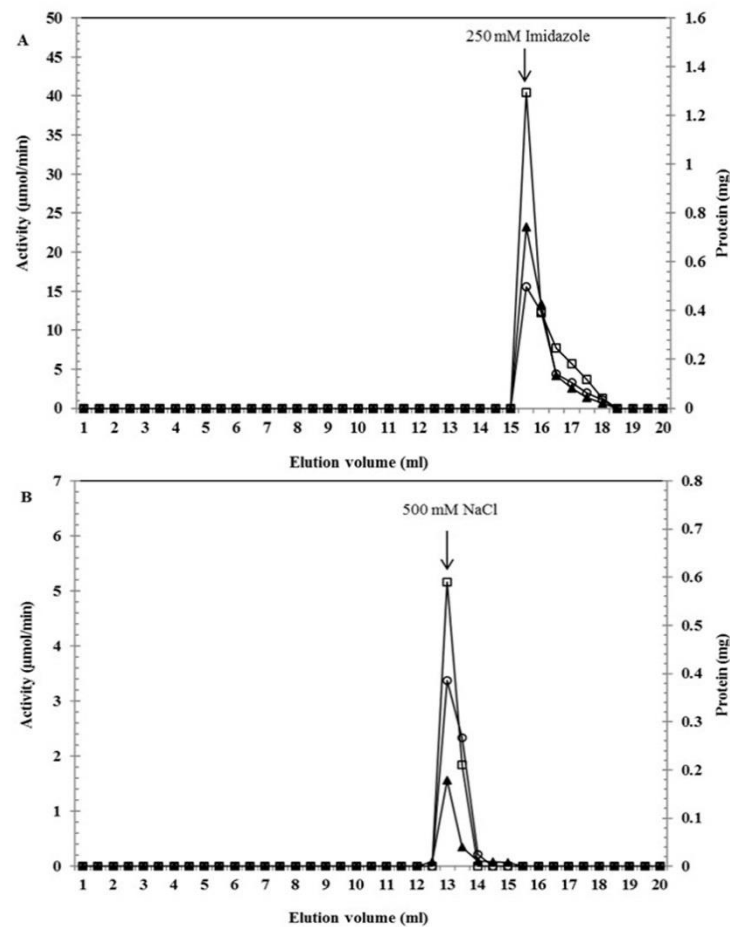


Figure 14 Ni-NTA affinity and HiTrapQ anion-exchange chromatographic profiles of the fused bifunctional *PfOMPDC-PfOPRT* enzyme.

The 0.5-ml fractions were collected and assayed for both enzymatic activities (□ for *PfOMPDC*, □○ for *PfOPRT* and ▲ protein concentration). (A). The Ni-NTA affinity column (0.5 ml bed volume) equilibrated with buffer A (50 mM TrisHCl, pH 8.0, 300 mM NaCl and 10 mM imidazole), and the crude enzyme (from supernate fraction of *E. coli* lysate) was loaded onto the column was washed twice with 5 ml of buffer A and buffer B (50 mM TrisHCl, pH 8.0, 300 mM NaCl and 20 mM imidazole) and eluted

with 3 ml of buffer C (50 mM TrisHCl, pH 8.0, 300 mM NaCl and 250 mM imidazole). The bifunctional enzymatic activities were co-eluted as overlapping peaks on the Ni-NTA affinity column. (B). The recombinant protein, pooled from the Ni-NTA affinity step was then eluted from the HiTrapQ anion-exchange column, equilibrated with 50 mM TrisHCl, pH 8.0 and eluted with 50 mM TrisHCl, pH 8.0, 500 mM NaCl. The enzymatic activities were co-eluted as overlapping peaks on the HiTrapQ anion-exchange column.

At the Ni-NTA affinity chromatographic step, the specific activities of *PfOMPDC* and *PfOPRT* component in the bifunctional enzyme were 48.90 and 26.58  $\mu\text{mol}/\text{min}/\text{mg}$  protein (n=3), respectively. At the HiTrapQ anion-exchange chromatographic step, the specific activities of *PfOMPDC* and *PfOPRT* component in the bifunctional enzyme were 27.22 and 23.02  $\mu\text{mol}/\text{min}/\text{mg}$  protein (n=3), respectively (Table 1). Recovery yields of both enzymatic activities at the HiTrapQ anion-exchange step were relatively low (9.8% for *PfOMPDC*, 15.3% for *PfOPRT*). These results indicate that both enzymatic activities of the bifunctional enzyme are markedly labile.

**Table 1** Purification of bifunctional *PfOMPDC-PfOPRT* enzyme.

Step	<i>PfOMPDC</i>		<i>PfOPRT</i>		
	Total protein (mg)	Activity ( $\mu\text{mol}/\text{min}$ )	Specific activity ( $\mu\text{mol}/\text{min}/\text{mg}$ )	Activity ( $\mu\text{mol}/\text{min}$ )	Specific activity ( $\mu\text{mol}/\text{min}/\text{mg}$ )
Ni-NTA <sup>a</sup>	1.4528	71.04	48.90	38.62	26.58
HiTrapQ <sup>b</sup>	0.2572	7.00	27.22	5.92	23.02

<sup>a</sup> Ni-NTA-agarose affinity chromatographic column, eluting at 250 mM imidazole

<sup>b</sup> HiTrapQ-anion-exchange chromatographic column, eluting at 500 mM NaCl

Starting with 1 liter of the *E. coli* TOP10 culture, approximately 1-2 mg of the purified enzyme was obtained. The SDS-PAGE analysis of the purified bifunctional *PfOMPDC-PfOPRT* enzyme is shown in Figure 15. Molecular mass of monomeric bifunctional *PfOMPDC-PfOPRT* enzyme was calculated to be  $68 \pm 4$  kDa (n=18), corresponding to the predicted molecular mass of 70,812 Da from the deduced amino acid sequence of the protein.

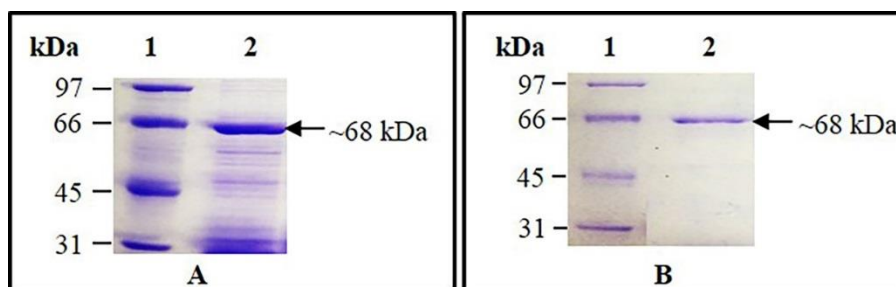


Figure 15 SDS-PAGE analysis on a 10% polyacrylamide gel of the bifunctional *PfOMPDC-PfOPRT* enzyme after subjecting onto a Ni-NTA affinity and the HiTrapQ anion-exchange shows in panel A and B, respectively.

Panel A shows a heterogeneous enzyme preparation (58.11  $\mu\text{g}$ ), purified using the Ni-NTA affinity step (lane 2). Panel B shows a homogeneous enzyme preparation (10.29  $\mu\text{g}$ ), purified from two sequential step of the Ni-NTA affinity and the HiTrapQ anion-exchange steps with molecular mass of  $68 \pm 4$  kDa (lane 2). Low range molecular mass markers are given in kDa (lane 1) of panel A and B.

#### 4.1.3. Confirmation of fused bifunctional *PfOMPDC-PfOPRT* enzyme by

##### Western blot analysis

Western blot analysis was performed to confirm the bifunctional *PfOMPDC-PfOPRT* protein expressed as described in section 4.1.2, by using monoclonal antibody directed against His<sub>6</sub>-tag on the fused enzyme with horseradish peroxidase conjugates. The Western blot shows a positive band at a position of  $\sim 70$  kDa molecular mass (Figure 16).



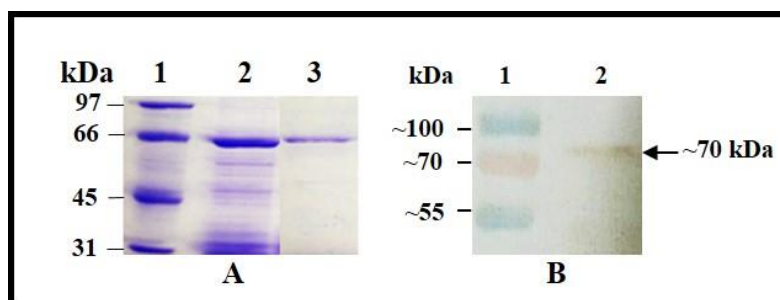


Figure 16 SDS-PAGE and Western blot analysis of the purified bifunctional *PfOMPDC-PfOPRT* enzyme.

Panel A indicates 10% SDS-PAGE gel of the purified enzyme, taken from the Ni-NTA affinity step (lane 2) and from two sequential step of the Ni-NTA affinity and the HiTrapQ anion-exchange chromatography (lane 3). Lane 1 is low range molecular mass markers in kDa. Panel B shows the Western blot of the bifunctional enzyme at ~70 kDa molecular mass (lane 2). Lane 1 is PageRuler prestained protein ladder in kDa.

## 4.2. Physical property of fused bifunctional *PfOMPDC-PfOPRT* enzyme

### 4.2.1. Determination of molecular mass of native bifunctional enzyme

The molecular mass of the native bifunctional enzyme was determined by using a Superose 12 gel-filtration FPLC column. The purified bifunctional enzyme, taken from the second purification step on the HiTrapQ anion- exchange chromatography, was subjected onto the Superose 12 gel-filtration column which had been equilibrated with 50 mM TrisHCl (pH 8.0), 300 mM NaCl, 1 mM DTT. Both enzymatic activities were co-eluted as a single overlapping peak (Figure 17), corresponding to an apparent molecular mass of  $158 \pm 10$  kDa ( $n= 4$ ) (Figure 17 inset). This value is consistent with a dimeric state of quaternary structure of the enzyme, which would have a calculated molecular mass of  $\sim 142$  kDa. The eluting enzyme was further analyzed by SDS-PAGE with a molecular mass of  $68 \pm 4$  kDa ( $n=4$ ) (Figure 18), as what found in the monomeric form of the bifunctional enzyme.

The results indicate that the native form of fused bifunctional *PfOMPDC-PfOPRT* enzyme is catalytically active in a dimeric structure.

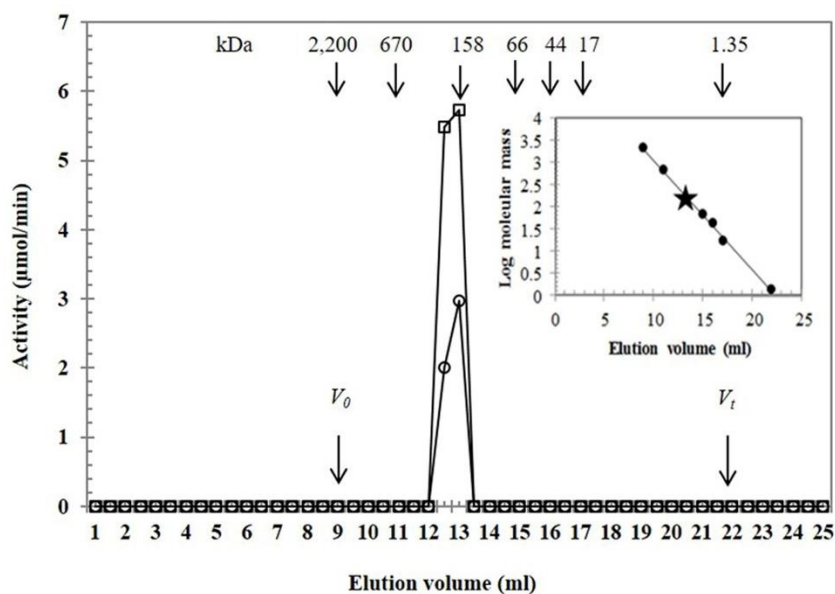
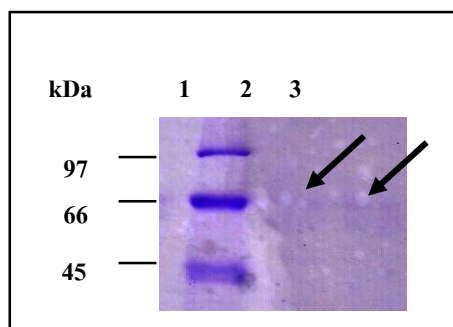


Figure 17 Superose 12 gel-filtration FPLC of the purified bifunctional *PfOMPDC-PfOPRT* enzyme.

The column was equilibrated with a buffer containing 50 mM TrisHCl (pH 8.0), 300 mM NaCl, 1mM DTT. The 0.5-ml fractions were collected for enzymatic activities. Both activities were eluted at 13.0-ml, estimated to a molecular mass of 158.0 kDa ( $\square$  for *PfOMPDC*,  $\circ$  for *PfOPRT*). Molecular mass marks, void volume ( $V_0$ ) and total eluting volume ( $V_t$ ) are indicated with arrows. Inset shows the plot between log molecular mass of the markers and elution volume ( $R^2 = 0.8$ ), the star indicates the bifunctional *PfOMPDC-PfOPRT* enzyme eluted at 13 ml with a molecular mass of 158 kDa.



**Figure 18** SDS-PAGE analysis on a 10% polyacrylamide gel of the purified bifunctional enzyme after subjecting onto a Superose 12 gel-filtration FPLC column.

Lanes 2 and 3 are fractions 26 and 25 from Figure 17, respectively. Low range molecular mass markers are given in kDa (lane 1). The black arrow indicates band of the bifunctional enzyme after Coomassie brilliant blue R250 staining, with a molecular mass of ~68 kDa.

จุฬาลงกรณ์มหาวิทยาลัย  
CHULALONGKORN UNIVERSITY

#### 4.2.2. Stabilization of recombinant bifunctional enzyme

Since the recombinant bifunctional *Pf*OMPDC-*Pf*OPRT enzyme is known to be markedly unstable as evident in section 4.1.2. In order to stabilize the activities of both OPRT and OMPDC enzymes, purification of the recombinant enzyme was performed in all buffers used by having 0.5 mM PRPP and 0.5 mM UMP, a substrate and a product of OPRT and OMPDC, respectively (Figure 19). The chromatographic profiles of enzymatic activities were similar to that had been done previously in

Figure 14. However, the total protein and activity obtained from the purification in the presence of the stabilizers (PRPP and UMP) were ~2-3-fold higher than those without stabilizers. At the Ni-NTA affinity chromatographic step, the specific activities of *Pf*OMPDC and *Pf*OPRT component in the bifunctional enzyme with stabilizer were 30.55 and 38.72  $\mu\text{mol}/\text{min}/\text{mg}$  protein (n=3), respectively. At the HiTrapQ anion-exchange chromatographic step, the specific activities of *Pf*OMPDC and *Pf*OPRT component in the bifunctional enzyme with stabilizer were 29.42 and 35.29  $\mu\text{mol}/\text{min}/\text{mg}$  protein (n=3), respectively (Table 2). Recovery yields of both enzymatic activities at the second step of HiTrapQ anion-exchange chromatographic step were relatively high (29.5% for *Pf*OMPDC, 27.9% for *Pf*OPRT). Recovery yields of both enzymatic activities at the second step of HiTrapQ anion-exchange column were up to ~30-35%, comparing to the first step of Ni-NTA affinity column, and the specific activities of OMPDC and OPRT in a range of ~29-35  $\mu\text{mol}/\text{min}/\text{mg}$  protein were also achieved (Table 2), especially the OPRT enzyme had more pronounced effect than the OMPDC enzyme. These results indicate that both enzymatic activities of the bifunctional enzyme are stabilized by PRPP and UMP.

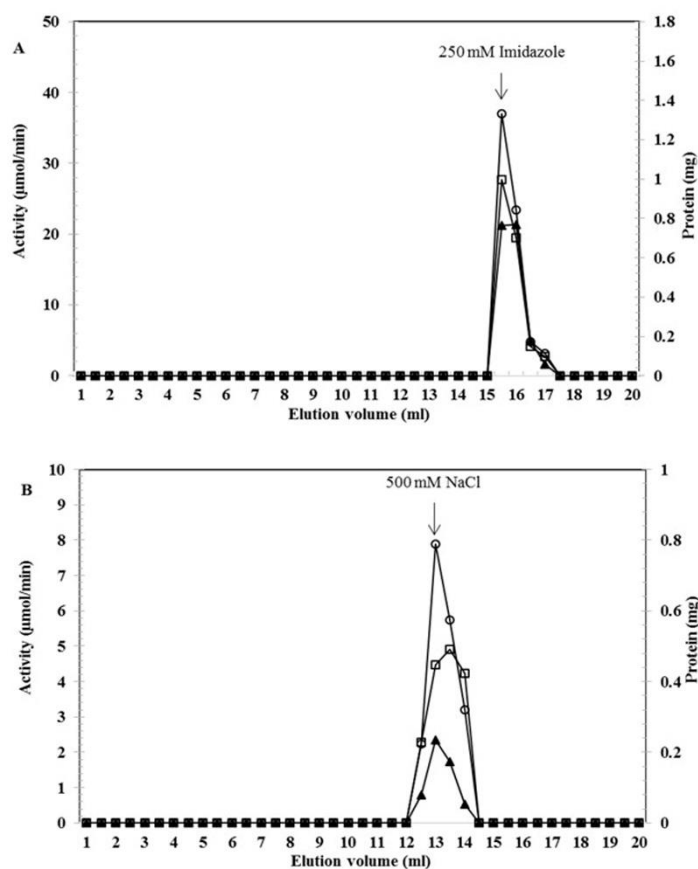


Figure 19 Ni-NTA affinity and HiTrapQ anion-exchange chromatographic profiles of the bifunctional *PfOMPDC-PfOPRT* enzyme with stabilizers.

The 0.5-ml fractions were collected and assayed for both enzymatic activities ( $\square$  for *PfOMPDC*,  $\bigcirc$  for *PfOPRT* and  $\blacktriangle$  protein concentration), (A). The Ni-NTA affinity column (0.5 ml bed volume) equilibrated with buffer A (50 mM TrisHCl, pH 8.0, 300 mM NaCl and 10 mM imidazole), and the crude enzyme (from supernate fraction of *E. coli* lysate) was loaded onto the column was washed twice with 5 ml of buffer A and buffer B (50 mM TrisHCl, pH 8.0, 300 mM NaCl and 20 mM imidazole) and eluted

with 3 ml of buffer C (50 mM TrisHCl, pH 8.0, 300 mM NaCl and 250 mM imidazole) containing 0.5 mM PRPP and 0.5 mM UMP. The bifunctional enzymatic activities were co-eluted as overlapping peaks on the Ni-NTA affinity column. (B). The recombinant protein, pooled from the Ni-NTA affinity step, was then eluted from the HiTrapQ anion-exchange column, equilibrated with 50 mM TrisHCl, pH 8.0 and eluted with 50 mM TrisHCl, pH 8.0, 500 mM NaCl, containing 0.5 mM PRPP and 0.5 mM UMP. The enzymatic activities were co-eluted as overlapping peaks on the HiTrapQ anion-exchange column.



Table 2 Purification of bifunctional PfOMPDC- PfOPRT enzyme in the presence of stabilizers.

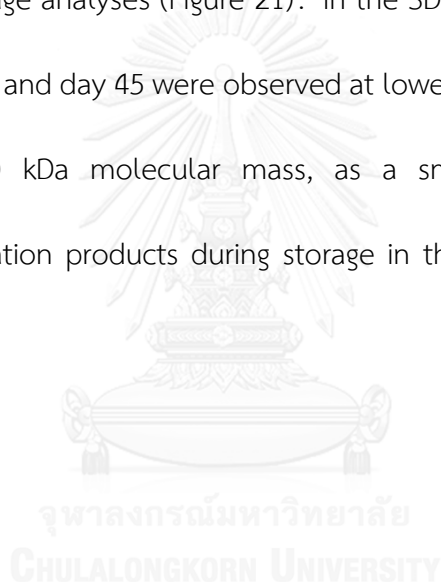
Step	Total protein (mg)	<i>PfOMPDC</i>		<i>PfOPRT</i>	
		Activity ( $\mu\text{mol}/\text{min}$ )	Specific activity ( $\mu\text{mol}/\text{min}/\text{mg}$ )	Activity ( $\mu\text{mol}/\text{min}$ )	Specific activity ( $\mu\text{mol}/\text{min}/\text{mg}$ )
Ni-NTA <sup>a</sup>	1.7670	53.98	30.55	68.42	38.72
HiTrapQ <sup>b</sup>	0.5403	15.90	29.42	19.07	35.29

<sup>a</sup> Ni-NTA-agarose affinity chromatographic column, eluting at 250 mM imidazole, 0.5 mM PRPP and 0.5 mM UMP.

<sup>b</sup> HiTrapQ- anion- exchange chromatographic column, eluting at 500 mM NaCl, 0.5 mM PRPP and 0.5 mM UMP.



Examination of stability property of both catalytic activities in the bifunctional enzyme was performed by keeping its in the absence and presence of 0.5 mM PRPP and 0.5 mM UMP at 4 °C. After storage half-life of the OPRT activity was ~0.5 week and ~3 weeks, respectively. But the OMPDC activity was much more stable with a half-life of about ~3-4 weeks (Figure 20). It was also found that more than 90% of the bifunctional protein, stored at 4 weeks, remained at 68-kDa band, as observed by SDS-PAGE and image analyses (Figure 21). In the SDS-PAGE gel, degradations of the protein on day 30 and day 45 were observed at lower bifunctional protein bands of approximately 50 kDa molecular mass, as a smear pattern, forming the heterologous degradation products during storage in the absence of stabilizers at 4 °C.



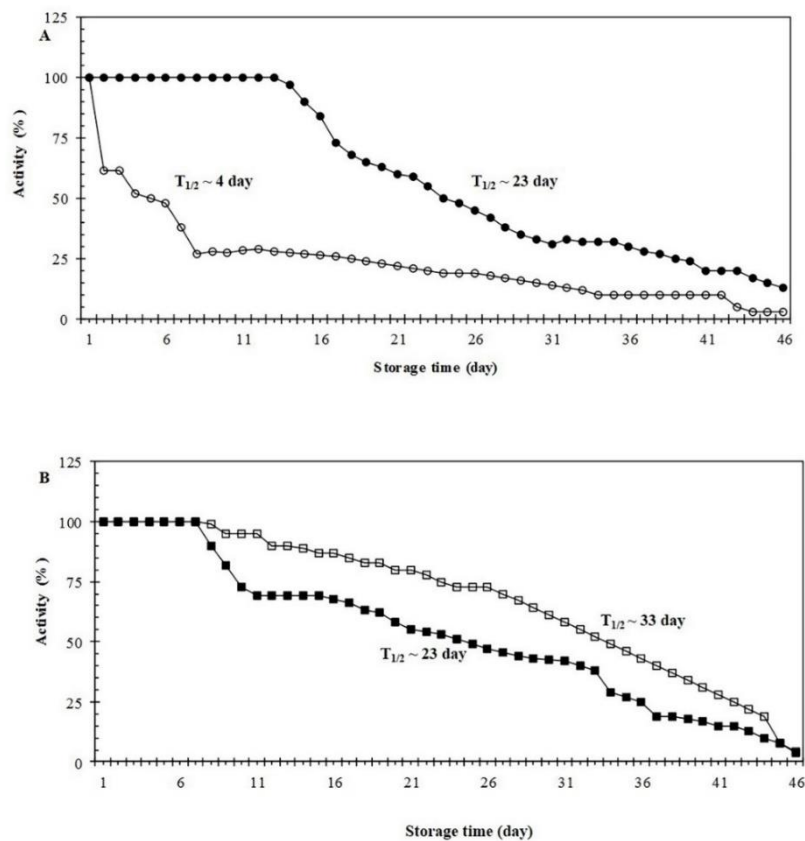


Figure 20 Stabilization of the bifunctional enzyme by stabilizers, PRPP and UMP.

The concentrations of 0.5 mM PRPP and 0.5 mM UMP were used for *PfoPRT* and *PfoOMPDC* component in bifunctional enzyme, respectively (○ for *PfoPRT*, absence of stabilizer, ● for *PfoPRT* presence of stabilizer, □ for *PfoOMPDC* absence of stabilizer, and ■ for *PfoOMPDC* presence of stabilizer). The half-life of OPRT in the bifunctional enzymes with stabilizer was 6-times higher than without stabilizer (A). The half-life of OMPDC was not much different between the absence and presence of stabilizers over 7 weeks (B).

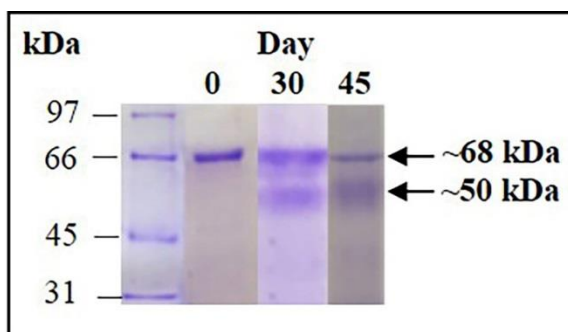


Figure 21 SDS-PAGE analysis of the purified bifunctional enzyme *PfOMPDC-PfOPRT* during storage in the absence of stabilizers.

At day 0, there was no degradation. At day 30 and day 45, there were degradation products as observed at lower bifunctional protein bands of 50 kDa, as a smear pattern.

The results suggest that the bifunctional enzyme has catalytic stability in the presence of substrate and product as stabilizers. Without the stabilizers, the intrinsic stability property was found in the OMPDC enzyme, but its labile property was associated to the OPRT enzyme only in the bifunctional *PfOMPDC-PfOPRT*.

### 4.3. Kinetic property of fused bifunctional *PfOMPDC-PfOPRT* enzyme

To determine whether the fused bifunctional enzymes express its kinetic property on either Michaelis-Menten or allosteric kinetics, the enzyme was then determined for various kinetic parameters, e.g. Michaelis constant ( $K_m$ ), maximal velocity ( $V_{max}$ ), turnover number ( $k_{cat}$ ), catalytic efficiency ( $k_{cat}/K_m$ ) etc.

#### 4.3.1. Kinetic constants of fused bifunctional *PfOMPDC-PfOPRT* enzyme

The  $K_m$  and  $V_{max}$  values of *PfOPRT* and *PfOMPDC* component in the fused bifunctional *PfOMPDC-PfOPRT* enzyme were determined by varying concentrations of each substrate and measuring initial velocity ( $V$ ), and then calculating  $K_m$ .

The catalysis of each component in the bifunctional enzyme (used at concentration of  $\sim 6 \mu\text{M}$ ) followed the Michaelis-Menten kinetics as a hyperbolic curve, and showed a straight line on the Lineweaver-Burk plots. For the *PfOPRT* enzyme, the varied substrates orotate and PRPP had the Michaelis-Menten kinetic behaviours (Figure 22, 23). For the *PfOMPDC* enzyme, the varied substrate OMP exhibited also the Michaelis-Menten kinetic (Figure 24).

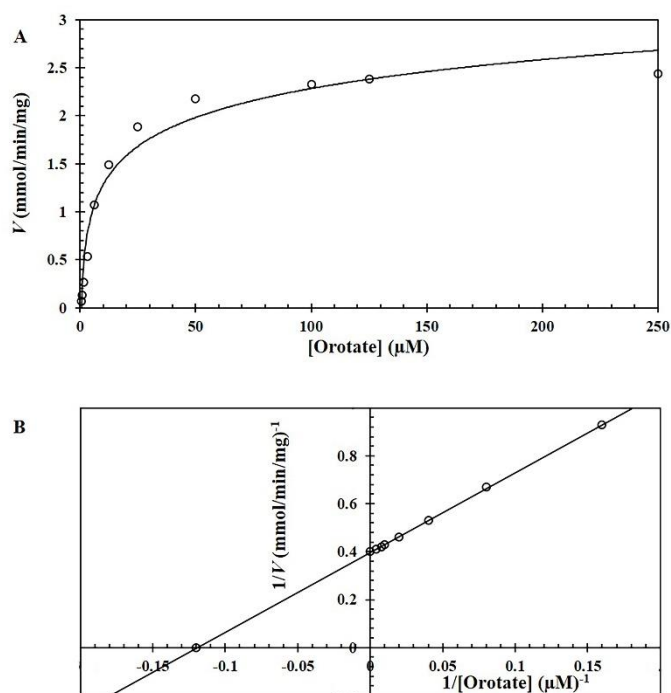


Figure 22 Michaelis- Menten and Lineweaver- Burk plots of the forward reaction of *PfOPRT* component in the bifunctional *PfOMPDC-PfOPRT* enzyme.

The initial velocity rates ( $V$ ) were measured at variable orotate concentrations and fixed PRPP concentration at 250  $\mu\text{M}$ , the concentration of orotate was varied from 6.25 to 250  $\mu\text{M}$  (A). The Lineweaver-Burk plots were illustrated for the OPRT component in the bifunctional enzyme, as a straight line with  $R^2$  of 0.9998 (B). The  $K_m$  and  $V_{\text{max}}$  values were then calculated from the Lineweaver-Burk plots.

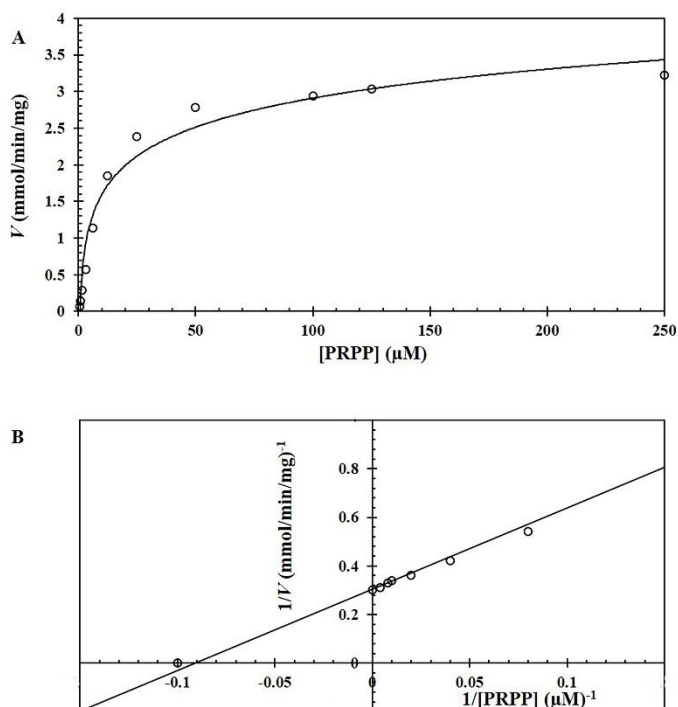


Figure 23 Michaelis- Menten and Lineweaver- Burk plots of the forward reaction of *Pf*OPRT component in the bifunctional *Pf*OMPDC-*Pf*OPRT enzyme.

The initial velocity rates ( $V$ ) were measured at variable PRPP concentrations and fixed orotate concentration at 250  $\mu\text{M}$ , the concentration of PRPP was varied from 6.25 to 250  $\mu\text{M}$  (A). The Lineweaver-Burk plots were illustrated for the OPRT component in the bifunctional enzyme, as a straight line with  $R^2$  of 0.9906 (B). The  $K_m$  and  $V_{\text{max}}$  values were then calculated from the Lineweaver-Burk plots.

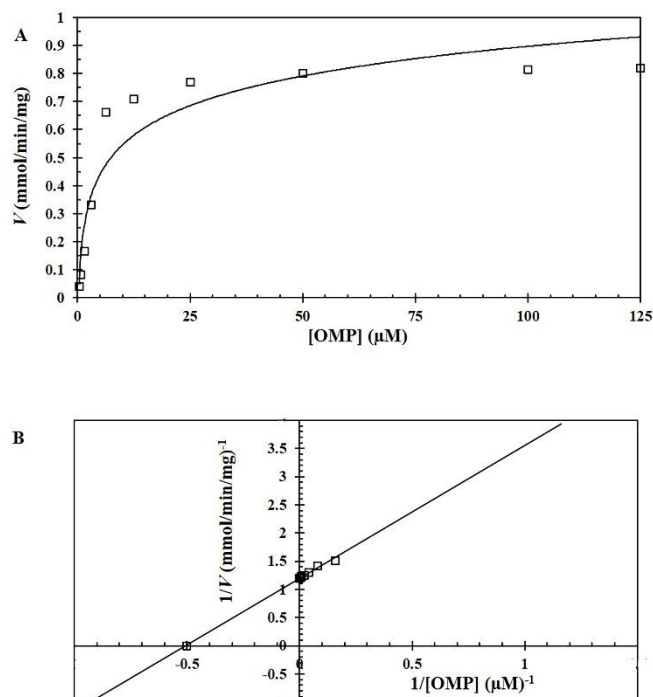


Figure 24 Michaelis-Menten and Lineweaver-Burk plots of the reaction of *PfOMPDC* component in *PfOMPDC-PfOPRT* bifunctional enzyme.

A, the Michaelis-Menten reaction of the *PfOMPDC* component in bifunctional enzyme. The concentration of OMP was varied from 6.25 to 125  $\mu\text{M}$ . B, the Lineweaver-Burk plots of the OMPDC component in the bifunctional enzyme, as a straight line with  $R^2$  of 0.9967. The  $K_m$  and  $V_{\text{max}}$  values were then calculated from the Lineweaver-Burk plots.

Determinations of kinetic parameters of both enzymes in the bifunctional enzyme (used at concentration of ~5-10  $\mu\text{M}$ ) are summarized in Table 3. The calculated data of the kinetic parameters were mean  $\pm$  SD, taken from at least three separate experiments.

**Table 3** Kinetic constants of *PfOPRT* and *PfOMPDC* components in the bifunctional enzyme.

	$K_m$ ( $\mu\text{M}$ )	$V_{\text{max}}$ ( $\mu\text{mol}/\text{min}/\text{mg}$ protein)	$k_{\text{cat}}$ ( $\text{s}^{-1}$ )	$k_{\text{cat}}/K_m$ ( $\text{M}^{-1}\text{s}^{-1}$ )
OPRT (n =3):				
Substrate: Orotate	$8.3 \pm 0.4$	2,518.3	2,972.0	$3.6 \times 10^8$
Substrate: PRPP	$9.3 \pm 0.5$	2,994.0	3,534.0	$3.8 \times 10^8$
OMPDC (n = 3):				
Substrate: OMP	$2.0 \pm 0.1$	835.3	985.8	$4.9 \times 10^8$

The results indicate that the kinetics of *PfOMPDC* and *PfOPRT* components in the bifunctional enzyme follow the Michaelis-Menten kinetics, as a hyperbolic curve, and show a straight line on the Lineweaver-Burk plots. In addition, there were no kinetic indications on an allosteric property of the bifunctional enzyme, their  $K_m$



values were at relatively low  $\mu\text{M}$  levels ( $\sim 2\text{-}9\ \mu\text{M}$ ) and the perfect catalytic efficiency ( $k_{\text{cat}}/K_m$ ) were achieved at greater than  $10^8\ \text{M}^{-1}\text{s}^{-1}$ .

#### 4.4. Bioinformatics and proteomics of fused bifunctional *Pf*OMPDC-*Pf*OPRT enzyme

##### 4.4.1. Multiple sequence alignments of all bifunctional OMPDC-OPRT enzymes

The multiple alignments of amino acid sequences of all available bifunctional OMPDC-OPRT proteins were performed by the Clustal Omega program. Alignment of the *Pf*OMPDC-OPRT amino acid sequence was also done, comparing to the sequences of four organisms. Species names and accession numbers are as follows: *T. Cruzi* (*Trypanosoma cruzi*) (EKG07751.1), *L. donovani* (*Leishmania donovani*) (XP\_003859743.1), *N. punctiforme* (*Nostoc punctiforme*) (ACC81973.1) and *Oscillatoria spp.* (CBN54487.1). Kinetoplastid protozoa are *T. cruzi* and *L. donovani*. Cyanobacteria are *N. punctiforme* and *Oscillatoria spp.*

The percent identity of *P. falciparum* OMPDC-OPRT sequence comparing among *T. cruzi*, *L. donovani*, *Oscillatoria spp.* and *N. punctiforme* were 31.89%, 30.65%, 22.72% and 22.65%, respectively. As shown in Figure 25, percent similarity of *P. falciparum* OMPDC-OPRT sequence comparing among *T. cruzi*, *L. donovani*, *N. punctiforme* and *Oscillatoria spp.* Were found to be 65.51%, 64.57%, 60.18% and 58.97%, respectively, according to Clustal Omega calculation.

It should be noted that the *P. falciparum* OMPDC-OPRT is the longest amino acid sequence (604 residues) having two internal insertions of amino acids, one is on the OMPDC component (residues 28-64) and the other is on the OPRT component (residues 331-379, a large insertion).



*T. cruzi* --MPMAFFDMLNERAKS--LLCGLDPRAL----- 27  
*L. donovani* ----MSFFDLLNERAKR--LLCGLDPRAL----- 25  
*N. punctiforme* ----MNFDFKLNRSILQNGLLFVGLDNPPE----- 27  
*Oscillatoria spp.* MNIQMNFDFKLLTAIERNQGLLYVALDDEPP----- 31  
*P. falciparum* ----MGEKVKLEKRRNAINCLCGLDDEPDIENFMKNEKENNYNNIKKNLKEKYINNV 56

*T. cruzi* -----TAEAAEBCMR-----IIDATAEYAAAYKPPAAFFIEFFGEEGW 65  
*L. donovani* -----TAAAAVEECKR-----IEQTHEYAAAYKPPAAFFIEFFGAEGW 63  
*N. punctiforme* -----MMVRYESEE----LIAGLEKWLQFIIAETADYVCAYKPPILGFIEALGIPGL 75  
*Oscillatoria spp.* -----IFITGSPASERVQILVTNLENELQSISKTADYVCAYKPPILGFIEALGIPGL 83  
*P. falciparum* SIKKDILLKADNIIREEKSEEFFYFFNFHFCFYIINETNKYALTEKMFIAFIPYGSVGI 116

*T. cruzi* KALQCVTAHVPAN-IPVLDAKRDLADTAEAAKSAFEHLAAHAIITSPYMGGLSISPF 124  
*L. donovani* AALSEVIRAPAG-IPVLDAKRDLADTADAAATSAFKHLAAHAIITSPYMGGLSISQPF 122  
*N. punctiforme* ELLYTTAAAPAH-IPVLDAKHEDLN-TSTIQAQTVFTEWVDAITLSPYTGQSHWAPF 133  
*Oscillatoria spp.* ELLQQTIKSPPH-IPVLDAKHEDLN-TSTAFARNAEDWVDAVTLSPYAGVQVTPF 141  
*P. falciparum* DVLKNVBDYIYELNIPILDMKINDIGNTVKNIRKFIIEYLLSDSCTVNIYMGTIMKDI 176

*T. cruzi* LQYASK----AVFLCKTSNKGSNETQC-LRVNGRHLYESVAEHEETVMYNYKN----- 173  
*L. donovani* MRYPDK----AVFLCKTSNKGSNDQC-LRVGDRYLYEAAEAREGEPWVYNGN----- 171  
*N. punctiforme* LVYPEK----AVFLCCTSNPSEALQQ-YPTNESPLYLQVYVEEK-TWETPEQ----- 181  
*Oscillatoria spp.* LVYPGK----AVFLCATNPSPATIQE-YPTAEHPLYLELVQAQ-SWETLDQ----- 189  
*P. falciparum* CYBEEKNKYYEAFLVKTTNPSSAIEQKNLSLDNKQAVVIAGEELNMSYLNLEQNNEF 236

*T. cruzi* VGVVVGATDPIASRVRVRAPTLWFLVPGIGAGG-----LKAALNAGLRAIGSGILL 227  
*L. donovani* VGVVVGATDPVALARVRARAPTLWFLVPGIGAGG-----SLKASLDAGLRAIGSGILL 225  
*N. punctiforme* LGEVGTNAEVALRAIAPERIMARSIWAGS-----MLRQILEAGLNDIGDGLL 235  
*Oscillatoria spp.* LGEVGV-VMADMARIRKAAPERLIIHGDIAEEDLTEEDLTQILAAGLSKNVEGILL 248  
*P. falciparum* LGEVVGANSYDENYIRTYFNCYLLSPIGAGN-----LHKTLTNGYHKYIEKILL 290

*T. cruzi* NYSRAMARAKDPRAAAKLSEDNLVR----- 254  
*L. donovani* NYSRGLARAADPRAAAELCEENAIR----- 252  
*N. punctiforme* PVPQDLGNTQLSEEVSLRAEINQLKTEIIHENSTCSVW----- 275  
*Oscillatoria spp.* PVPSPILVKEDNGKAIKLRDAVNEQRLRVVVEGSPCTDLW----- 288  
*P. falciparum* NIGRAITKNYPQKAAIMYYDQINAILKQNMESMTTIKENEFDCDEEYKSFVHLKDKIC 350

*T. cruzi* -----FGKACSTDAAAIVASRCNRFNGFT 279  
*L. donovani* -----FAKGASVELAKALVDSHCNRFNGFT 277  
*N. punctiforme* -----FPDVCFLNQHPYQDLLQLYDIDCMFNGFEV 306  
*Oscillatoria spp.* -----LPDVCFLQPEPHRDLILQLYDIGCIFGDFV 319  
*P. falciparum* EERKKKELVNNINDVNFNDDDDNNYDDGNSYSSYIKEMKLLKVVLLKVKAIKFGFT 410

*T. cruzi* LKSGKNSPIITDLRRIVTSPSILRVVAREYANLRLTDFDRIVGLYAAIPIATAIILE 338  
*L. donovani* LKSGKSSPIITDLRRIVTYPAIMRLVAREYAKVLRHYDFDRIAGLYAAIPIASAIINE 336  
*N. punctiforme* QASGAIFFPYITDLRKTINPQVFNQVLTAYEDLRLNLFDRLAGIYGSIFPTATGLALR 365  
*Oscillatoria spp.* QASGAVFPYITDLRPTIIPQIFHLIVSAYADLRLDLDFDRLAGIYGSIFPTATGLALR 378  
*P. falciparum* LKSKRKSNEYFSSGVVNVIVSSNII CFLLESELNKLSPDYLLGAYKGIPTMVSILTTFH 470

*T. cruzi* ANI-----LVYPRVEAKSCTKAAIEGTYMKGR-----VVVI 372  
*L. donovani* ANV-----LVYPRVEAKICTKAAIEGTYMKGR-----VVVI 370  
*N. punctiforme* LHCT-----MIFPRVEKAGTRRRVIEGTFPGET-----VVVV 399  
*Oscillatoria spp.* NERT-----MIFPRVEKAGGAGRIEGTFQAGEM-----VVVV 412  
*P. falciparum* LFEKPKYSNIFYLDRVEKKEVGDKNVIVGLLDLDDKDI LNLKKTKNQDEEKN 1311 530

*T. cruzi* DDIIVTGGTLEAEI EKLAAG-LEIVSIVVLDNEMGAKQLLGLGYELAAVTLTSLP 431  
*L. donovani* DDLVSTGETKVEAIEKLSAG-LEIVSIVVLDNEMGAKAFLLNLGYDFEAVGLHQILP 429  
*N. punctiforme* DDIIISGKIVMEGAGKLSAG-LNVNDIVVLDNEQGVKDRLONGYRSHSLTISEITN 458  
*Oscillatoria spp.* DDIIISGKIVMEGAAKLSAG-LEVEDIVVLDNEQGVKDRLONGYRAHALLTLEAE 471  
*P. falciparum* DDVETCGTLETEILAKLTYEHLKVVAVTVLNNNEYEINENNKIYFKIIEKRVGAPL 590

*T. cruzi* LWRKAGAITQKMKDVQSFMLEAS-SKL 458  
*L. donovani* LWRKGNAITSCOEADVRAFLGQWKQSKL 457  
*N. punctiforme* TLYQAGRINECFLFAEAS----- 477  
*Oscillatoria spp.* ILYQSGRVDSFCFNLLETVQ----- 491  
*P. falciparum* YSILYKDDIISMI----- 604

**Figure 25 Multiple sequence alignments of all known bifunctional OMPDC-OPRT enzymes.**

The sequence alignments of five different OMPDC-OPRT were performed using Clustal Omega program. Species names and accession numbers are as follows: kinetoplastid protozoa [*T. cruzi* (EKG07751.1), *L. donovani* (XP\_003859743.1)], cyanobacteria [*N. punctiforme* (ACC81973.1), *Oscillatoria spp.* (CBN54487.1)]. The yellow and pink highlighted boxes indicate identical and similar amino acids, respectively.

**4.4.2. Proteomic analysis of bifunctional *Pf*OMPDC-*Pf*OPRT enzyme**

The LC-MS/MS data of the bifunctional *Pf*OMPDC-*Pf*OPRT (Table 4) identified the sequences of 476-KYSNIFYLYDRK-487, 554-KVVAFIVLLNRN-565 and 585-RVGIPLYSILSYKD-598, containing amino acids responsible for the *Pf*OPRT component in the bifunctional *Pf*OMPDC-*Pf*OPRT.

Table 4 LC-MS/MS data analysis of the bifunctional *Pf*OMPDC-*Pf*OPRT enzyme.

Peptide <sup>a</sup>	Peptide score <sup>b</sup>	MH <sup>+</sup> (Da) <sup>c</sup>
KYSNIFYLYDRK	28	1352.6401
KVVAFIVLLNRN	29	1142.7176
RVGIPLYSILSYKD	39	1351.7751

<sup>a</sup> The peptide matches the OPRT of *P. falciparum* (3D7) protein with an ID of gi|529281050.

<sup>b</sup> The results were tested by the Decyder MS program with significance at  $p < 0.05$ , whereas peptide score is the score for each peptide identification, high peptide score indicates high significance.

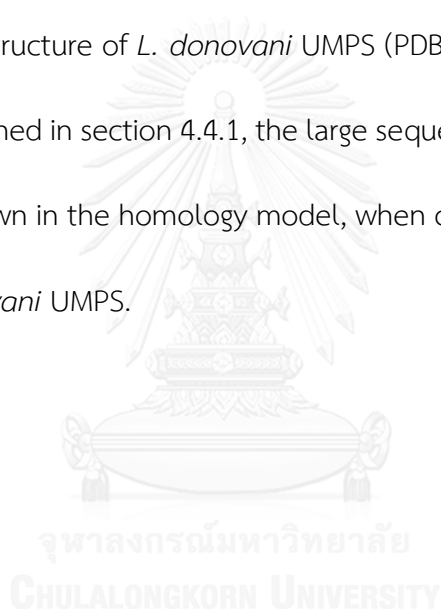
<sup>c</sup> MH<sup>+</sup> (Da) is a peptide mass.

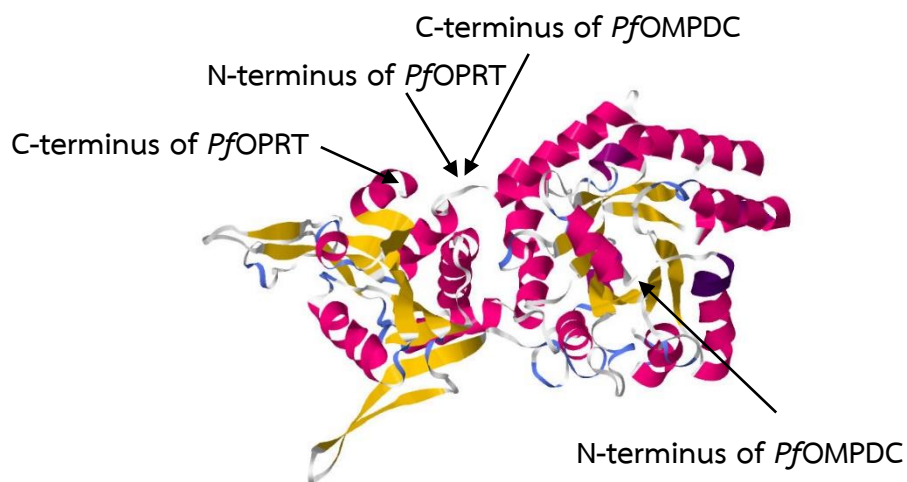
The peptide score of an MS/MS search is derived from the ions scores. The ion score is the MS/MS match on the data based, with significance threshold at  $p < 0.05$ , representing the total numbers of molecular mass matches for each query. The results suggest that the amino acid sequences of the peptides are bifunctional *Pf*OMPDC-*Pf*OPRT enzyme.

#### 4.4.3. Homology models of the bifunctional *PfOMPDC-PfOPRT* enzyme

The Phyre program predicts the secondary structure (e.g.  $\alpha$ -helix,  $\beta$ -strand, etc.) and the homology model of three dimensional (3D) structure of the bifunctional *PfOMPDC-PfOPRT* enzyme (residues 1-323 for *PfOMPDC* and 324-604 for *PfOPRT*, respectively) (Figure 26).

Here, the homology model of monomeric *PfOMPDC-PfOPRT* was constructed by using the crystal structure of *L. donovani* UMPS (PDB code 3QW4) as a template (Figure 27). As mentioned in section 4.4.1, the large sequence insertions of *PfOMPDC-PfOPRT* were not shown in the homology model, when compared to the amino acid sequence of *L. donovani* UMPS.





Jmol

Figure 26 Proposed homology model of the bifunctional *PfOMPDC-PfOPRT* enzyme in monomeric form.

The model was constructed by the Phyre program. The arrows indicate N- and C-terminus of *PfOMPDC* and *PfOPRT*. Pink ribbons represent the  $\alpha$ -helices, and yellow ribbons represent the  $\beta$ -strands.

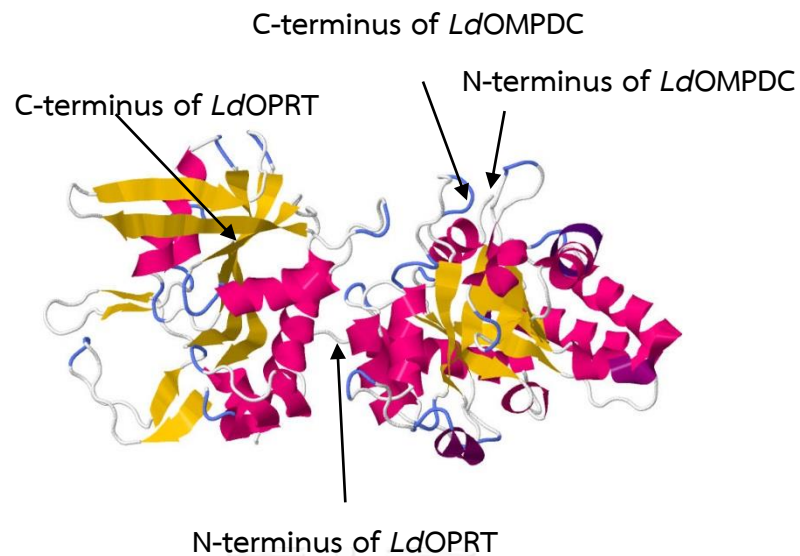


Figure 27 Crystal structure of the *L. donovani* UMPS (*LdUMPS*) enzyme in monomeric form.

The crystal structure model was constructed by the Phyre program. The arrows indicate N- and C-terminus of *LdOMPDC* and *LdOPRT*. Pink ribbons represent the  $\alpha$ -helices, and yellow ribbons represent the  $\beta$ -strands.

The monomeric *PfOMPDC*-*PfOPRT* model consisted of 23  $\alpha$ -helices and 17  $\beta$ -strands, whereas the monomeric *LdUMPS* model consisted of 19  $\alpha$ -helices and 19  $\beta$ -strands. The LC-MS/MS data of monofunctional *PfOPRT* identified the 168-EYGDKNVIVGNLDDDDKDILNLK-191 and 173-NVIVGNLDDDDKDILNLK-191 (75),



containing the amino acids responsible for  $\beta$ 14 strand and  $\alpha$ 20 helix of the bifunctional model, which presumably locate at the domain-domain interacting sites and bind between chain A and B of *PfOPRT*. On the other hand, the LC-MS/MS data of monofunctional *PfOMPDC* identified the sequence 175-DICYDEEKNK-184 locating at  $\alpha$ 8 helix (75), as a homodimeric binding between chain A and B of *PfOMPDC*. Based on the previous results on the LC-MS/MS data, the dimeric *PfOMPDC-PfOPRT* model was then constructed (Figure 28).



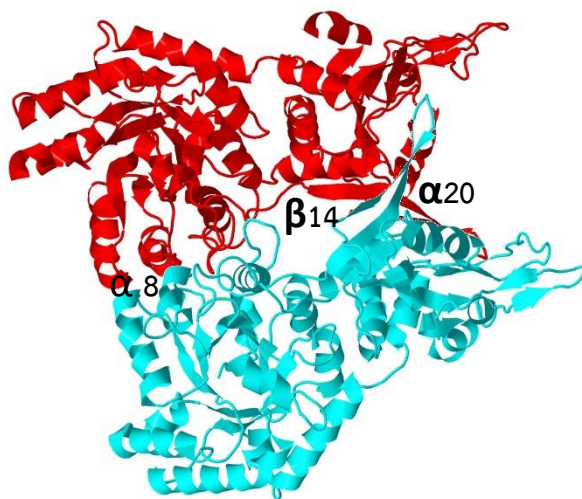


Figure 28 Proposed homology model of the bifunctional *PfOMPDC-PfOPRT* enzyme in dimeric form.

The model was constructed by the Phyre program. Red ribbons represent the monomeric *PfOMPDC-PfOPRT* enzyme (chain A), cyan ribbons represent the monomeric *PfOMPDC-PfOPRT* enzyme (chain B). The interacting sites are identified on  $\alpha 8$ , for *PfOMPDC*, and  $\beta 14$  and  $\alpha 20$  for *PfOPRT*.

The Phyre program also predict the homology model of 3D structure of *L. donovani* UMPS in dimeric form (Figure 29) (PDB code 3QW4), based on homodimeric interactions of *P. falciparum* enzyme (75). These homology models suggest that the bifunctional *PfOMPDC-PfOPRT* enzyme might have a folding 3D structure similar to the known crystal structure of *L. donovani* UMPS.

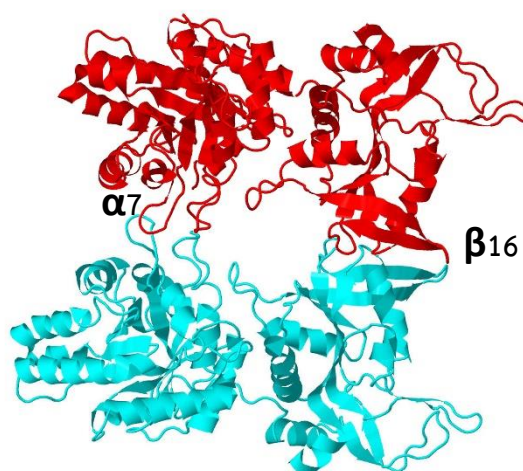


Figure 29 Homology model of the *LdUMPS* enzyme in dimeric form.

The model was constructed by the Phyre program. Red ribbons represent the *LdUMPS* monomer (chain A), cyan ribbons represent the *LdUMPS* monomer (chain B). The interacting sites are located on  $\alpha 7$  and  $\beta 16$  for *LdOMPDC* and *LdOPRT*, respectively, based on homodimeric interactions of *P. falciparum* enzyme (75).

## CHAPTER V

### DISCUSSION AND CONCLUSION

The fifth and sixth enzymes of the *de novo* pyrimidine biosynthetic pathway in *P. falciparum* were prepared as a fused bifunctional protein in the inversed order, as NH<sub>2</sub>-OMPDC-OPRT-COOH. The same fusion events are found in other protozoan parasites and in some cyanobacteria (18, 21, 79), which are different from human enzyme showing in the forward order as NH<sub>2</sub>-OPRT-OMPDC-COOH (16, 17, 80). The bifunctional *P. falciparum* OMPDC-OPRT fused gene was constructed and functionally expressed under stringent conditions in *E. coli*, as soluble form.

In this study, we had the PCR products processing and ligating into a Zero Blunt TOPO cloning vector. The OMPDC gene was firstly subcloned into a pTrcHisA expression vector and the OPRT gene was secondly subcloned into the pTrcHisA containing the OMPDC, encoding the PfOMPDC-PfOPRT and functionally expressed in *E. coli* TOP10 cells. The recombinant protein was expressed under a high concentration of IPTG induction. The fused bifunctional PfOMPDC-PfOPRT enzyme was purified by chromatography on the Ni-NTA-agarose affinity column and subsequently on the HiTrapQ anion-exchange column, as a fused bifunctional protein with catalytic activities of both enzymatic components. The purified enzyme had relatively high specific activities of both PfOPRT and PfOMPDC components in a range of 23-27 μmol/min/mg protein in the presence of stabilizers, comparing to their monofunctional and the

enzyme complex forms, which were also expressed in the single plasmid transformation to *E. coli* ranges of 7-21 and 8-25  $\mu\text{mol}/\text{min}/\text{mg}$  protein, respectively (24-27). The purity of the recombinant enzyme, assessed by 10% gel of SDS-PAGE and image analyses, was more than 90%. The enzyme had a monomeric form of 604 amino acid residues with a molecular mass of  $68 \pm 4$  kDa, corresponding to the predicted molecular mass of 70.812 kDa from the deduced amino acid sequence of the bifunctional protein. Confirmation of the fused bifunctional *Pf*OMPDC-*Pf*OPRT enzyme was performed by Western blot analysis, this experiment suggests that a positive band at a position of approximately 70 kDa molecular mass. The amino acid sequence of the bifunctional *Pf*OMPDC-*Pf*OPRT enzyme was confirmed after tryptic in-gel digestion of the bifunctional protein band in the SDS-PAGE gel by using LC-MS/MS and proteomic analyses. In *L. donovani* OMPDC-OPRT crystal structure, it is a tetramer containing two dimers each of OMPDC and OPRT (20). Oligomerization of the *P. falciparum* enzyme was determined by subjecting the purified enzyme onto the Superose 12 gel-filtration FPLC column. Co-elution of both activities as a single peak, corresponded to an apparent molecular mass of  $158 \pm 10$  kDa, this value is consistent with a dimeric state of quaternary structure of the enzyme, which would have a calculated molecular mass of approximately 142 kDa. It is then concluded that the prepared enzyme *Pf*OMPDC-*Pf*OPRT fusion is bifunctionally active and consists of two subunits of *Pf*OMPDC-*Pf*OPRT monomer, as dimeric formation in its native quaternary form. And then, the construction of recombinant plasmid containing fused bifunctional

*PfOMPDC-PfOPRT* gene to be studied of the fused bifunctional enzyme for kinetic characterization.

In this study, the catalysis of the OPRT and OMPDC component of the bifunctional enzyme followed the hyperbolic curve, as predicted by Michaelis-Menten kinetics, and showed a straight line on the Lineweaver-Burk plots. There were no kinetic indications as to indicate the allosteric property of the enzyme (i.e., exhibiting a sigmoidal plot due to multiple active sites), however, their  $K_m$  values at relatively low  $\mu\text{M}$  levels were also noted. It is shown that the upon purification both catalytic domains in fused bifunctional *PfOMPDC-PfOPRT* enzyme were markedly unstable. So, we figured out a novel approach to stabilize the activities of both OPRT and OMPDC enzymes in all buffers at the purification steps, by using substrate and product of OPRT and OMPDC, respectively (at concentrations of 0.5 mM PRPP and 0.5 mM UMP, respectively). However, the results also showed similar pattern of the chromatographic profiles on both the Ni-NTA affinity chromatography and subsequently on the HiTrapQ anion-exchange chromatography. Surprisingly, the total protein and enzymatic activities after the purification in the presence of the stabilizers (PRPP and UMP) were ~2-3-fold higher than those without stabilizers. The recovery yields of both enzymatic activities at the second step of the HiTrapQ anion-exchange column were upto ~30-35%, comparing to the first step of the Ni-NTA affinity column, and the specific activities of OMPDC and OPRT in a range of ~29-35  $\mu\text{mol}/\text{min}/\text{mg}$  protein were also achieved, especially the OPRT enzyme had more pronounced effect on instability than

the OMPDC enzyme. These results indicate that both enzymatic activities of the bifunctional enzyme can be stabilized by PRPP and UMP. As a previous report, purification and characterization of UMP synthase from the human placenta showed the co-elution of both OPRT and OMPDC with the molecular mass of 51 kDa. The OPRT of human placenta UMP synthase showed the marked lability during the purification. This labile behavior of our fused enzymes was very similar to that observed in UMP synthase purification from human placenta and mouse Ehrlich ascites carcinoma (16, 17). The loss of OPRT activity upon purification of the human placental UMP synthase is due to enzymatic inactivity rather than from the loss of OPRT component from the enzyme (16). After that, we examined the stability property of both domains in the bifunctional enzyme by keeping its in the absence and presence of 0.5 mM PRPP and 0.5 mM UMP at 4 °C. The half-life of the OPRT activity was ~0.5 and ~3 weeks, respectively. But the OMPDC activity was much more stable with the half-life of about ~3-4 weeks. Taken together, the *P. falciparum* enzyme has enhanced intrinsic instability, comparing the more stability of the monofunctional forms as described (26). The bacteria, such as *E. coli*, and yeast have increased concentrations of the monofunctional enzymes by about 10-50-fold, and the stability of both enzymes is apparently decreased (17). The large differences of the *in vivo* protein concentrations would reflect greater lability of the monofunctional enzymes than the bifunctional human enzyme (17), or *P. falciparum* multienzyme complex in previous studies in our laboratory (24-27). Moreover, the instable property has been noted in

the bifunctional *Leishmanial* OMPDC-OPRT or UMPS enzyme (20). It is noted that the part of the N-terminus of the *Ld*OPRT domain is obstructing of catalysis or optimal folding of the enzyme, this region was not appeared in the *Ld*UMPS crystal structure and quite far from the active site. It is possible that the *Ld*OPRT enzyme is itself intrinsic instable and is then stabilized by fusion to the *Ld*OMPDC. In 1996, Yablonski et al. had the same explanation for the fusion of the two domains in mammalian UMPS enzyme (17). This might be the increased stability of monofunctional *Ld*OPRT, which may have been the evolutionary driving force for the gene fusion event that brought these domains together. Because the limits of OPRT reaction, rate of UMP production by limiting the amount of OMP available to OMPDC, an increase in stability of *Ld*OPRT lead to increased enzyme efficiency, this would yield a higher orotate and PRPP to UMP production (20). However, the similar pattern of *P. falciparum* and human is that the OPRT activity existing in fused bifunctional *Pf*OMPDC-*Pf*OPRT enzyme and *Hs*UMPS showed a marked lability during the purification of fused bifunctional *Pf*OMPDC-*Pf*OPRT enzyme and *Hs*UMPS from *P. falciparum* and human placenta, respectively (16, 17). It can be concluded that the loss of OPRT activity upon the purification due to inactivation rather than from the loss of OPRT subunit (16, 17). Since there is a paucity information on the stability of another bifunctional enzymes, nevertheless, a case study of the native bifunctional rearranged domains of NH<sub>2</sub>-terminal ATP-sulfurylase and COOH-terminal adenosine 5'-phosphosulfate kinase explain the ability of individual domains in bifunctional enzyme to function independently has recently received



increasing attention. This enzyme has bifunctional role (both sulfurylase and kinase activities). For this reason, the selective advantages of the bifunctional enzyme over the expressed monofunctional enzyme, engineered sulfurylase and kinase to produce the two individual enzyme activities on separately expressed polypeptides (81). On the other hand, in 1997, Beaucamp et al. studied the stability and function of phosphoglycerate kinase-triosephosphate isomerase (PGK-TIM) fusion protein in a bacterium *Thermotoga maritima*. This study tells us that the fusion of PGK to TIM does not only enhances the intrinsic stability of TIM, but also its catalytic efficiency. Thus, it should be noted that the higher order of quaternary structure of the fusion protein contributes significantly to the intrinsic stability of TIM (82). The similar result was observed for the *HsUMPS*, showing that the activity of monofunctional domains are relatively lower stable when compared with the *HsUMPS*. To overcome the instability property, microorganisms often generate higher amounts of the monofunctional enzymes, compared with the bifunctional analogue in mammals (17).

Indeed, the fused bifunctional *PfOMPDC-PfOPRT* enzyme has more details on kinetic properties, comparing the OPRT and OMPDC in any other forms (monofunctional and enzyme complex forms). The bifunctional *PfOMPDC-PfOPRT* enzyme prepared in our studies were used to investigate details of kinetic and physical properties. Our studies found that the fused bifunctional *PfOMPDC-PfOPRT* enzyme shows the highest kinetic parameters. The parameters (e.g.,  $K_m$ , and catalytic efficiency ( $k_{cat}/K_m$ )) of the bifunctional *PfOMPDC-PfOPRT* enzyme are much more effective than

kinetic values of the enzyme complex and monofunctional forms, respectively. The bifunctional enzyme expressed a perfect catalytic efficiency ( $k_{\text{cat}}/K_m$ ) with  $3.6 \times 10^8 \text{ M}^{-1}\text{s}^{-1}$  for OPRT domain and  $4.9 \times 10^8 \text{ M}^{-1}\text{s}^{-1}$  for OMPDC domain, whereas the  $k_{\text{cat}}/K_m$  of the enzyme complex and monofunctional enzymes had the values of  $1.0 \times 10^6$  and  $2.3 \times 10^5 \text{ M}^{-1}\text{s}^{-1}$ , respectively, for OPRT, and  $2.9 \times 10^6$  and  $5.6 \times 10^5 \text{ M}^{-1}\text{s}^{-1}$ , respectively, for OMPDC. Most of these kinetic effects were due to the selectively enhanced up to 400-fold and 700-fold, respectively of the  $k_{\text{cat}}$  values for OPRT and 30-fold and 130-fold, respectively for OMPDC, on the other hand the  $K_m$  values were ~2-7 times lower than those of the monofunctional enzymes, but  $K_m$  values of enzyme complex were only slightly lower than bifunctional *Pf*OMPDC-*Pf*OPRT enzyme for OPRT components. All kinetic values for all forms of OPRT and OMPDC are shown in Table 5.

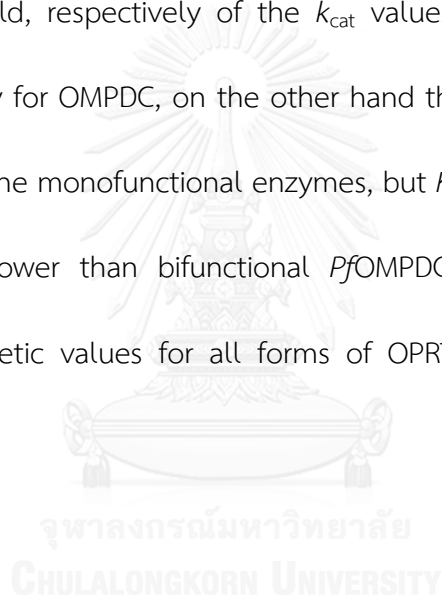


**Table 5** Comparison of kinetic constants of *P. falciparum* OPRT and OMPDC domains in bifunctional, enzyme complex and monofunctional enzymes.

	$K_m$ ( $\mu\text{M}$ )	$k_{\text{cat}}$ ( $\text{s}^{-1}$ )	$k_{\text{cat}}/K_m$ ( $\text{M}^{-1}\text{s}^{-1}$ )
OPRT: substrate orotate			
Bifunctional form	$8.3 \pm 0.4$	2,972.0	$3.6 \times 10^8$
Enzyme complex <sup>a</sup>	$7.0 \pm 0.3$	7.3	$1.0 \times 10^6$
Monofunctional form <sup>b</sup>	$18.2 \pm 0.9$	4.2	$2.3 \times 10^5$
OPRT: substrate PRPP			
Bifunctional form	$9.3 \pm 0.5$	3,534.0	$3.8 \times 10^8$
Enzyme complex <sup>a</sup>	$7.9 \pm 0.2$	7.8	$9.9 \times 10^5$
Monofunctional form <sup>b</sup>	$28.6 \pm 1.3$	3.2	$1.1 \times 10^5$
OMPDC: substrate OMP			
Bifunctional form	$2.0 \pm 0.1$	985.8	$4.9 \times 10^8$
Enzyme complex <sup>a</sup>	$10.5 \pm 0.5$	30.7	$2.9 \times 10^6$
Monofunctional form <sup>b</sup>	$13.4 \pm 1.2$	7.5	$5.6 \times 10^5$

<sup>a</sup> Data were taken from (27).

<sup>b</sup> Data were taken from (24, 26).

Comparison of the catalytic efficiency of the bifunctional *Pf*OMPDC-*Pf*OPRT enzyme ( $3.6\text{-}4.9 \times 10^8 \text{ M}^{-1}\text{s}^{-1}$ ) and *Ld*UMPS ( $\sim 10^4\text{-}10^6 \text{ M}^{-1}\text{s}^{-1}$ ) indicate that the malarial enzyme would favor efficient catalysis by markedly enhancing enzyme turnovers ( $k_{\text{cat}}$  values), especially the OPRT catalytic domain. Moreover, the two domains covalently linked by a longer amino acid sequence of the bifunctional enzyme were found to have a properly folded protein, shown by the Phyre homology model using the crystal structure of *L. donovani* OMPDC-OPRT as template and by having low  $\mu\text{M}$   $K_{\text{m}}$  values, as found in the monofunctional forms (Table 6). Our studies signify that the unstable OMPDC-OPRT enzyme is completely active under the conditions used.

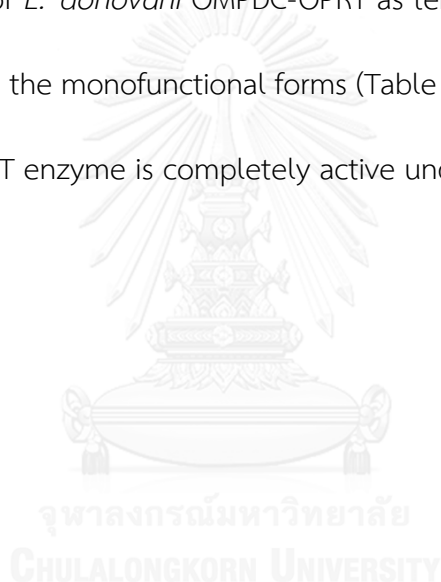


Table 6 Comparison of kinetic constants of OPRT and OMPDC domains in bifunctional *P. falciparum* (*Pf*) OMPDC-OPRT and *L. donovani* (*Ld*) UMPS enzyme.

	$K_m$ ( $\mu\text{M}$ )	$k_{\text{cat}}$ ( $\text{s}^{-1}$ )	$k_{\text{cat}}/K_m$ ( $\text{M}^{-1}\text{s}^{-1}$ )
OPRT: substrate orotate			
<i>Pf</i> OMPDC- <i>Pf</i> OPRT	$8.3 \pm 0.4$	2,972.0	$3.6 \times 10^8$
<i>Ld</i> UMPS <sup>a</sup>	127	1.2	$9.4 \times 10^4$
OPRT: substrate PRPP			
<i>Pf</i> OMPDC- <i>Pf</i> OPRT	$9.3 \pm 0.5$	3,534.0	$3.8 \times 10^8$
<i>Ld</i> UMPS <sup>a</sup>	151	1.2	$7.9 \times 10^4$
OMPDC: substrate OMP			
<i>Pf</i> OMPDC- <i>Pf</i> OPRT	$2.0 \pm 0.1$	985.8	$4.9 \times 10^8$
<i>Ld</i> UMPS <sup>a</sup>	9.9	12.9	$1.2 \times 10^6$

<sup>a</sup> Data were taken from (20).

Although previous studies on the intrinsic activity and stability of bifunctional human UMPS showed that the instability was due to the OPRT inactivity. In our experiments, the enzyme was used at a low concentration to assure that the protein existing in monomeric form in the absence of ligands, was at near  $K_m$  value so that a significant fraction of the enzyme population would remain ligand free at any time and therefore be in the monomeric form. The previous studies showed that the isolated human OMPDC domain, as well as the yeast OMPDC monofunctional protein, were very unstable in the monomeric form (17). The instability of the human OPRT domain was remarkable in demonstrating the complete stability of each catalytic center when it is fused in the bifunctional enzyme, even when UMPS was partly in the monomeric form. Explanation of the evidence for stability of the OMPDC and OPRT of the bifunctional UMPS is that there might be an interaction between the two different domains within the same subunit. Even if such interaction between the OPRT and OMPDC domains is transient, it could add sufficient stabilization to maintain the active structural conformation of each domain that the protein domain is monomeric form, so that there is no measurable loss of activity. By comparison, both the human OMPDC and OPRT domains were unstable at the monofunctional forms, as evident by dramatic loss of enzymatic activity (17).

Taken together, all available kinetic constants are shown in Table 7 and 8. Subsequently, comparison of catalytic efficiency of the bifunctional *Pf*OMPDC-*Pf*OPRT enzyme were  $3.6-4.9 \times 10^8 \text{ M}^{-1}\text{s}^{-1}$  and human UMPS (*Hs*UMPS) ( $\sim 10^6-10^7$

$M^{-1}s^{-1}$ ), and monofunctional *Pf*OPRT and *Pf*OMPDC were  $2.3-5.6 \times 10^5 M^{-1}s^{-1}$  and *Hs*OPRT and *Hs*OMPDC ( $\sim 10^5-10^7 M^{-1}s^{-1}$ ), indicate that the malarial enzyme, as bifunctional form, is higher efficient catalysis than *Hs*UMPS. On the one hand, the human enzyme in monofunctional forms has catalytic efficiency higher than the malarial enzyme, with a difference of about 100-fold.

**Table 7** Comparison of kinetic constants of OPRT and OMPDC domains in bifunctional *P. falciparum* OMPDC-OPRT and human UMPS enzyme.

	$K_m$ ( $\mu M$ )	$k_{cat}$ ( $s^{-1}$ )	$k_{cat}/K_m$ ( $M^{-1}s^{-1}$ )
OPRT: substrate orotate			
<i>Pf</i> OMPDC- <i>Pf</i> OPRT	8.3 $\pm$ 0.4	2,972.0	$3.6 \times 10^8$
<i>Hs</i> UMPS <sup>a</sup>	2.1 $\pm$ 0.12	4	$1.9 \times 10^6$
OMPDC: substrate OMP			
<i>Pf</i> OMPDC- <i>Pf</i> OPRT	2.0 $\pm$ 0.1	985.8	$4.9 \times 10^8$
<i>Hs</i> UMPS <sup>a</sup>	0.23 $\pm$ 0.0087	16	$7.0 \times 10^7$

<sup>a</sup> Data were taken from (17).

All available kinetic constants are shown in Table 8. Subsequently, comparison of catalytic efficiency of the monofunctional *Pf*OPRT and *Pf*OMPDC were  $2.3\text{-}5.6 \times 10^5 \text{ M}^{-1}\text{s}^{-1}$  and *Hs*OPRT and *Hs*OMPDC ( $\sim 10^5\text{-}10^7 \text{ M}^{-1}\text{s}^{-1}$ ), indicate that the human enzyme in monofunctional forms has higher catalytic efficiency than the malarial enzyme, with difference of about 100-fold.

**Table 8** Comparison of kinetic constants of OPRT and OMPDC in *P. falciparum* and human monofunctional enzymes.

	$K_m$ ( $\mu\text{M}$ )	$k_{\text{cat}}$ ( $\text{s}^{-1}$ )	$k_{\text{cat}}/K_m$ ( $\text{M}^{-1}\text{s}^{-1}$ )
OPRT: substrate orotate			
<i>Pf</i> OPRT <sup>a</sup>	18.2 $\pm$ 0.9	4.2	$2.3 \times 10^5$
<i>Hs</i> OPRT <sup>b</sup>	7.1 $\pm$ 0.27	2.9	$4.1 \times 10^5$
OMPDC: substrate OMP			
<i>Pf</i> OMPDC <sup>a</sup>	13.4 $\pm$ 1.2	7.5	$5.6 \times 10^5$
<i>Hs</i> OMPDC <sup>b</sup>	0.30 $\pm$ 0.018	13	$4.3 \times 10^7$

<sup>a</sup> Data were taken from (24, 26).

<sup>b</sup> Data were taken from (17).



As Cleland noted that the catalytic efficiency,  $k_{\text{cat}}/K_m$  values of many enzymes (e.g., carbonic anhydrase, triose phosphate isomerase, fumarase, etc.) approach the diffusion limit at which the rate of substrate diffuses to the enzyme, and are therefore “perfect” catalytic power (83, 84). The perfect enzyme has a  $k_{\text{cat}}/K_m$  of about  $10^8$ - $10^9$   $\text{M}^{-1}\text{s}^{-1}$ . And also Benner proposed that enzyme flexibility is important for the catalytic power; hence, the more flexible or unstable enzymes are better catalysis (85). Based on our studies, creating the fusion enzyme having the perfect catalytic power and enhanced flexibility, would support the Rosetta Stone model on molecular evolution of protein-protein interactions (64, 65). In 1958, the deliberation of the function of flexibility in enzyme catalysis, the well known “induced fit” hypothesis proposed by Koshland et.al. (86, 87), the exemplify change the active site conformation while substrate binding. In the enzyme catalysis, especially the active site position, is in a specific conformational change, which is different from one another. The X-ray crystallographic study of different forms of *E. coli* dihydrofolate reductase (DHFR), consist of holoenzyme, Michaelis complex, ternary product complex, tetrahydrofolate binary complex and tetrahydrofolate-nicotinamide adenine dinucleotide phosphate complex. The results indicate that the flexibility of enzyme is required for maximal catalytic activity (88). The activation of DHFR is accompanied by an increase in sensitivity of the enzyme molecule to heat and proteolysis and this is against with the perfection of Cleland and Benner proposal, however, this recommends substitution for conformational change from a compact and stable to somewhat an open and more

flexible structure (89). In addition, the necessity of enzyme catalysis is the flexibility instead of a well compact structure of the active site which is responsible for the catalysis (88). Comparing the catalytic efficiency with those of the enzyme complex and monofunctional enzymes indicate that the bifunctional *PfOMPDC-PfOPRT* enzyme is the best enzyme, a possible advantage of bifunctionality. Thus OMPDC-OPRT is an almost perfect enzyme, having evolved to nearly maximum catalytic efficiency, serving as a super-enzyme, expressing characteristics of more flexibility and maximal catalytic efficiency. Our studies provide proof-of-concept for the evidence to molecular evolution in the gene fusion on enzyme kinetic benefits.

The multiple alignments of amino acid sequences of all available bifunctional OMPDC-OPRT proteins were performed by using the Clustal Omega program. Alignment of the *PfOMPDC-OPRT* amino acid sequence was also done, comparing to the sequences of other four organisms. Our results indicate that the percent identity of *P. falciparum* OMPDC-OPRT sequence comparing among *T. cruzi*, *L. donovani*, *Oscillatoria spp.* and *N. punctiforme* were 31.89%, 30.65%, 22.72% and 22.65% respectively. Surprisingly, the *P. falciparum* OMPDC-OPRT is found to be the longest amino acid sequence (604 residues) having two internal insertions of amino acids (on the OMPDC component and on the OPRT component). This indicates that the *PfOMPDC-OPRT* property is identical to that of kinetoplastids, which are supported by Makiuchi T., et al. (18, 53). Additionally, the rationality of originated fused gene can be used as a phylogenetic marker.

By performing SDS-PAGE analysis in the previous reports, it is demonstrated that the monomeric forms of each monofunctional *Pf*OMPDC and *Pf*OPRT have molecular masses of 38 and 33 kDa, respectively (24-26). These studies showed that the monomeric forms of both enzymes are inactive (24-26), but the heterotetrameric form (enzyme complex) of both enzymes are active (26-28). In our studies, the dimeric form of bifunctional (*Pf*OMPDC-*Pf*OPRT)<sub>2</sub> enzyme is enzymatic active with approximately 142 kDa, determined by the Superose 12 gel-filtration FPLC column (Figure 17). The quaternary structure of the bifunctional *Pf*OMPDC-*Pf*OPRT enzyme is shown as a (*Pf*OMPDC-*Pf*OPRT)<sub>2</sub> homodimeric form, as shown in Figure 30. The bifunctional *Pf*OMPDC-*Pf*OPRT or *Plasmodium* UMPS enzyme is structurally similar to *Leishmania* UMPS (20) and human UMPS (17). Surprisingly, many enzymes are found to be active in the bifunctional form, such as DHFR and TS, whereas DHFR is a key enzyme in folate metabolism of the malaria parasite. The *Plasmodial* DHFR and TS enzymes are active in both the monofunctional and bifunctional enzymes (58, 62).

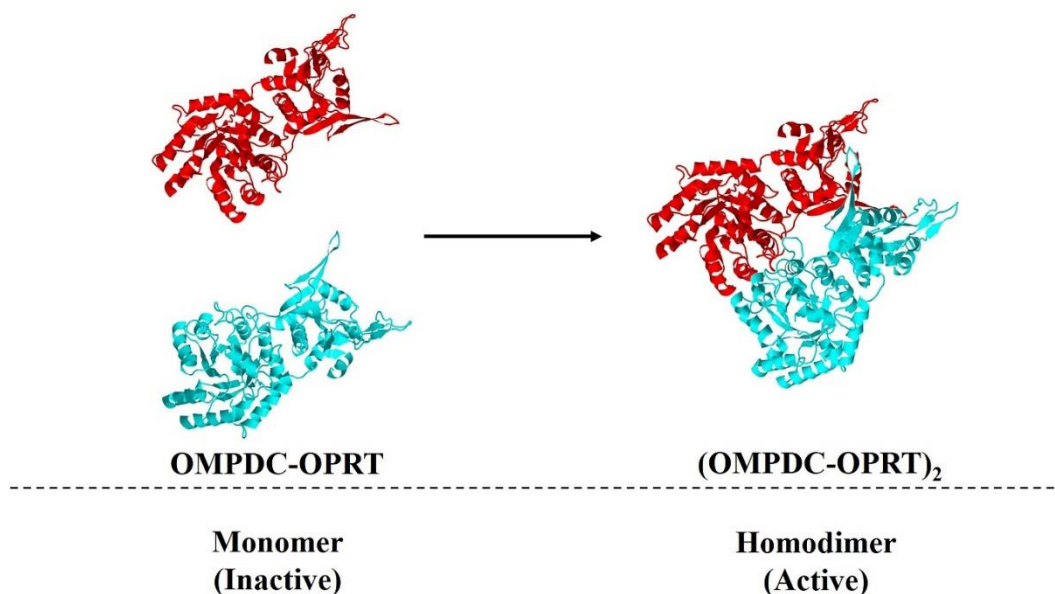


Figure 30 The sequential steps for monomer and dimer formation of the bifunctional *PfOPRT-PfOMPDC* enzyme.

Each of the inactive monomer of *PfOMPDC-PfOPRT* is associated into homodimer (*PfOMPDC-PfOPRT*)<sub>2</sub> without allosteric coupled active sites.

The evolution of protein-protein interactions is proposed as the “Rosetta Stone” model (Figure 31). Firstly, they are initiated with fusion of the genes that the non-interacting separate proteins, leading to expression of the fused two-domain protein. In the fused protein, the domains as colocalized proteins have high level of effective concentrations, and somewhat few mutations have created a basal binding site between the domains, which are optimized by sequential mutations. The

interacting domains are then separated by recombination with another gene to create an interacting pair of proteins. The interaction of pair proteins are produced by the gene fission, thus the Rosetta Stone hypothesis of the gene fusion in the first step is not essential. The another probable mutation, a loop shortening that bears to a domain-swapped homodimer. This path of evolution to homo-oligomers has been discussed earlier, and is analogous to homo-oligomers of the evolutionary path, as proposed for hetero-oligomers formation (64, 65).



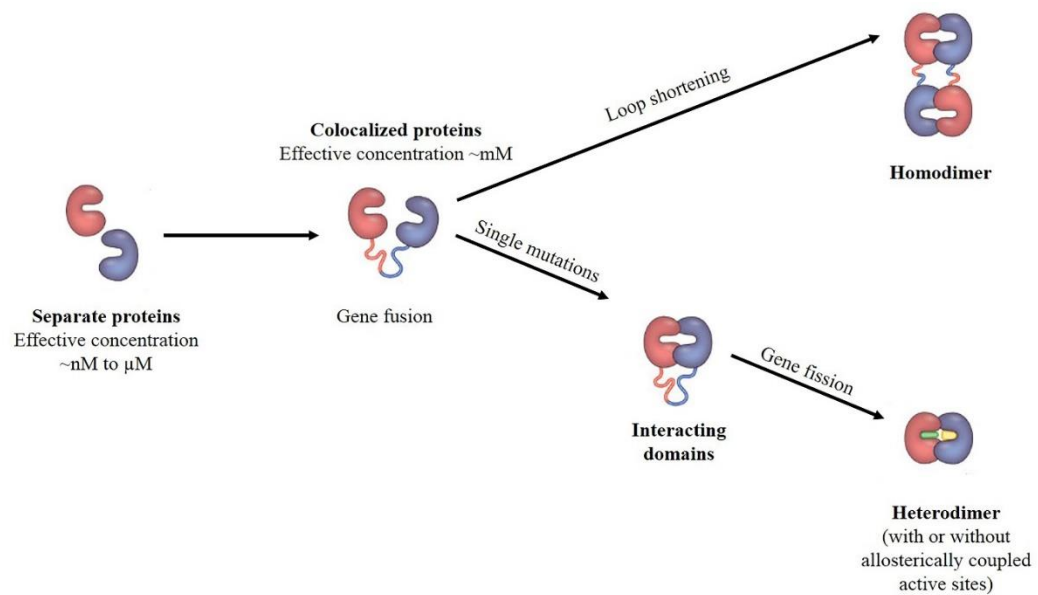


Figure 31 Rosetta Stone hypothesis of evolution for protein- protein interactions in colocalization and allostery by mutations.

Most cellular proteins have effective concentrations at about nM to  $\mu$ M levels, as separate proteins. Interaction between these two proteins are likely to be occurred when they are colocalized. The colocalization is originated by gene fusion that results in both proteins being part of the same polypeptide chain, with effective by concentrations at mM levels. Furthermore, single mutations that increase the affinity of the two domains for each other, or that introduce allostery, are then selected, resulting in tight interactions between these sites or allosteric coupling. Additional single genetic events such as gene fission or loop shortening can result in a strongly interacting heterodimer and homodimer, respectively (Adapted from (65)).

The fused bifunctional enzyme of the malaria parasite has illustrated the efficiency of functional kinetic advantage, which in the colocalized proteins principles for evolutionary origin, that the increase random mutation of protein, may be reduced the free energy to create a tightly binding monomer resulting increased its concentration, that can amplify the effect of protein function. And also with allosteric property in the protein-protein interaction, in which protein networks or complex system are regulated by allosteric control (64, 65) (Figure 32).

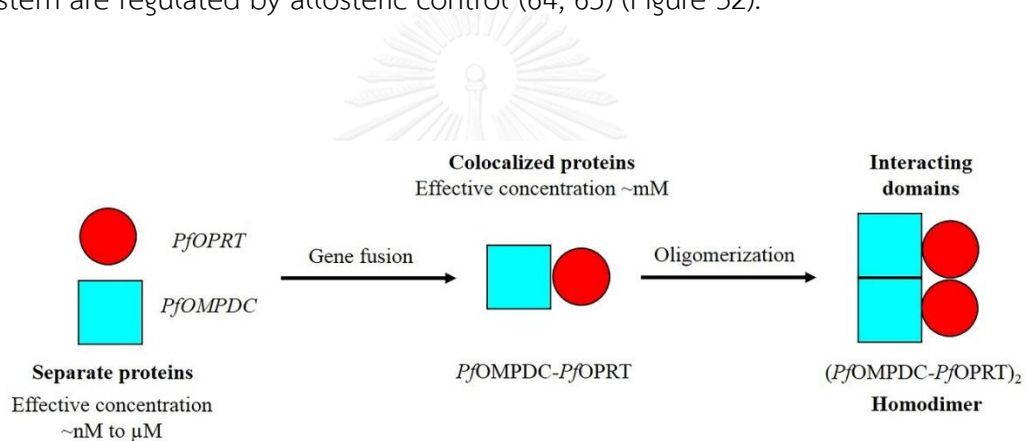


Figure 32 Evolution of protein-protein interactions of the fused bifunctional *PfOMPDC-PfOPRT* enzyme.

Interaction between these both proteins are likely to be occurred when they are colocalized as gene fusion to have a fused bifunctional enzyme. Other details are shown in Figure 31.

The protein-protein interactions of the fused bifunctional (*Pf*OMPDC-*Pf*OPRT)<sub>2</sub> (Figure 33A) are then compared to *Leishmania* (Figure 33B) and human UMPS (Figure 33C) enzymes. In our studies, the *OPRT* and *OMPDC* genes and their corresponding enzymes in *Plasmodium* are constructed similarly to *L. donovani* UMPS, as OMPDC-OPRT orientation. They are different from the human UMPS, whereas the *Pf*OPRT and *Pf*OMPDC are the inversely linked fusion as what found in *L. donovani* and other species (20). In addition, the bifunctional *Ld*UMPS structural models do not possess any significant domain-domain interaction between OPRT and OMPDC, and exist as the active tetrameric structure (20) (Figure 33B). Studies of the *L. donovani* enzyme structure have superimposed the position of human OPRT and OMPDC monofunctional enzymes on *L. donovani* UMPS, illustrating the C-terminus of OPRT is linked together with the N-terminus of OMPDC by having 20 amino acid residues missing at the joining region (20) (Figure 33C). Furthermore, the studies of the bifunctional human UMPS (OPRT-OMPDC) demonstrate that the active form is dimer (17). However, the previous studies show that the homology 3D model in space-filling representation of human UMPS enzyme is in the dimeric form, as (OPRT-OMPDC)<sub>2</sub> (80, 90). The homology models are constructed and compared for the possible homology models by the Phyre program of dimeric (*Pf*OMPDC-*Pf*OPRT)<sub>2</sub> in the malaria parasite and human UMPS (OPRT-OMPDC)<sub>2</sub> (Figure 33).





Figure 33 Comparative structural models of *P. falciparum* OMPDC-OPRT, *L. donovani* and human UMPS.

Panel A, the homology model of dimeric (*Pf*OPRT-*Pf*OMPDC)<sub>2</sub> of *P. falciparum*; panel B, the crystal structure of tetramer (OMPDC-OPRT)<sub>4</sub> of *L. donovani* UMPS (PDB ID 3QW4); and panel C, superimposition of human OPRT and OMPDC monofunctional enzymes on *Ld*UMPS. The structures of the human OPRT (blue, PDB ID 2WNS) and OMPDC (green, PDB ID 2EAW) domains of UMPS are shown by superimposition on the template structure of *Ld*UMPS, where the N-terminus represent red color and C-terminus represent yellow color. Panels B and C were taken from French JB., et al. (20).

The Phyre program predicts the secondary structure (e.g.,  $\alpha$ -helix,  $\beta$ -strand, etc.) and the homology model of three dimensional (3D) structure of the bifunctional *Pf*OMPDC-*Pf*OPRT enzyme residues 1- 323 for *Pf*OMPDC and 324- 604 for *Pf*OPRT, respectively) (Figure 26), was constructed by using the crystal structure of *Ld*UMPS (PDB code 3QW4) as a template. The large sequence insertions of *Pf*OMPDC-*Pf*OPRT

were not shown in the homology model, when compared to the amino acid sequence of *LdUMPS*. The *LdUMPS* 3D structure was predicted using search models of *LdOMPDC* and *Corynebacterium diphtheriae* OPRT (PDB code 2P1Z). The linker between the OMPDC and OPRT domains were shown in both *LdUMPS* monomers; though, these two monomers could not be superimposed due to their differences in the position of the domains relatively to the adjacent domains. In the *LdUMPS* structure, two OMPDC domains are formed as a tight dimer, similarly to the monofunctional *LdOMPDC* structure. In the *LdUMPS* structure, two domains of each chain are linked by covalent bond. The tetrameric form had dimeric *LdOMPDC* and *LdOPRT* functional domains, consistent with homologous structures of the monofunctional enzymes. The PISA server analyzed the most stable structure in solution of quaternary structure as the tetrameric form. Additionally, the surface contact between the OPRT and OMPDC domains was firmly packed on one face of the OMPDC and the OPRT dimer (20).

The formation of dimeric  $((PfOPRT)(PfOMPDC))_2$  is therefore stable in soluble. As indicated by the gel filtration chromatography (Figure 17), the presence of a ligand (e.g. substrate, product, high salt) causes a conformational change to occur (26). The 3D structure of the bifunctional *PfOMPDC-PfOPRT* enzyme indicates that this change can take place. The ligand-dependent conformational change is likely to cause dimerization of domains, leading to a complete dimeric form of the bifunctional *PfOMPDC-PfOPRT* enzyme. The dimeric enzyme would be catalytically competent for both OMPDC and OPRT reactions.

In addition, some bifunctional enzymes are demonstrated in *Plasmodium*, for examples, DHFS-TS ( 58, 62) , G6PD-6PGL ( 63) and S-adenosylmethionine decarboxylase/ ornithine decarboxylase (AdoMetDC- ODC) ( 91). In case, ODC and AdoMetDC are originated as two separate proteins in all organisms so far examined. In *P. falciparum*, both enzymes are exceptional linked to form the bifunctional enzyme. The AdoMetDC domain is located at the N-terminus, where the ODC domain is at C-terminus (92).

In summary, the fused bifunctional OMPDC-OPRT enzyme is described in many organisms from bacteria to protozoan parasites. We produced gene fusions of *P. falciparum* OMPDC-OPRT, and expressed as the recombinant bifunctional protein in *E. coli* Top10 cells, as soluble form. The enzyme was purified to near homogeneity using the Ni-NTA-agarose affinity and the anion-exchange chromatographies. The fused bifunctional PfOMPDC-PfOPRT enzyme was confirmed by Western blot analysis and proteomic approach. The molecular mass of native fused bifunctional enzyme was determined by gel-filtration chromatographic column, having an apparent molecular mass of 158 kDa. The enzyme was active and functioned in a dimeric form. The enzymatic activities, although unstable, were stabilized by its substrate and product during purification and long-term storage. Furthermore, the enzyme expressed a perfect catalytic efficiency ( $k_{cat}/K_m$ ). The turnover number ( $k_{cat}$ ) was selectively enhanced up to three orders of magnitude, while the  $K_m$  was not much affected and remained at low  $\mu\text{M}$  levels. Comparing the catalytic efficiency with the monofunctional

enzymes and the multienzyme complex indicate that the bifunctional *Pf*OMPDC-*Pf*OPRT enzyme would favor efficient catalysis by markedly increasing the turnover number, a possible advantage of bifunctionality. The bifunctional *Pf*OMPDC-*Pf*OPRT enzyme is also important in evolutionary pattern of the malaria parasite. Taken from the benefits of kinetic characterizations, the bifunctional *Pf*OMPDC-*Pf*OPRT enzyme is much more catalytically active than monofunctional enzymes and multienzyme complex. The  $K_m$  values of the bifunctional *Pf*OMPDC-*Pf*OPRT enzyme are lower than monofunctional enzymes and multienzyme complex.

The gene fusion study, shown in Figure 32, is supported by Rosetta Stone model (Figure 31) with lines of evidence as follows: (1) the cellular proteins have effective concentrations at about nM to  $\mu$ M, as separate proteins, (2) and then interaction between two proteins occurred when they are colocalized, (3) finally, the gene fission or loop shortening can result in a strongly interacting homodimer. The kinetic parameters are favored for the fused bifunctional *P. falciparum* enzyme, as compared to the bifunctional *L. donovani* UMPS enzyme. By analogy, loss of stability of both enzymes are noted, their activities can be stabilized by using substrate and product of OPRT and OMPDC in all buffers at the purification steps and long-term storage.

Our study lends proof-of-concept that the two enzymes, creating a “super-enzyme” with perfect catalytic power and more flexibility (83, 85), reflects

cryptic relationship of enzymatic reactivities and metabolic functions on molecular evolution. This unique property, thus the possibility of a new drug target for the bifunctional *Pf*OMPDC-*Pf*OPRT enzyme, which can be further exploited for a rational drug design approach for more effective antimalarials (93).



## REFERENCES

1. Singh B, Kim SL, Matusop A, Radhakrishnan A, Shamsul SS, Cox-Singh J, et al. A large focus of naturally acquired *Plasmodium knowlesi* infections in human beings. *Lancet*. 2004;363(9414):1017-24.
2. Flannery EL, Chatterjee AK, Winzeler EA. Antimalarial drug discovery approaches and progress towards new medicines. *Nat Rev Microbiol*. 2013;11(12):849-62.
3. Krungkrai SR, Krungkrai J. Insights into the pyrimidine biosynthetic pathway of human malaria parasite *Plasmodium falciparum* as chemotherapeutic target. *Asian Pac J Trop Med*. 2016;9(6):525-34.
4. Palacpac NM, Arisue N, Tougan T, Ishii KJ, Horii T. *Plasmodium falciparum* serine repeat antigen 5 (SE36) as a malaria vaccine candidate. *Vaccine*. 2011;29(35):5837-45.
5. Snow RW, Guerra CA, Noor AM, Myint HY, Hay SI. The global distribution of clinical episodes of *Plasmodium falciparum* malaria. *Nature*. 2005;434(7030):214-7.
6. Hay SI, Okiro EA, Gething PW, Patil AP, Tatem AJ, Guerra CA, et al. Estimating the global clinical burden of *Plasmodium falciparum* malaria in 2007. *PLoS Med*. 2010;7(6):e1000290.
7. Boivin MJ, Bangirana P, Byarugaba J, Opoka RO, Idro R, Jurek AM, et al. Cognitive impairment after cerebral malaria in children: a prospective study. *Pediatrics*. 2007;119(2):e360-6.
8. Blut A. Malaria. *Transfus Med Hemother*. 2009;36(1):48-60.
9. Gero AM, O'Sullivan WJ. Purines and pyrimidines in malarial parasites. *Blood Cells*. 1990;16(2-3):467-84; discussion 85-98.
10. Jones ME. Pyrimidine nucleotide biosynthesis in animals: genes, enzymes, and regulation of UMP biosynthesis. *Annu Rev Biochem*. 1980;49:253-79.
11. Evans DR, Guy HI. Mammalian pyrimidine biosynthesis: fresh insights into an ancient pathway. *J Biol Chem*. 2004;279(32):33035-8.

12. Krungkrai J, Krungkrai SR, Phakanont K. Antimalarial activity of orotate analogs that inhibit dihydroorotase and dihydroorotate dehydrogenase. *Biochem Pharmacol.* 1992;43(6):1295-301.
13. Cassera MB, Zhang Y, Hazleton KZ, Schramm VL. Purine and pyrimidine pathways as targets in *Plasmodium falciparum*. *Curr Top Med Chem.* 2011;11(16):2103-15.
14. Umezumi K, Amaya T, Yoshimoto A, Tomita K. Purification and properties of orotidine-5'-phosphate pyrophosphorylase and orotidine-5'-phosphate decarboxylase from bakers' Yeast. *J Biochem.* 1971;70(2):249-62.
15. Quinn CL, Stephenson BT, Switzer RL. Functional organization and nucleotide sequence of the *Bacillus subtilis* pyrimidine biosynthetic operon. *J Biol Chem.* 1991;266(14):9113-27.
16. Livingstone LR, Jones ME. The purification and preliminary characterization of UMP synthase from human placenta. *J Biol Chem.* 1987;262(32):15726-33.
17. Yablonski MJ, Pasek DA, Han BD, Jones ME, Traut TW. Intrinsic activity and stability of bifunctional human UMP synthase and its two separate catalytic domains, orotate phosphoribosyltransferase and orotidine-5'-phosphate decarboxylase. *J Biol Chem.* 1996;271(18):10704-8.
18. Makiuchi T, Nara T, Annoura T, Hashimoto T, Aoki T. Occurrence of multiple, independent gene fusion events for the fifth and sixth enzymes of pyrimidine biosynthesis in different eukaryotic groups. *Gene.* 2007;394(1-2):78-86.
19. Mejean A, Mazmouz R, Mann S, Calteau A, Medigue C, Ploux O. The genome sequence of the cyanobacterium *Oscillatoria sp.* PCC 6506 reveals several gene clusters responsible for the biosynthesis of toxins and secondary metabolites. *J Bacteriol.* 2010;192(19):5264-5.
20. French JB, Yates PA, Soysa DR, Boitz JM, Carter NS, Chang B, et al. The *Leishmania donovani* UMP synthase is essential for promastigote viability and has an unusual tetrameric structure that exhibits substrate-controlled oligomerization. *J Biol Chem.* 2011;286(23):20930-41.

21. Gao G, Nara T, Nakajima-Shimada J, Aoki T. Novel organization and sequences of five genes encoding all six enzymes for de novo pyrimidine biosynthesis in *Trypanosoma cruzi*. *J Mol Biol*. 1999;285(1):149-61.
22. Nara T, Hshimoto T, Aoki T. Evolutionary implications of the mosaic pyrimidine-biosynthetic pathway in eukaryotes. *Gene*. 2000;257(2):209-22.
23. Krungkrai J, Prapunwatana P, Wichitkul C, Reungprapavut S, Krungkrai SR, Horii T. Molecular biology and biochemistry of malarial parasite pyrimidine biosynthetic pathway. *Southeast Asian J Trop Med Public Health*. 2003;34 Suppl 2:32-43.
24. Krungkrai SR, Aoki S, Palacpac NM, Sato D, Mitamura T, Krungkrai J, et al. Human malaria parasite orotate phosphoribosyltransferase: functional expression, characterization of kinetic reaction mechanism and inhibition profile. *Mol Biochem Parasitol*. 2004;134(2):245-55.
25. Krungkrai SR, Prapunwattana P, Horii T, Krungkrai J. Orotate phosphoribosyltransferase and orotidine 5'-monophosphate decarboxylase exist as multienzyme complex in human malaria parasite *Plasmodium falciparum*. *Biochem Biophys Res Commun*. 2004;318(4):1012-8.
26. Krungkrai SR, DelFraino BJ, Smiley JA, Prapunwattana P, Mitamura T, Horii T, et al. A novel enzyme complex of orotate phosphoribosyltransferase and orotidine 5'-monophosphate decarboxylase in human malaria parasite *Plasmodium falciparum*: physical association, kinetics, and inhibition characterization. *Biochemistry*. 2005;44(5):1643-52.
27. Kanchanaphum P, Krungkrai J. Kinetic benefits and thermal stability of orotate phosphoribosyltransferase and orotidine 5'-monophosphate decarboxylase enzyme complex in human malaria parasite *Plasmodium falciparum*. *Biochem Biophys Res Commun*. 2009;390(2):337-41.
28. Kanchanaphum P, Krungkrai J. Co-expression of human malaria parasite *Plasmodium falciparum* orotate phosphoribosyltransferase and orotidine 5'-monophosphate decarboxylase as enzyme complex in *Escherichia coli*: a novel strategy for drug development. *Asian Biomed*. 2010;4(2):297-306.



29. Abdo M, Zhang Y, Schramm VL, Knapp S. Electrophilic aromatic selenylation: new OPRT inhibitors. *Org Lett*. 2010;12(13):2982-5.
30. Takashima Y, Mizohata E, Krungkrai SR, Fukunishi Y, Kinoshita T, Sakata T, et al. The in silico screening and X-ray structure analysis of the inhibitor complex of *Plasmodium falciparum* orotidine 5'-monophosphate decarboxylase. *J Biochem*. 2012;152(2):133-8.
31. Breman JG, Alilio MS, Mills A. Conquering the intolerable burden of malaria: what's new, what's needed: a summary. *Am J Trop Med Hyg*. 2004;71(2 Suppl):1-15.
32. Cowman AF, Healer J, Marapana D, Marsh K. Malaria: biology and disease. *Cell*. 2016;167(3):610-24.
33. Riley EM. Is T-cell priming required for initiation of pathology in malaria infections. *Immunol Today*. 1999;20(5):228-33.
34. Ndungu FM, Urban BC, Marsh K, Langhorne J. Regulation of immune response by *Plasmodium*-infected red blood cells. *Parasite Immunol*. 2005;27(10-11):373-84.
35. Organization WH. Global Health Observatory (GHO) data 2015 [cited 2017. Available from: <http://www.who.int/gho/malaria/en/>.
36. Renia L, Goh YS. Malaria parasites: the great escape. *Front Immunol*. 2016;7:463.
37. Gardner MJ, Hall N, Fung E, White O, Berriman M, Hyman RW, et al. Genome sequence of the human malaria parasite *Plasmodium falciparum*. *Nature*. 2002;419(6906):498-511.
38. Hall N, Carlton J. Comparative genomics of malaria parasites. *Curr Opin Genet Dev*. 2005;15(6):609-13.
39. Carlton JM, Escalante AA, Neafsey D, Volkman SK. Comparative evolutionary genomics of human malaria parasites. *Trends Parasitol*. 2008;24(12):545-50.
40. Pain A, Bohme U, Berry AE, Mungall K, Finn RD, Jackson AP, et al. The genome of the simian and human malaria parasite *Plasmodium knowlesi*. *Nature*. 2008;455(7214):799-803.

41. Xue HY, Forsdyke DR. Low-complexity segments in *Plasmodium falciparum* proteins are primarily nucleic acid level adaptations. *Mol Biochem Parasitol.* 2003;128(1):21-32.
42. Frugier M, Bour T, Ayach M, Santos MA, Rudinger-Thirion J, Theobald-Dietrich A, et al. Low complexity regions behave as tRNA sponges to help co-translational folding of *plasmodial* proteins. *FEBS Lett.* 2010;584(2):448-54.
43. Pizzi E, Frontali C. Low-complexity regions in *Plasmodium falciparum* proteins. *Genome Res.* 2001;11(2):218-29.
44. Baca AM, Hol WGJ. Overcoming codon bias: A method for high-level overexpression of *Plasmodium* and other AT-rich parasite genes in *Escherichia coli*. *Int J Parasitol.* 2000;30(2):113-8.
45. Winzeler EA. Malaria research in the post-genomic era. *Nature.* 2008;455(7214):751-6.
46. Devlin TM. Textbook of biochemistry with clinical correlations. 7<sup>th</sup> ed. New York: John Wiley & Sons; 2011.
47. Roskoski R. Biochemistry. 1<sup>st</sup> ed. Philadelphia: Saunders; 1996.
48. Huang M, Graves LM. De novo synthesis of pyrimidine nucleotides; emerging interfaces with signal transduction pathways. *Cell Mol Life Sci.* 2003;60(2):321-36.
49. de Montigny J, Belarbi A, Hubert JC, Lacroute F. Structure and expression of the URA5 gene of *Saccharomyces cerevisiae*. *Mol Gen Genet.* 1989;215(3):455-62.
50. Tokuoka K, Kusakari Y, Krungkrai SR, Matsumura H, Kai Y, Krungkrai J, et al. Structural basis for the decarboxylation of orotidine 5'-monophosphate (OMP) by *Plasmodium falciparum* OMP decarboxylase. *J Biochem.* 2008;143(1):69-78.
51. Zhang Y, Deng H, Schramm VL. Leaving group activation and pyrophosphate ionic state at the catalytic site of *Plasmodium falciparum* orotate phosphoribosyltransferase. *J Am Chem Soc.* 2010;132(47):17023-31.
52. Kumar S, Krishnamoorthy K, Mudeppa DG, Rathod PK. Structure of *Plasmodium falciparum* orotate phosphoribosyltransferase with autologous inhibitory protein-protein interactions. *Acta Crystallogr F Struct Biol Commun.* 2015;71(Pt 5):600-8.

53. Makiuchi T, Annoura T, Hashimoto T, Murata E, Aoki T, Nara T. Evolutionary analysis of synteny and gene fusion for pyrimidine biosynthetic enzymes in Euglenozoa: an extraordinary gap between kinetoplastids and diplomonads. *Protist*. 2008;159(3):459-70.
54. Suchi M, Mizuno H, Kawai Y, Tsuboi T, Sumi S, Okajima K, et al. Molecular cloning of the human UMP synthase gene and characterization of point mutations in two hereditary orotic aciduria families. *Am J Hum Genet*. 1997;60(3):525-39.
55. Miller BG, Hassell AM, Wolfenden R, Milburn MV, Short SA. Anatomy of a proficient enzyme: the structure of orotidine 5'-monophosphate decarboxylase in the presence and absence of a potential transition state analog. *Proc Natl Acad Sci U S A*. 2000;97(5):2011-6.
56. Ahuja A, Purcarea C, Ebert R, Sadecki S, Guy HI, Evans DR. *Aquifex aeolicus* dihydroorotase: association with aspartate transcarbamoylase switches on catalytic activity. *J Biol Chem*. 2004;279(51):53136-44.
57. Zhang P, Martin PD, Purcarea C, Vaishnav A, Brunzelle JS, Fernando R, et al. Dihydroorotase from the hyperthermophile *Aquifex aeolicus* is activated by stoichiometric association with aspartate transcarbamoylase and forms a one-pot reactor for pyrimidine biosynthesis. *Biochemistry*. 2009;48(4):766-78.
58. Osorio E, Aguilera C, Naranjo N, Marin M, Muskus C. Biochemical characterization of the bifunctional enzyme dihydrofolate reductase-thymidylate synthase from *Leishmania (Viannia)* and its evaluation as a drug target. *Biomedica*. 2013;33(3):393-401.
59. Garrett CE, Coderre JA, Meek TD, Garvey EP, Claman DM, Beverley SM, et al. A bifunctional thymidylate synthetase-dihydrofolate reductase in protozoa. *Mol Biochem Parasitol*. 1984;11:257-65.
60. Ivanetich KM, Santi DV. Bifunctional thymidylate synthase-dihydrofolate reductase in protozoa. *FASEB J*. 1990;4(6):1591-7.

61. Atreya CE, Anderson KS. Kinetic characterization of bifunctional thymidylate synthase-dihydrofolate reductase (TS-DHFR) from *Cryptosporidium hominis*: a paradigm shift for ts activity and channeling behavior. *J Biol Chem*. 2004;279(18):18314-22.
62. Chanama M, Chitnumsub P, Yuthavong Y. Subunit complementation of thymidylate synthase in *Plasmodium falciparum* bifunctional dihydrofolate reductase-thymidylate synthase. *Mol Biochem Parasitol*. 2005;139(1):83-90.
63. Stover NA, Dixon TA, Cavalcanti AR. Multiple independent fusions of glucose-6-phosphate dehydrogenase with enzymes in the pentose phosphate pathway. *PLoS One*. 2011;6(8):e22269.
64. Marcotte EM, Pellegrini M, Ng HL, Rice DW, Yeates TO, Eisenberg D. Detecting protein function and protein-protein interactions from genome sequences. *Science*. 1999;285(5428):751-3.
65. Kuriyan J, Eisenberg D. The origin of protein interactions and allostery in colocalization. *Nature*. 2007;450(7172):983-90.
66. Fletcher S, Hamilton AD. Targeting protein-protein interactions by rational design: mimicry of protein surfaces. *J R Soc Interface*. 2006;3(7):215-33.
67. Wells JA, McClendon CL. Reaching for high-hanging fruit in drug discovery at protein-protein interfaces. *Nature*. 2007;450(7172):1001-9.
68. Yuvaniyama J, Chitnumsub P, Kamchonwongpaisan S, Vanichtanankul J, Sirawaraporn W, Taylor P, et al. Insights into antifolate resistance from malarial DHFR-TS structures. *Nat Struct Biol*. 2003;10(5):357-65.
69. Towbin H, Staehelin T, Gordon J. Electrophoretic transfer of proteins from polyacrylamide gels to nitrocellulose sheets: procedure and some applications. *Proc Natl Acad Sci U S A*. 1979;76(9):4350-4.
70. Cleland WW. Statistical analysis of enzyme kinetic data. *Methods Enzymol*. 1979;63:103-38.
71. Segel IH. Enzyme kinetics: behavior and analysis of rapid equilibrium and steady state enzyme systems. New York: John Wiley & Sons; 1993.
72. Sievers F, Higgins DG. Clustal omega. *Curr Protoc Bioinformatics*. 2014;48:3.13.1-6.

73. Kelley LA, Sternberg MJ. Protein structure prediction on the web: a case study using the Phyre server. *Nat Protoc.* 2009;4(3):363-71.
74. Shevchenko A, Tomas H, Havlis J, Olsen JV, Mann M. In-gel digestion for mass spectrometric characterization of proteins and proteomes. *Nat Protoc.* 2006;1(6):2856-60.
75. Imprasittichail W, Roytrakul S, Krungkrai SR, Krungkrai J. A unique insertion of low complexity amino acid sequence underlies protein-protein interaction in human malaria parasite orotate phosphoribosyltransferase and orotidine 5'-monophosphate decarboxylase. *Asian Pac J Trop Med.* 2014;7(3):184-92.
76. Sambrook J, Fritsch EF, Maniatis T. Molecular cloning : a laboratory manual. 2<sup>nd</sup> ed. New York: Cold Spring Harbor Laboratory Press; 1989.
77. Laemmli UK. Cleavage of structural proteins during the assembly of the head of bacteriophage T4. *Nature.* 1970;227(5259):680-5.
78. Bradford MM. A rapid and sensitive method for the quantitation of microgram quantities of protein utilizing the principle of protein-dye binding. *Anal Biochem.* 1976;72:248-54.
79. Annoura T, Nara T, Makiuchi T, Hashimoto T, Aoki T. The origin of dihydroorotate dehydrogenase genes of kinetoplastids, with special reference to their biological significance and adaptation to anaerobic, parasitic conditions. *J Mol Evol.* 2005;60(1):113-27.
80. Wittmann JG, Heinrich D, Gasow K, Frey A, Diederichsen U, Rudolph MG. Structures of the human orotidine-5'-monophosphate decarboxylase support a covalent mechanism and provide a framework for drug design. *Structure.* 2008;16(1):82-92.
81. Deyrup AT, Krishnan S, Singh B, Schwartz NB. Activity and stability of recombinant bifunctional rearranged and monofunctional domains of ATP-sulfurylase and adenosine 5'-phosphosulfate kinase. *J Biol Chem.* 1999;274(16):10751-7.

82. Beaucamp N, Hofmann A, Kellner B, Jaenicke R. Dissection of the gene of the bifunctional PGK-TIM fusion protein from the hyperthermophilic bacterium *Thermotoga maritima*: design and characterization of the separate triosephosphate isomerase. *Protein Sci.* 1997;6(10):2159-65.
83. Cleland WW. What limits the rate of an enzyme-catalyzed reaction. *Acc Chem Res.* 1975;8(5):145-51.
84. Cleland WW. Determining the chemical mechanisms of enzyme-catalyzed reactions by kinetic studies. *Adv Enzymol Relat Areas Mol Biol.* 1977;45:273-387.
85. Benner SA. Enzyme kinetics and molecular evolution. *Chem Rev.* 1989;89(4):789-806.
86. Koshland DE. Application of a theory of enzyme specificity to protein synthesis. *Proc Natl Acad Sci U S A.* 1958;44(2):98-104.
87. Koshland DE, Jr., Ray WJ, Jr., Erwin MJ. Protein structure and enzyme action. *Fed Proc.* 1958;17(4):1145-50.
88. Tsou CL. The role of active site flexibility in enzyme catalysis. *Biochemistry (Mosc).* 1998;63(3):253-8.
89. Duffy TH, Beckman SB, Peterson SM, Vitols KS, Huennekens FM. L1210 dihydrofolate reductase kinetics and mechanism of activation by various agents. *J Biol Chem.* 1987;262(15):7028-33.
90. Bello AM, Konforte D, Poduch E, Furlonger C, Wei L, Liu Y, et al. Structure-activity relationships of orotidine-5'-monophosphate decarboxylase inhibitors as anticancer agents. *J Med Chem.* 2009;52(6):1648-58.
91. Birkholtz LM, Wrenger C, Joubert F, Wells GA, Walter RD, Louw AI. Parasite-specific inserts in the bifunctional S-adenosylmethionine decarboxylase/ornithine decarboxylase of *Plasmodium falciparum* modulate catalytic activities and domain interactions. *Biochem J.* 2004;377(Pt 2):439-48.

92. Krause T, Luersen K, Wrenger C, Gilberger TW, Muller S, Walter RD. The ornithine decarboxylase domain of the bifunctional ornithine decarboxylase/S-adenosylmethionine decarboxylase of *Plasmodium falciparum*: recombinant expression and catalytic properties of two different constructs. *Biochem J.* 2000;352 Pt 2:287-92.
93. Olliaro P, Wells TN. The global portfolio of new antimalarial medicines under development. *Clin Pharmacol Ther.* 2009;85(6):584-95.



APPENDIX



จุฬาลงกรณ์มหาวิทยาลัย  
CHULALONGKORN UNIVERSITY



**Nucleotide sequence *P. falciparum* OMPDC-OPRT gene**

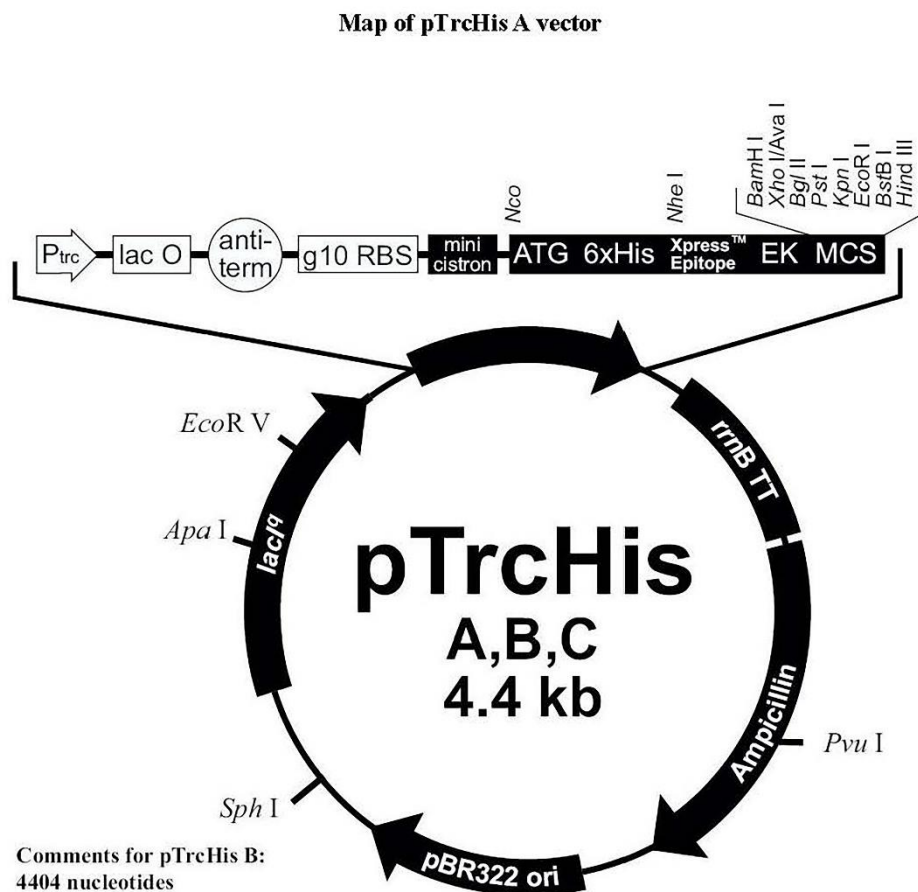
5'ATGGGTTTTAAGGTTAAATTAGAAAAACGAAGGAATGCAATAAACACGTGTTTTATGTATTGGG  
CTTGATCCTGATGAGAAGGATATTGAGAACTTTATGAAGAATGAGAAAGAAAATAATTATAATA  
ATATAAAGAAAAATTTGAAAGAGAAGTATATAAATAATGTATCTATAAAGAAGGATATTTTATTG  
AAAGCACCTGATAATATTATAAGAGAAGAAAAAAGTGAGGAATTCTTTTACTTTTTTAATCATT  
TTGTTTTTATATAATTAATGAAACGAATAAATATGCCTTAACGTTTAAGATGAATTTTGCTTTTT  
ATATTCCTTATGGATCAGTAGGTATAGATGTATTAAGAATGTGTTTGATTATTTATATGAATTA  
AATATTCCAACAATATTAGATATGAAAATTAATGATATAGGAAATACGGTGAAAAATTATCGAAA  
ATTTATATTTGAATATTTAAAGAGTGATTCATGTACTGTTAATATATATATGGGAACAAATATGT  
TAAAAGATATATGTTATGATGAAGAAAAAATAAATATTATAGTGCATTTGTTCTTGTTAAACT  
ACTAACCTGATTCAGCTATATTTCAAAAAATCTCTCTTTAGATAATAACAAGCATATGTAAT  
AATGGCACAAGAAGCTTTAAATATGTCCAGTTACTTAAATCTAGAACAAAATAATGAATTTATAG  
GTTTTGTTGTTGGAGCAAATAGTTATGATGAAATGAATTATATACGAACTTATTTTCAAATTGT  
TATATTTTATCACCAGGAATAGGAGCTCAAAATGGAGACTTACATAAAACCTTAACAAATGGATA  
TCATAAAAGTTATGAAAAAATCTTATAAATATTGGAAGAGCTATAACAAAAAATCCATACCCTC  
AAAAAGCAGCTCAAATGTATTACGATCAGATTAATGCAATCTTAAAGCAAAATATGGAATCG**3'5'**  
ATGACGACGATAAAAGAGAATGAATTTTTGTGTGATGAGGAGATATATAAAAGTTTTGTACATCT  
GAAGGATAAGATATGTGAGGAAAGAAAAAGAAGGAACTTGTTAATAATAATATTGATAATGTT  
AATTTTAATGATGATGATGATAATAATTATGATGATGATGGTAATTCTTATAGTTCCTACATTAA  
AGAGATGAAGAAATTATTAAGTTGTTCTTTTAAATATAAGGCATTAATTTGGAGAATTTA  
TTTTAAATCGAAAAGAAAAATCAAATTTTTTTTTCAAGTGGAGTATTAATAATATTGTTTCT

TCAAATATAATTTGTTTTTTATTATCCGAATTAATATTAATAAACAATTATCATTGATTATTTA  
TTAGGTGCTTCATATAAAGGTATTCCTATGGTATCCTTAACAAGTCACTTTTTATTTGAATCCAA  
AAAATATTCTAACATTTTTTTATTTATATGATAGAAAAGAAAAAAGAATATGGTGATAAAAATG  
TTATTGTGGGAAATCTTGATGATGATGATAAAGATATACTAACTTAAAAAAAAAACA AAAAAT  
AATCAAGATGAAGAAAAGAAAAATATCATAATTATTGATGATGTTTTTACTTGTGGAACAGCATT  
AACGGAAATATTAGCCAAATTA AAAACATATGAACATTTAAAAGTAGTAGCGTTTATAGTATTGC  
TTAATAGAAATGAATATGAGATAAACGAAAATAATCAAAAGATATATTTTAAGGATATCTTTGAG  
AAAAGGGTAGGAATACCTCTCTACAGTATATTATCTTACAAAGACGATATACAGTCGATGATAT  
GA3'

**Total base pairs; 1,815 bp.**

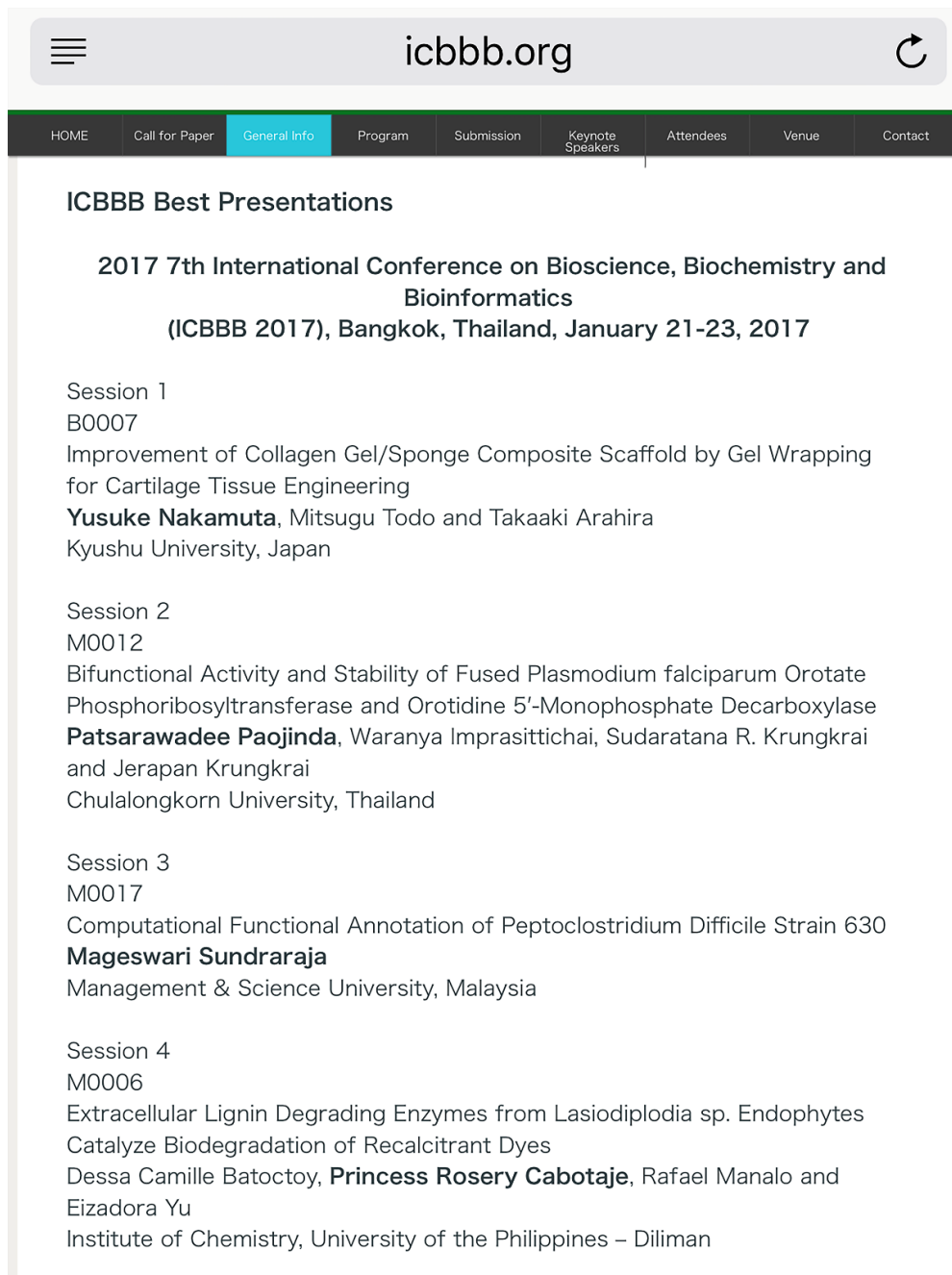


## Map of pTrcHis A vector



From: <https://www.thermofisher.com/order/catalog/product/V36020>

## The Best Presentations



The screenshot shows the website interface for icbbb.org. At the top, there is a navigation bar with a hamburger menu icon on the left, the website URL 'icbbb.org' in the center, and a refresh icon on the right. Below this is a dark navigation menu with the following items: HOME, Call for Paper, General Info (highlighted in light blue), Program, Submission, Keynote Speakers, Attendees, Venue, and Contact.

The main content area is titled 'ICBBB Best Presentations' and lists the details for the 2017 7th International Conference on Bioscience, Biochemistry and Bioinformatics (ICBBB 2017), held in Bangkok, Thailand, from January 21-23, 2017.

The presentations are organized into four sessions:

- Session 1**  
B0007  
Improvement of Collagen Gel/Sponge Composite Scaffold by Gel Wrapping for Cartilage Tissue Engineering  
**Yusuke Nakamuta**, Mitsugu Todo and Takaaki Arahira  
Kyushu University, Japan
- Session 2**  
M0012  
Bifunctional Activity and Stability of Fused Plasmodium falciparum Orotate Phosphoribosyltransferase and Orotidine 5'-Monophosphate Decarboxylase  
**Patsarawadee Paojinda**, Waranya Imprasittichai, Sudaratana R. Krungkrai and Jerapan Krungkrai  
Chulalongkorn University, Thailand
- Session 3**  
M0017  
Computational Functional Annotation of Peptoclostridium Difficile Strain 630  
**Mageswari Sundraraja**  
Management & Science University, Malaysia
- Session 4**  
M0006  
Extracellular Lignin Degrading Enzymes from Lasiodiplodia sp. Endophytes Catalyze Biodegradation of Recalcitrant Dyes  
Dessa Camille Batocoy, **Princess Rosery Cabotaje**, Rafael Manalo and Eizadora Yu  
Institute of Chemistry, University of the Philippines – Diliman

**VITA**

Name : Patsarawadee Paojinda  
Student ID : 5587829220  
Sex : Female  
Date of birth : March 17, 1988  
Place of birth : Samut Songkhram, Thailand  
Nationality : Thai  
Education : 2006-2009 Bachelor of Medical Technology  
(First class Honor), Rangsit University, Thailand  
Publication :

The manuscript entitled “Bifunctional activity of fused Plasmodium falciparum orotate phosphoribosyltransferase and orotidine 5'-monophosphate decarboxylase” has been accepted for publication in Parasitology International (Journal Impact Factor: 1.860).

Oral presentation :

The paper entitled “Bifunctional activity and stability of fused Plasmodium falciparum orotate phosphoribosyltransferase and orotidine 5'-monophosphate decarboxylase” was presented orally at The 7th International Conference on Bioscience, Biochemistry and Bioinformatics (7th ICBBB, 21-23 January 2017), Bangkok, Thailand. (The Best Presentations).